Title
Mechanisms of mTORC1 signal regulation by the Rag GTPases

Author
Lawrence, Rosalie E

Publication Date
2019

Peer reviewed|Thesis/dissertation

Mechanisms of mTORC1 signal regulation by the Rag GTPases

by

Rosalie E Lawrence

A dissertation submitted in partial satisfaction

of the requirements for the degree of

Doctor of Philosophy

in

Molecular and Cell Biology

in the

Graduate Division

of the

University of California, Berkeley

Committee in charge:

Professor Roberto Zoncu, Chair
Professor Jeremy Thorner
Professor Jacob Corn
Professor Ke Xu

Summer 2019

ABSTRACT

Mechanisms of mTORC1 signal regulation by the Rag GTPases
by
Rosalie E Lawrence

Doctor of Philosophy in Molecular and Cell Biology
University of California, Berkeley

Assistant Professor Roberto Zoncu, Chair

The decision of whether to allocate resources toward cellular growth or toward quality control is a matter of cellular life and death; disruption of growth pathways is an emerging driving force in diseases ranging from cancer to neurodegeneration. In mammalian cells, the protein kinase activity of mTORC1 promotes cellular anabolism and impedes cellular catabolism, ultimately achieving a balance that dictates the rate of cell growth. In response to nutrient levels, mTORC1 is activated upon recruitment to the lysosome, an organelle whose role as a nutrient sensing integrator has recently come into focus. The Rag GTPases are required for mTORC1 recruitment to the lysosome, but the mechanisms via which the Rags sense nutrients and precisely couple the degree of mTORC1 lysosomal recruitment levels to the level of available nutrients were unknown.

I report new live-imaging and reconstitution approaches that enabled the discovery that when the Rags transition from their inactive nucleotide binding state to their active nucleotide state in response to nutrient stimulation, they also loosen their binding affinity for their lysosomal scaffold, Ragulator. The resulting spatial cycling between the lysosome and the cytoplasm ultimately limits mTORC1 accumulation on its Rag-Ragulator lysosomal scaffold, and promotes rapid responsiveness of mTORC1.

Next, I asked whether the nucleotide states of the two Rag GTPase domains are coordinated. Prior work had established that a complex of Folliculin (FLCN) and FLCN-interacting protein 2 (FLCN:FNIP2) serves as a RagC-specific GTPase-activating protein (GAP) and thus has a positive role in mTORC1 stimulation. However, genetic evidence placed FLCN as a tumor suppressor, suggesting a negative role. I reconstituted the “Lysosomal Folliculin Complex” (LFC), a supercomplex composed of Ragulator, inactive-loaded Rags, and FLCN:FNIP2 that localizes to lysosomes. I discovered that in the LFC, FLCN:FNIP2 clamps Rags in their inactive state ($RagA^{GDP}$:$RagC^{GTP}$) by directly inhibiting nucleotide exchange in RagA, concomitant with inhibition of its RagC GAP activity, a conclusion reinforced by a high-resolution (3.6 Å) structure of the LFC. Thus, when nutrients are low, FLCN:FNIP2 is able to maintain the Rag heterodimer in its inactive state, but, in response to a rise in nutrients, FLCN:FNIP2 is converted into a functional GAP.

Finally, by assessing newly available structures of active nucleotide-bound and inactive nucleotide-bound Rag heterodimers, along with recent structural information about Rag interactors, I was able to assemble an integrated structure-guided model of the Rag-mediated cycle of recruitment and activation of mTORC1 at the lysosome. My findings increase our understanding of the molecular logic of nutrient sensing and point to new opportunities for manipulating mTORC1 signaling in disease contexts.

Dedication

to

Walton ‘Wink’ Lawrence, Jr.

for encouraging me to fly

to

Joseph Sterling Ingraham

for the company

to

Mary Edith Ingraham

for everything

Acknowledgments

Thank you to all of my teachers: professors of course, but also classmates, mentees, friends, labmates. Thank you to all of my supporters: family, friends, housemates, teammates, adventure buddies, my therapist.

To Roberto and Brian for sharing the journey of launching a new lab together. Brian, you taught me fearlessness: to ask questions, to say the thing that is hard to say, to love those around you unconditionally. Roberto, you taught me so much: your unflappable optimism and perseverance raised the ceiling for what I thought to be possible. Your openness and unwavering support have made all of the difference—thank you for taking on an excited young graduate student who knew basically nothing about mTORC1 but had big dreams.

To my other labmates and collaborators: Kelvin, for sharing the journey of the dynamic Rags project, Oliver for always being the adult in the room and simultaneously having the best meme game, Ashley for sharing your brilliance in always-thoughtful ways, Justin for being the fellow geek who walks through lab in cycling cleats and for being a great baymate and friend. To Anna and Yangxue, who charted new ground in the dynamic Rags and Folliculin projects. To Emma, who continues to inspire me, and was a true friend in addition to being a stellar mentee and scientist. To the many postdocs who shared their knowledge: Ofer, Regina, Chun-Yan, Andrew, Subhra, Rose.

To my many Hurley lab collaborators: Do Jin for patiently teaching me everything about HEK cell purification, Ming for generosity in discussion and with reagents. To Simon for being the most thoughtful, patient, and good-humored co-author I could ask for (despite our asynchronous circadian rhythms!). To Lindsey, whose generosity as a scientist and as a friend has buoyed me through many challenging moments, from being roommates at our Berkeley interview to giving talks at Asilomar to getting the folliculin project off the ground.

Thank you to my Berkeley mentors: to Susan for her ongoing mentorship and support. To Jim for the many long scientific discussions, for challenging me, and for the excellent bikerides! To Jacob for his consistently incisive feedback and for encouraging me to take risks. To Jeremy for his dedication to teaching and mentorship, and the many times he provided thoughtful feedback on talks or drafts and offered career advice.

To the many scientists whose friendship and good humor has made this whole experience memorable: Madeleine, Shion, Laura, Amy, Melissa, John, Akshay, James, thank you for inspiring me, putting things in perspective, and keeping me laughing! To my Swarthmore and Santa Cruz friends for sending love from near and far. To my Swarthmore roommate and Berkeley housemate Halleh for embarking on this journey together, and making sure we rode grad school in style with lots of snacks. Because of you, the toughest times and the best times in grad school were never devoid of humor and good wine, and always feel like home.

To Mom and Flora for unconditional support and for understanding when grad school took over my brain. Thank you for taking care of me and encouraging me to take

care of myself—none of this would be possible without you! Thank you to my extended family for continual support: Loring, Ruth Ann, Randy, and everyone.

To Avi. I am unfathomably lucky to have shared my graduate school experience with someone as caring, thoughtful, intelligent, and loving as you are. Thank you for growing with me, for feeding me, for your scientific insights, for helping me to step back and take breaks when I needed to. I look forward to what the future holds.

Contents

List of Figures

Chapter 1

Chapter 2

Chapter 3

Chapter 4

Appendix 1

Chapter 1

Introduction: mTORC1 is recruited to the lysosome upon nutrient stimulation by the Rag GTPases

1.1 Human cells manage complex metabolic programs in response to internal and external cues.

The ability to convert matter into energy to drive cellular activities and promote growth is a fundamental property of life (Koshland 2002). Many components of the machineries that facilitate cellular metabolism are conserved across phyla—nucleotide triphosphates as energy currency; membranes as facilitators of chemical gradients.

Unicellular organisms have adapted mechanisms to adjust metabolic activities to survive in diverse environmental conditions. Multicellular organisms utilize these ancient principles, and also have evolved mechanisms to facilitate distinct metabolic profiles in differentiated cell types, from energy storage in adipose tissue to ATP flux in muscle cells. Furthermore, human cells harbor genetic programs that enable metabolism to be regulated simultaneously by autocrine and endocrine factors, resulting in individualized cell-autonomous decisions governing levels of anabolism and catabolism (Albert and Hall 2015).

The cellular mechanisms that control growth and metabolism must be sturdy enough to execute faithfully in a complex environment, and also flexible enough to enable cells to survive in dynamically changing conditions. What are the network properties of human cell metabolism that robustly execute growth decisions in the varying physical contexts of diverse cell types and nutrient conditions? What properties of the network enable cells to evade pathological states, and what features confer vulnerability to disease?

In this dissertation, I will describe key properties of the nutrient sensing arm of the mechanistic Target of Rapamycin Complex 1 (mTORC1) pathway, a central decision-maker in cellular growth. mTORC1 activity is dependent on its subcellular localization and dynamics. Specifically, mTORC1 localizes to the lysosomal surface in response to nutrients via a mechanism dependent on the heterodimeric Rag GTPases.

In Chapter 2, I present the identification of a novel ‘affinity switch’ mechanism between the Rag GTPases and their lysosomal scaffold, Ragulator, that constrains mTORC1 activity in healthy cells and is bypassed in some disease contexts. Chapter 3 reports a novel role for the Folliculin/Folliculin Interacting Protein 2 (FLCN:FNIP2) complex in gating a Rag-dependent transition between an inactivating and an activating mode toward mTORC1. I also report a high-resolution structure of FLCN:FNIP2, the Rag GTPases, and Ragulator, which facilitated structure-guided mutagenesis

experiments to delineate multiple independent FLCN:FNIP2 roles in Rag-dependent mTORC1 regulation. I conclude by discussing recent structural advances in the field in Chapter 4, and present the first structural comparison between Rag GTPases in their active and inactive conformations. I conclude by putting forth a structure-informed unified model of the Rag GTPase nucleotide cycle and implications for mTORC1 lysosomal recruitment, discussing open questions in the field and potential future directions.

1.2 mTORC1 is a master regulator of cell growth

A central regulator of eukaryotic cellular growth is named for its susceptibility to the macrolide Rapamycin, a small molecule with immunosuppressive and antiproliferative effects, isolated from a soil sample on Rapa Nui (Easter) Island in 1964 (Sabatini 2017; Saxton and Sabatini 2017). The mechanistic Target of Rapamycin (mTOR), a PI3K-like serine-threonine kinase, is a member of two distinct protein complexes that control cellular anabolism: mTOR Complex 1 (mTORC1) is a master regulator of cell growth, whereas mTOR Complex 2 (mTORC2) controls cellular survival and proliferation (Saxton and Sabatini 2017).

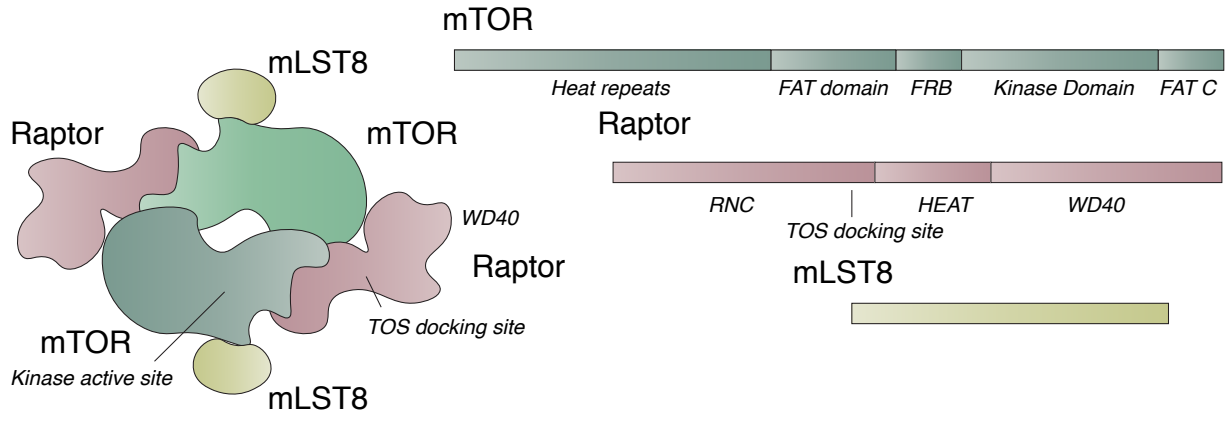

Figure 1.1 mTORC1 complex components and structural schematic. *The mTORC1 complex contains obligate members mTOR, RAPTOR, and mLST8, which form a hexameric supercomplex containing two symmetric copies of each protein. The mTOR protein is composed of several distinct domains, including a HEAT-repeat containing domain, a FAT domain, an FRB domain (which is the binding site for the rapamycin-FKBP complex), and the kinase active site domain. The RAPTOR protein is also composed of multiple domains; RNC, HEAT, and WD40. The substrate-binding interface with which TOS-containing substrates interact was mapped onto a region at the interface of the RNC and HEAT domains. The mLST8 protein binds directly to mTOR and forms a beta-propellor architecture (Yip et al. 2010). Schematic is adapted from structure published in Yang* et al.*(Yang et al. 2017)*

The mTORC1 complex is composed of mTOR along with obligate subunits Regulatory Associated Protein of mTOR (RAPTOR) and mammalian lethal with SEC13

protein 8 (mLST8). The 289-kDA mTOR polypeptide is composed of an N-terminal Huntingtin, Elongation factor 3, protein phosphatase 2A, Tor1 (HEAT) repeat alpha-solenoid domain, a Focal Adhesion kinase Targeting (FAT) domain, an FKBP-rapamycin Binding (FRB), and a canonical PI3K-like kinase domain (Figure 1.1) (Yip et al. 2010; Yang et al. 2013; Yang et al. 2017).

The 150-kDa Raptor protein is composed of a Raptor N-terminal Caspase-like (RNC) domain, a HEAT domain, and a WD40 domain, and is thought to act to concentrate and position substrates. Many mTORC1 substrates contain a TOR Signaling (TOS) sequence signature, and a TOS binding interface was mapped on Raptor between its RNC and HEAT domains (Yang et al. 2017). The 36-kDa mLST8 protein, whose function is not well characterized, is a component of both the mTORC1 and mTORC2 complexes, and adopts a Beta Propeller fold (Saxton and Sabatini 2017). Two existing Cryo-EM structures are of an mTORC1 dimer, composed of two copies each of mTOR, Raptor, and mLST8, suggesting that the complex may function as a dimer in cells. (Yang et al. 2013; Yang et al. 2017).

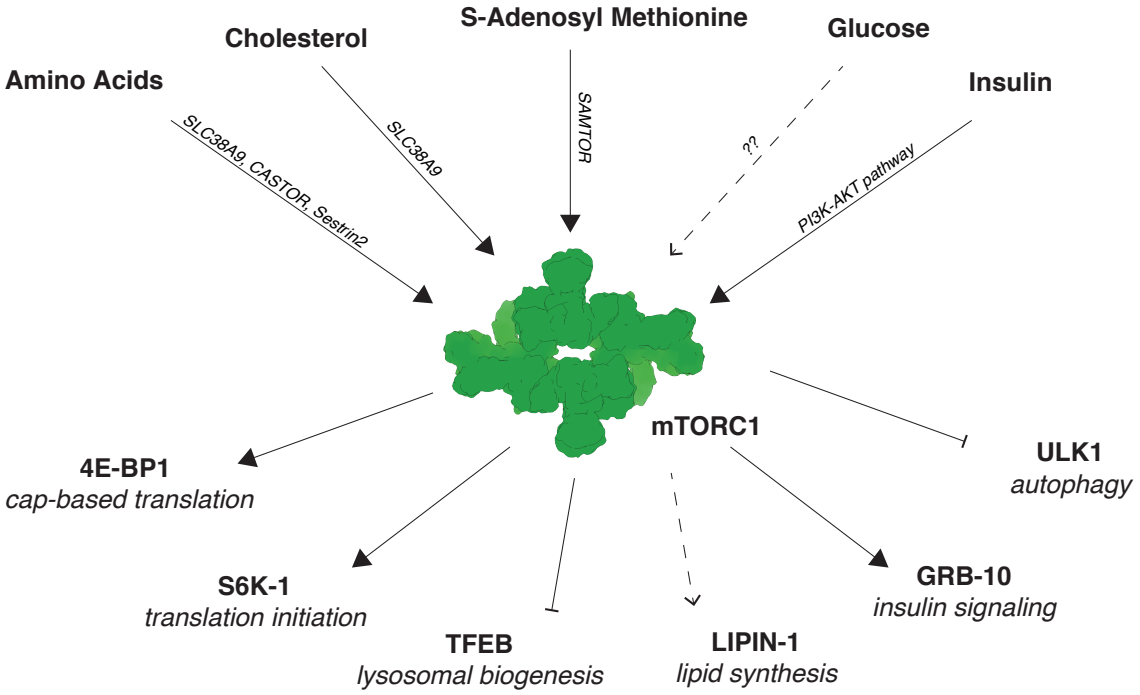

Figure 1.2 Upstream inputs and downstream substrates of mTORC1. *Molecules that activate mTORC1 are indicated at the top of the figure. The proteins that sense levels of the indicated inputs are indicated in italics along the arrows, when known. Below mTORC1, substrates are indicated in bold and the pathways that they regulate are indicated below in italics.*

mTORC1 controls many cellular processes, ranging from protein translation to lipid synthesis, energy production, and autophagy (Perera and Zoncu 2016). An ever-growing list of mTORC1 substrates includes translational/ribosomal biogenesis

controllers 4E-BP1 and S6 Kinase, the lysosomal biogenesis transcription factor TFEB, the autophagy initiating kinase Ulk1, and Grb10, a regulator of insulin-derived signaling (Gingras et al. 1999; Holz et al. 2005; Kang et al. 2013) (Figure 1.2). It was reported that mTORC1 regulates SREBP-dependent lipid biosynthesis via controlling the nuclear localization of Lipin-1, but whether Lipin-1 is a direct mTORC1 target remains controversial (Peterson et al. 2011; Eid et al. 2017). Generally speaking, mTORC1 kinase activity promotes anabolic processes such as translation and lipid synthesis, and inhibits catabolic processes such as autophagy and lysosomal biogenesis (Perera and Zoncu 2016).

1.3 mTORC1 activity is controlled by multiple inputs

Multiple inputs regulate mTORC1 activity. mTORC1 activity depends on a "coincidence detection" mechanism that renders mTORC1 activity contingent upon inputs signifying sufficient levels of both nutrients and growth factors (Perera and Zoncu 2016; Saxton and Sabatini 2017) (Figure 1.3). Growth factor sufficiency is communicated to mTORC1 by a GTP-loaded Rheb GTPase, which is downstream of the PI3K-Akt pathway and whose GTP-binding state is directly controlled by the TSC1/2 GTPase Activating Protein (GAP) complex (Inoki et al. 2012). Nutrient sufficiency is communicated to mTORC1 via a set of heterodimeric GTPases (the Rag GTPases, which will be discussed in detail below). The nucleotide binding state of the Rag GTPases is controlled by levels of nutrients including amino acids, lipids, nucleotide derivatives, and glucose (Saxton and Sabatini 2017).

A key feature in mTORC1 nutrient sensing is its dramatic relocalization from a cytosolic pool in low nutrients to the surface of lysosomes in response to nutrient stimulation (Sancak et al. 2010; Zoncu et al. 2011). This action is mediated by the Rag GTPases. It is thought that localization of mTORC1 to the lysosome facilitates direct interaction with Rheb, which is lipidated and membrane-associated (Sancak et al. 2010; Perera and Zoncu 2016).

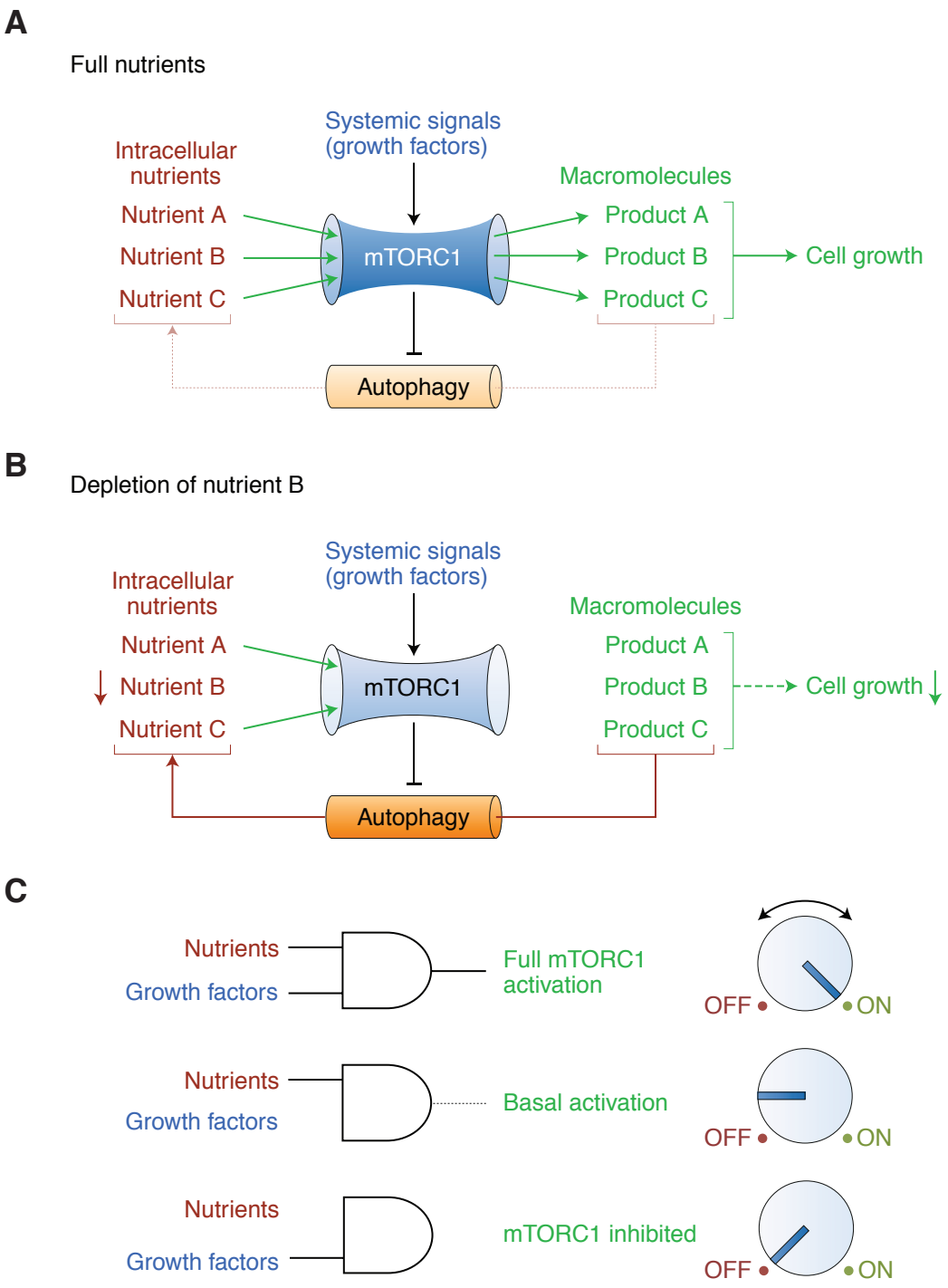

Figure 1.3. mTORC1 senses growth factors and nutrients via a coincidence detection mechanism. *(**a**) Under growth factor- and nutrient-replete conditions, mTORC1 suppresses autophagy while driving parallel synthesis of nutrient- derived macromolecules to support cell growth. (**b**) Depletion of any individual nutrient decreases mTORC1 activity and dampens the synthesis of all macromolecules downstream of mTORC1. The resulting inhibition of mTORC1 also enables induction of*

*autophagy, which recycles macromolecules into their nutrient components. (**c**) The logic of mTORC1 regulation as an AND gate requiring both sufficient nutrients and a signal from exogenous growth factors for full activation. Nutrients are generally sufficient to yield low basal activation of mTORC1, sufficient to suppress autophagy, for instance, and required for mTORC1 activation by growth factors. Adapted from Valvezan* et al.*, 2019.*

1.4 mTORC1 is activated at the lysosome, a nutrient sensing hub

The discovery that mTORC1 is recruited to the lysosome in response to nutrients led to a new understanding that the lysosome acts not only as a center for catabolism and recycling, but also as a key nutrient sensing hub (Perera and Zoncu 2016).

Lysosomes have long been appreciated as the degradative end-points for both intracellular and exogenous cargo. The catabolic function of the lysosome is accomplished by an array of approximately 60 proteases, lipases, nucleases and other hydrolytic enzymes that break down complex macromolecules into their constituent building blocks (Settembre et al. 2013; Perera and Zoncu 2016). These hydrolases require an acidic pH of ~4.5, which is established by an ATP-driven proton pump, the vacuolar H^+-ATPase (v-ATPase), in cooperation with ion channels (Zhao et al. 2015). The basic metabolites generated by lysosomal degradation are eventually exported to the cytoplasm via dedicated permeases that span the lysosomal membrane(Sagne et al. 2001; Rong et al. 2011; Jezegou et al. 2012; Liu et al. 2012; Verdon et al. 2017; Wyant et al. 2017) (Figure 1.4).

Studies in yeast and mammalian cells combining genetic, biochemical and mass spectrometric approaches are beginning to delineate the pools of metabolites stored within the lumen of lysosomes and vacuoles, including amino acids, sugars, lipids and nucleotides (Settembre et al. 2013; Perera and Zoncu 2016). Some products of lysosomal digestion are exported to the cytoplasm for immediate utilization, whereas others are stored for later use or to buffer the cytoplasmic concentrations of these species(Russnak et al. 2001; Li and Kane 2009; Abu-Remaileh et al. 2017; Verdon et al. 2017). Lysosomes and vacuoles also concentrate metal ions such as zinc, iron, copper and calcium within their lumen; iron and copper storage within the lysosome prevents their harmful accumulation in the cytoplasm(Li and Kane 2009; Polishchuk et al. 2014).

There is evidence that mTORC1 integrates levels of both intra-lysosomal and cytosolic pools of nutrients and converts these signals into an appropriate activity level (Valvezan and Manning 2019). The specific mechanisms proposed for sensing of individual nutrients are discussed below.

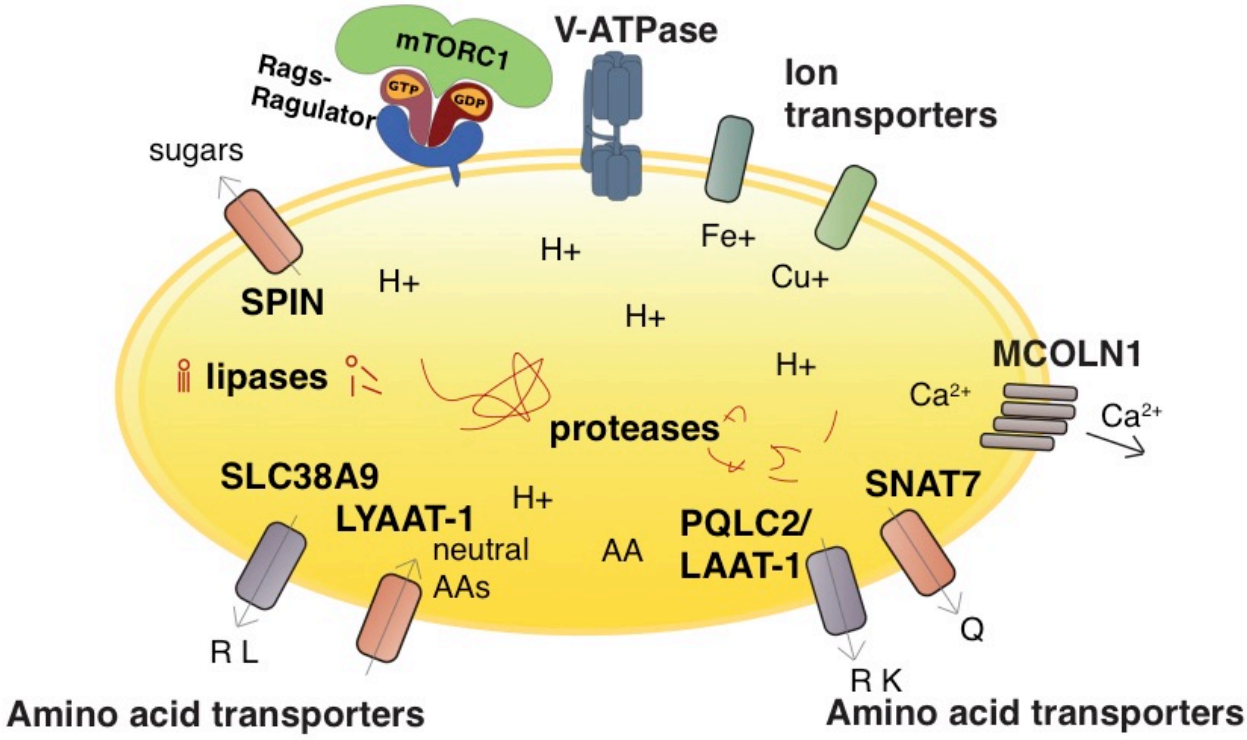

Figure 1.4 The lysosome is a sink for molecular building blocks and small molecules. *The lysosomal V-ATPase acidifies the lysosome and participates in nutrient sensing. Amino acid transporters including SLC38A9, LYAAT-1, PQLC2/LAAT-1 and SNAT7, sugar channels including SPIN, and ion channels including MCOLN1 maintain stores of amino acids, sugars and ions such as Cu+, Fe+, and Ca2+ within the lysosomal lumen. Lysosomal lipases, proteases, and nucleotidases digest cellular macromolecules into building blocks, many of which accumulate within the lysosomal lumen. The lysosome is the site of mTORC1 localization in nutrient replete cells, via its binding to the Ragulator-Rag GTPase scaffold.*

1.5 The Rag GTPases convey nutrient status to mTORC1 and control mTORC1 recruitment to the lysosome

The Rag GTPases were the first lysosomal components to be discovered that regulate mTORC1 lysosomal localization, and are thought to be direct mTORC1 binding partners (Kim et al. 2008; Sancak et al. 2008). The Rag GTPase complex is a heterodimer composed of RagA or RagB in complex with RagC or RagD. RagA and RagB are thought to be functionally equivalent, as are RagC and RagD (Sancak et al. 2008). While few experiments have established differential functions for RagA versus RagB, it was shown that RagB is primarily expressed in brain, while the RagA isoform predominates in most other tissues (Efeyan et al. 2014). RagC and RagD have more similar expression profiles, but a novel function for RagD has been reported: in

response to starvation, RagD is transcriptionally induced by and acts to promote mTORC1 induction and cellular hyperproliferation (Di Malta et al. 2017). *In* vitro experiments have failed to elucidate meaningful distinctions between RagA and RagB, nor between RagC and RagD in terms of nucleotide affinity or interactions with binding partners. Experiments presented in future chapters are thus conducted one selected heterodimer, and are thought to represent the properties of all possible heterodimers.

The Rags each contain two domains: an N-terminal G-domain with homology to Ras-like GTPase domains, and a C-terminal domain with a predicted roadblock architecture that acts as a heterodimerization interface (Gong et al. 2011; Su et al. 2017). Roadblock domains are commonly found as scaffolding modules in endocytic signaling pathways(Levine et al. 2013). Roadblock domains are homologous to longin domains, often as members of DENN modules which are often commonly found in endocytic GTPase-associated proteins (Levivier et al. 2001; Marat et al. 2011).

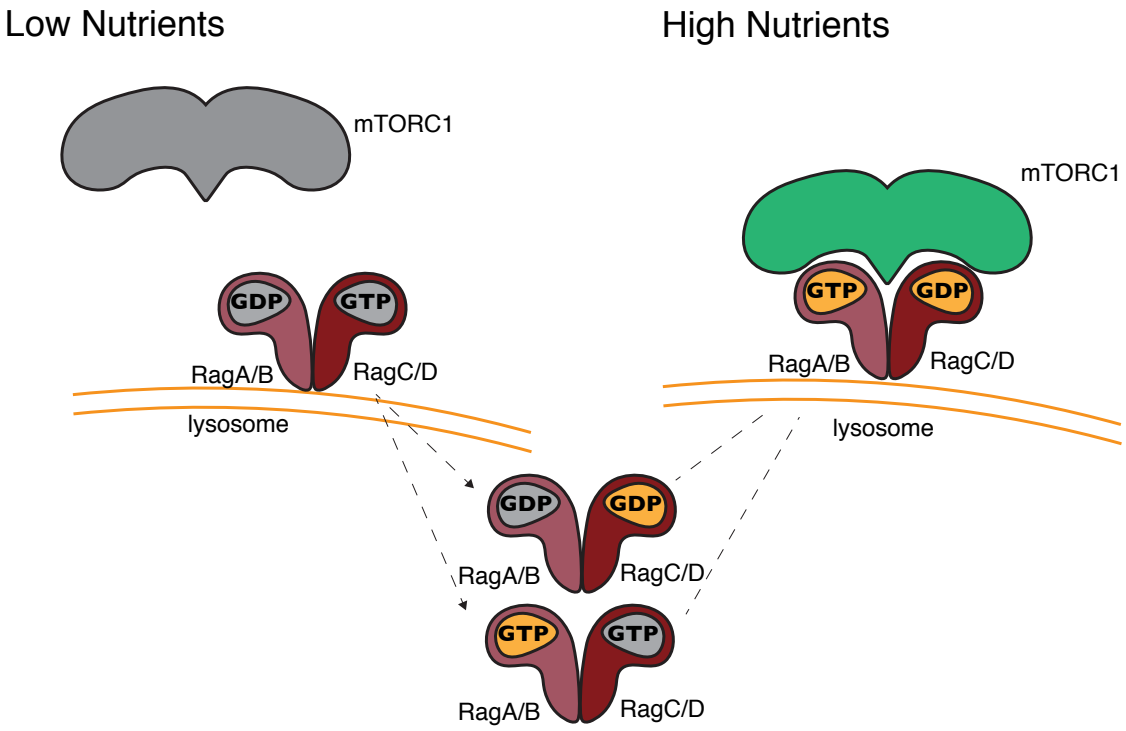

Figure 1.5 Rag nucleotide binding states control mTOR1 localization and activity. *In low nutrient conditions, it is thought that the Rags are predominantly in the RagA/B^{GDP}:RagC/D^{GTP} conformation, which maintains mTORC1 in an inactive, cytoplasmic state. In response to nutrients, the Rags are converted to the active RagA/B^{GTP}:RagC/D^{GDP} state, which results in mTORC1 recruitment to the lysosome and activation of kinase activity. It is unclear which, if any, transition state (RagA/B^{GTP}:RagC/D^{GTP} or RagA/B^{GDP}:RagC/D^{GDP}) the Rag complex passes through upon nutrient stimulation, and whether multiple populations of Rag nucleotide binding states coexist in different nutrient conditions.*

The Rag GTPases communicate nutrient sufficiency to mTORC1 via their nucleotide binding status. It is thought that Rags are primarily found in two distinct nucleotide binding conformations: RagA/B^{GDP}:RagC/D^{GTP} in low nutrient conditions, and RagA/B^{GTP}:RagC/D^{GDP} in nutrient replete conditions (Kim et al. 2008; Sancak et al. 2008) (Figure 1.5). This view became dogma in the field in response to early experiments in cells expressing various combinations of Rag proteins that were locked in particular nucleotide binding states via point mutations(Sancak et al. 2008; Sancak et al. 2010). These point mutations were designed based on homology to well-characterized Ras mutants (Nakashima et al. 1999; Sancak et al. 2008), but whether these mutations actually mimicked the GTP- or GDP-binding state of the Rags was later called into question (Appendix I). The above combinations were maximally inactivating (RagA/B^{GDP}:RagC/D^{GTP}) or activating (RagA/B^{GTP}:RagC/D^{GDP}) toward mTORC1. However, no experiment has rigorously ruled out the possibility that substantial populations of RagA/B^{GDP}:RagC/D^{GDP} or RagA/B^{GTP}:RagC/D^{GTP} heterodimers exist in cells.

Expression of maximally inactivating or activating Rag mutants were also shown to dominantly control mTORC1 localization. The inactivating Rag combination RagA/B^{GDP}:RagC/D^{GTP} caused constitutive mTORC1 localization in the cytoplasm, even under nutrient replete conditions, while the activating combination rendered mTORC1 lysosomal localization insensitive to starvation (Sancak et al. 2008; Zoncu et al. 2011). These observations led to the model that the Rag GTPases activate mTORC1 in response to nutrients by recruiting mTORC1 to the lysosomal surface, where it is then allosterically activated via interaction with Rheb.

1.6 Nutrient Sensing Upstream of the Rag GTPases

A distinguishing feature of Rags when compared to Ras-type GTPase relatives is their lack of covalent modifications to enable attachment to the lysosomal membrane. Instead, the Rags are directed to the lysosome by the pentameric Ragulator complex (also known as Lamtor complex), one subunit of which is post-translationally lipidated (Sancak et al. 2010) (Figure 1.6).

Much recent work has focused on identifying GAPs and Guanine Exchange Factors (GEFs) that cause the Rags to switch between the active and inactive state in response to amino acids, glucose and cholesterol. The Gator1 complex, composed of the Nprl2, Nprl3, and Depdc5 proteins (homologous to Nprl2-Nprl3-Iml1 in yeast), has been reported to have GAP activity toward RagA/B (Bar-Peled et al. 2013; Panchaud et al. 2013). Deletion of Gator1 results in constitutive mTORC1 activity and localization to the lysosome that cannot be reversed by amino acid withdrawal. Gator1 deletions have been observed in human cancers, indicating that aberrant mTORC1 nutrient sensing could promote cancer cell growth and proliferation (Lerman and Minna 2000; Otani et al. 2009; Bar-Peled et al. 2013). Gator1 is directed to the lysosome by the Kicstor complex, composed of the proteins KPTN, ITFG2, C12orf66 and SZT2(Peng et al. 2017; Wolfson et al. 2017). Gator1 GAP activity is antagonized by Gator2, a five-protein complex that

has homology to the SEA complex in yeast(Dokudovskaya et al. 2011; Bar-Peled et al. 2013).

Nutrient sensors located in the cytoplasm bind Gator2 to control its inhibitory interaction with Gator1 in a nutrient-dependent manner (Chantranupong et al. 2016; Wolfson et al. 2016; Gu et al. 2017). The Sestrins are stress-inducible proteins implicated in mTORC1 and AMPK regulation(Budanov and Karin 2008). Recent biochemical and structural evidence show that Sestrin1 and 2 bind to both leucine and Gator2; binding of leucine to a pocket within Sestrin2 causes its dissociation from Gator2, which allows Gator2 to inhibit Gator1 GAP activity and hence activate RagA/B(Saxton et al. 2016b; Wolfson et al. 2016). The Castor1/2 proteins promote mTORC1 activation in a similar 'double-negative' manner but upon binding to another amino acid, arginine (Chantranupong et al. 2016; Saxton et al. 2016a). Finally, Samtor binds the methionine derivative S-adenosylmethionine, which antagonizes a synergistic interaction between Samtor and Gator1, again resulting in increased RagA/B GTP binding in the presence of S-adenosylmethionine (Gu et al. 2017). These findings are consistent with previous reports that mTORC1 signaling is particularly sensitive to arginine and leucine, and suggest an intriguing connection between mTORC1 and methionine, an amino acid implicated in lifespan regulation (Grandison et al. 2009).

The FLCN:FNIP2 complex was shown to be a potent GAP for RagC/D (Petit et al. 2013; Tsun et al. 2013). FLCN:FNIP2 is thought to play an important role in lysosomal recruitment of mTORC1 by converting the Rags to their fully active state (Petit et al. 2013; Tsun et al. 2013). It is not fully understood how the activity of FLCN:FNIP2 is regulated. In contrast to Gator1, no data has directly linked nutrient sensing with control of FLCN GAP activity. Intriguingly, FLCN:FNIP2 has been reported to localize to the lysosomal surface in low nutrients, and this localization was reported to be downstream of Gator1 activity (Meng and Ferguson 2018).

In addition to sensing cytoplasmic pools of nutrients, mTORC1 has been reported to sense a lysosomal pool of amino acids via Rag- and Ragulator-interacting transmembrane proteins, including the v-ATPase and the amino acid transporter SLC38A9, which is specifically required for mTORC1 activation by lysosomal arginine (Zoncu et al. 2011; Rebsamen et al. 2015; Wang et al. 2015).

Glucose and cholesterol also promote mTORC1 activation at the lysosome via the Rag GTPases (Efeyan et al. 2013; Zhang et al. 2014; Castellano et al. 2017; Wolfson et al. 2017). Starving cells for glucose causes loss of lysosomal mTORC1 localization, which can be rescued by constitutively active (GTP-bound) RagA mutants. $RagA^{GTP/GTP}$ transgenic mice were hypersensitive to glucose starvation, and exhibited hallmarks of mTORC1 hyperactivity, including the inability to trigger autophagy during fasting (Efeyan et al. 2013). Depleting cells for cholesterol causes delocalization of mTORC1 from the lysosome and its inactivation in a Rag-dependent manner (Castellano et al. 2017). Interestingly, SLC38A9 was required for mTORC1 activation not only by arginine but also by cholesterol, thus playing a role in integrating and conveying chemically diverse nutrient inputs to mTORC1(Castellano et al. 2017).

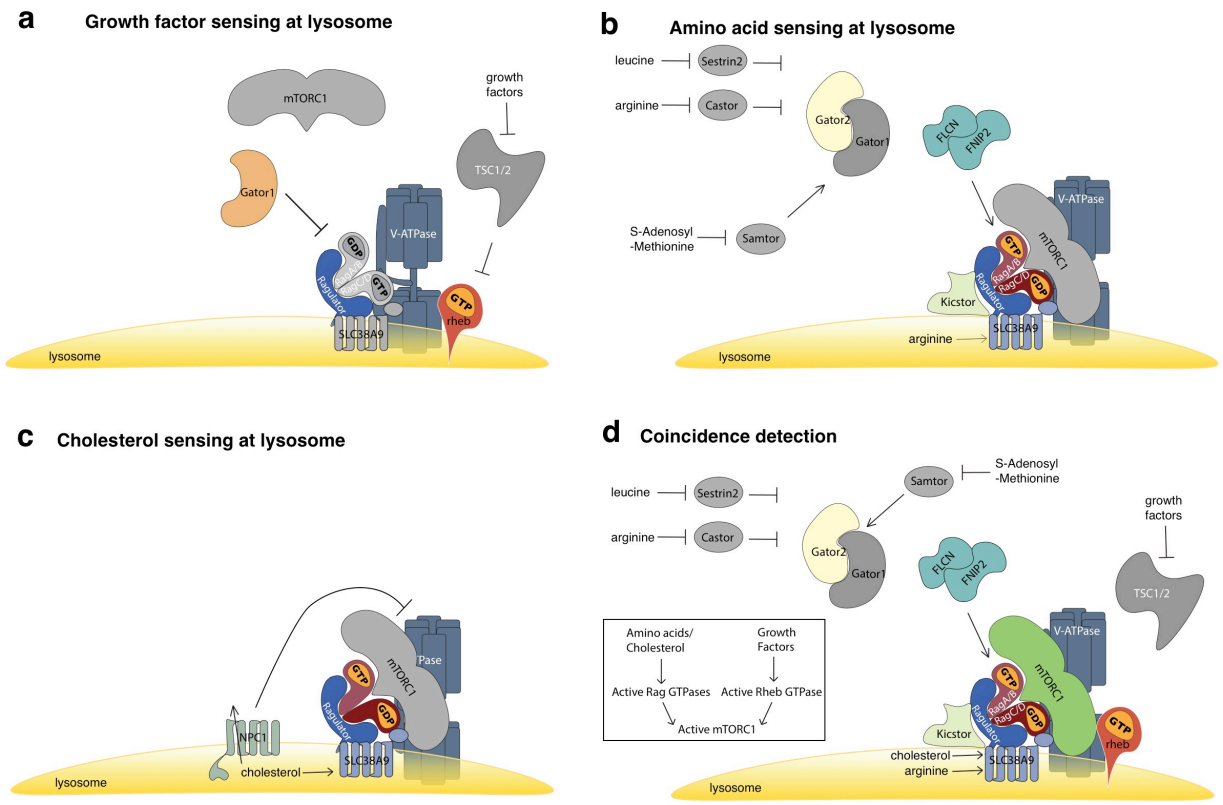

Figure 1.6 Nutrient sensing by mTORC1 at the lysosome *(a) In the absence of nutrients, mTORC1 is inactive in the cytoplasm (inactive proteins colored grey). Growth factors negatively regulate TSC1/2 Rheb GAP activity, allowing Rheb to become GTP-loaded and competent to activate lysosomal mTORC1. The Rag GTPases are localized to the lysosome by Ragulator, and RagA/B is GDP bound and RagC/D it GTP bound in the absence of nutrients. Gator1 GAP activity is active toward RagA/B, maintaining the GDP-bound state. (b) In response to nutrients, mTORC1 is recruited to the surface of the lysosome. Both cytoplasmic (Sestrin2, Castor, and Samtor) and lysosomal (SLC38A9) amino acid signals converge on the Rag GTPases. The Gator1 complex is a GAP for RagA/B; Leucine and arginine in the cytoplasm inhibit Gator2, which relieves its inhibition of Gator1 GAP activity toward RagA/B. Kicstor mediates Gator lysosomal recruitment. FLCN:FNIP2, the RagC GAP, is lysosomal in the absence of nutrients, and releases from the lysosome and promotes RagC activation in response to nutrients. mTORC1 activation by lysosomal arginine requires SLC38A9, which interacts with Ragulator and Rag GTPases via its cytoplasmic N-terminal domain. (c) Cholesterol activates mTORC1 activity in a Rag-dependent manner by binding SLC38A9 within the lysosomal transmembrane domain. NPC1 activity antagonizes cholesterol-driven V-ATPase-dependent mTORC1 activation. (d) Overview of coincidence detection mechanism: mTORC1 is activated only when both nutrient signals and growth factor signals are present. Nutrient signals (including amino acids, glucose, and cholesterol) converge on the Rag GTPases, which physically recruit mTORC1 to the lysosome. Growth factor signals converge on Rheb GTPase, which allosterically unlocks mTORC1 kinase activity at the lysosome.*

1.7 Comparison to and insights from the yeast TORC1 pathway

Thus far, this chapter has neglected mention of foundational studies on the yeast homologs of mTORC1 pathway components. This section will discuss key similarities and differences between components of the *S. cereviseae* Target of Rapamycin Complex I (TORC1) pathway and the mammalian mTORC1 pathway, and will highlight key insights derived from yeast studies (Figure 1.7).

The Rags and Ragulator share structural and functional features with the yeast Gtr1:Gtr2 GTPases and Ego1-3 scaffold, respectively (Kogan et al. 2010; Zhang et al. 2012). A crystal structure of the Gtr1:Gtr2 complex first demonstrated that that the Gtr1/2 C-terminal domains formed roadblock folds (Gong et al. 2011), and an Ego1-3 structure showed that a roadblock dimer was found in the Ego complex (Powis et al. 2015). Later, it was shown that the Ragulator complex, which is composed of five subunits in contrast with the 3-component yeast Eco complex, contained two roadblock dimers. The frequency with which the roadblock motif appears in the pathway, and the observation that a roadblock duplication may have taken place along the *S. cereviseae-H. sapiens* lineage suggest the possibility that other as-yet-uncharacterized roadblock domain-containing proteins may interact with these known components.

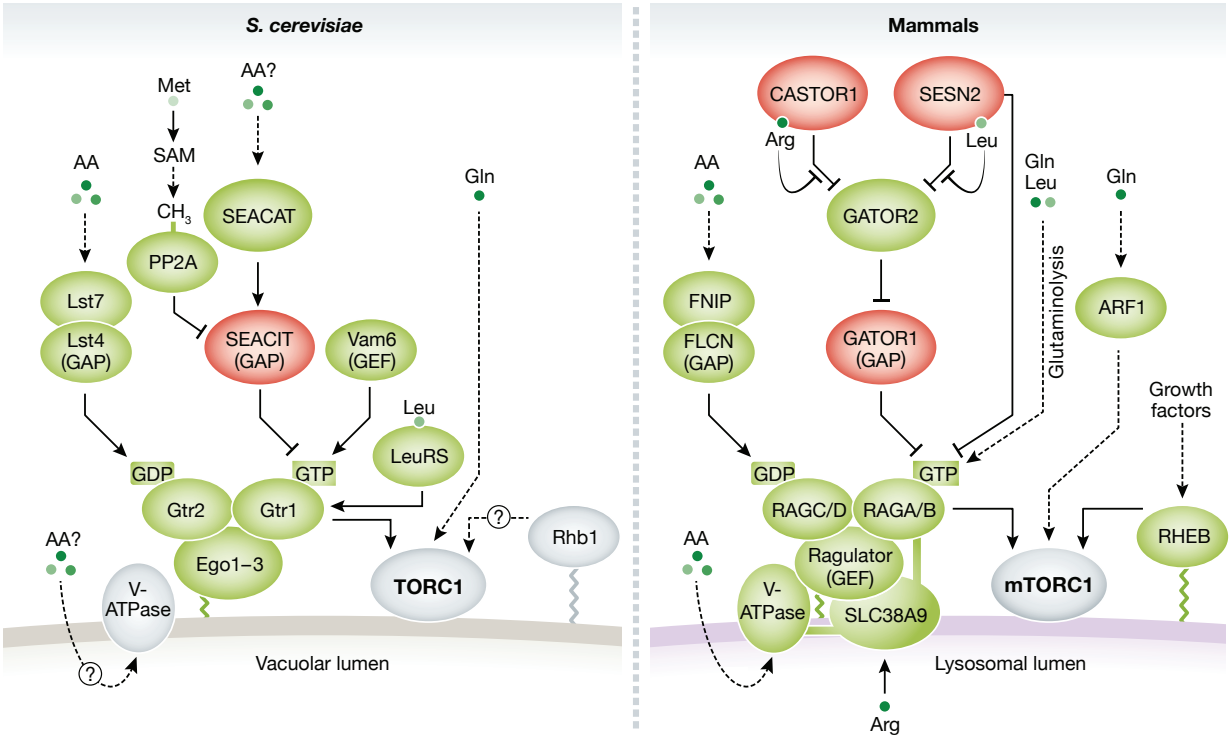

Figure 1.7 Comparison of* S. cereviseae *vacuolar TORC1 and* H. sapiens *lysosomal mTORC1 signaling. *Proteins shown in green promote (m)TORC1 activation. Proteins in red inhibit (m)TORC1. Dashed lines indicate indirect interactions. There is no evidence that the yeast RHEB-related protein Rhb1 plays a role in TORC1 regulation. Adapted from Gonzalez and Hall, 2017(Gonzalez and Hall 2017).*

Gtr1 and Gtr2 have known GAPs, which have homology to Rag GAPs. The SEACIT complex is homologous to the mammalian Gator1 complex, and is regulated by the SEACAT complex, which is homologous to mammalian Gator2. In yeast, nutrients are thought to be sensed in part through SEACAT/SEACIT. For example, a pathway in which methionine is convertd so S-Adenosyl Methionine, sensed by PP2A, whose activity relays information to SEACAT/SEACIT has been reported (Sutter et al. 2013). Importantly, *S. cerevisieae* TORC1 activity is thought to be dependent on nitrogen as well as amino acids(Stracka et al. 2014).

The yeast homologs of FLCN:FNIP2 are Lst7/Lst4, and they also display a starvation-dependent lysosomal localization pattern (Pacitto et al. 2015; Peli-Gulli et al. 2015; Peli-Gulli et al. 2017). Intriguingly, a recent study suggests a novel negative feedback mechanism of Lst4/7 mediated by mTORC1 (Peli-Gulli et al. 2017).

The yeast TORC1 system also differs critically from regulation of mammalian mTORC1 at the lysosome, as TORC1 is constitutively localized to the vacuole, rather than releasing under low nutrient conditions. Instead, several groups have observed the formation of TORC1 foci appearing associated with vacuoles in starvation conditions, and these structured were termed TORC1 Organized in Inhibited Domains (TOROIDs) (Prouteau et al. 2017; Sullivan et al. 2019).

1.8 Outstanding Questions in Rag-dependent regulation of mTORC1 signaling

Over the past decade, identification of many of the key lysosomal regulators of mTORC1 activity has opened the door for integrative studies probing how these components collaborate to achieve precise and responsive control over mTORC1 activity.

I first set out to understand the relationship between mTORC1 lysosomal localization and activity. Correlative evidence and my early observations suggested that the extent of mTORC1 localization to the lysosome was indicative of the magnitude of its activity (as assessed by amount of phosphorylated substrate). This hypothesis predicted that the setpoint level of mTORC1 accumulation on lysosomes should be moderate, such that the extent of mTORC1 lysosomal accumulation was a tunable parameter that could be adjusted to turn mTORC1 activity up or down in response to cellular need. It also suggested an understudied role for the intriguingly complex Rag GTPases. Might some of the unique features of the Rag GTPases, such as their lack of direct lipidation and heterodimeric nature imbue the capacity to dynamically manage mTORC1 lysosomal accumulation? Finally, this framing implies that mTORC1 kinase activity primarily occurs at the lysosome, rather than occurring after an activation event at the lysosome and subsequent diffusion to distant cellular locales. I present my work addressing these questions in Chapter 2 and end with experiments and modeling approaches that support the assertion that mTORC1 activity primarily occurs at the lysosomal surface.

While investigating the relationship between Rag GTPase nucleotide binding states and intracellular dynamics, I observed striking differences between “active” ($RagA/B^{GTP}$:$RagC/D^{GDP}$) and “inactive” ($RagA/B^{GDP}$:$RagC/D^{GTP}$) Rags in terms of cellular

distribution. Unexpectedly, the inactive Rags were more stably bound to lysosomes than were active Rags. Other groups reported that the FLCN:FNIP2 and homologous yeast Lst7/Lst4 complex were stably localized to lysosomes or vacuoles in low nutrient conditions (Petit et al. 2013; Peli-Gulli et al. 2015), and the coincidence between the stable lysosomal localizations of FLCN:FNIP2 and the inactive Rags complex led me to hypothesize that these two complexes could be direct interactors and co-regulators. This line of thought led to the findings presented in Chapter 3: FLCN:FNIP2 forms a stable complex that we term the Lysosomal Folliculin Complex (LFC) with Ragulator and inactive Rags at the lysosome. While part of the LFC, FLCN:FNIP2 GAP activity toward RagC is inhibited. Simulataneously, FLCN:FNIP2 regulates RagA nucleotide binding while in the LFC, effectively clamping the Rags in an inactive conformation. In this chapter I also report a structure of the LFC obtained in collaboration with Simon Fromm and members of the James Hurley lab.

In Chapter 4, I summarize structural insights from the LFC project as well as other projects investigating Rag/Ragulator interactions via structural and mechanistic means. I synthesize known information regarding the Rag nucleotide loading cycle, and propose an integrated model for the complete cycle. I conclude by presenting preliminary results relating to less-understood transitions in the Rag nucleotide binding cycle and identifying future directions.

1.9 References

Abu-Remaileh M, Wyant GA, Kim C, Laqtom NN, Abbasi M, Chan SH, Freinkman E, Sabatini DM. 2017. Lysosomal metabolomics reveals V-ATPase- and mTOR-dependent regulation of amino acid efflux from lysosomes. *Science* **358**: 807-813.

Albert V, Hall MN. 2015. mTOR signaling in cellular and organismal energetics. *Curr Opin Cell Biol* **33**: 55-66.

Bar-Peled L, Chantranupong L, Cherniack AD, Chen WW, Ottina KA, Grabiner BC, Spear ED, Carter SL, Meyerson M, Sabatini DM. 2013. A Tumor suppressor complex with GAP activity for the Rag GTPases that signal amino acid sufficiency to mTORC1. *Science* **340**: 1100-1106.

Budanov AV, Karin M. 2008. p53 target genes sestrin1 and sestrin2 connect genotoxic stress and mTOR signaling. *Cell* **134**: 451-460.

Castellano BM, Thelen AM, Moldavski O, Feltes M, van der Welle RE, Mydock-McGrane L, Jiang X, van Eijkeren RJ, Davis OB, Louie SM et al. 2017. Lysosomal cholesterol activates mTORC1 via an SLC38A9-Niemann-Pick C1 signaling complex. *Science* **355**: 1306-1311.

Chantranupong L, Scaria SM, Saxton RA, Gygi MP, Shen K, Wyant GA, Wang T, Harper JW, Gygi SP, Sabatini DM. 2016. The CASTOR Proteins Are Arginine Sensors for the mTORC1 Pathway. *Cell* **165**: 153-164.

Di Malta C, Siciliano D, Calcagni A, Monfregola J, Punzi S, Pastore N, Eastes AN, Davis O, De Cegli R, Zampelli A et al. 2017. Transcriptional activation of RagD GTPase controls mTORC1 and promotes cancer growth. *Science* **356**: 1188-1192.

Dokudovskaya S, Waharte F, Schlessinger A, Pieper U, Devos DP, Cristea IM, Williams R, Salamero J, Chait BT, Sali A et al. 2011. A conserved coatomer-related complex containing Sec13 and Seh1 dynamically associates with the vacuole in Saccharomyces cerevisiae. *Mol Cell Proteomics* **10**: M110 006478.

Efeyan A, Schweitzer LD, Bilate AM, Chang S, Kirak O, Lamming DW, Sabatini DM. 2014. RagA, but not RagB, is essential for embryonic development and adult mice. *Dev Cell* **29**: 321-329.

Efeyan A, Zoncu R, Chang S, Gumper I, Snitkin H, Wolfson RL, Kirak O, Sabatini DD, Sabatini DM. 2013. Regulation of mTORC1 by the Rag GTPases is necessary for neonatal autophagy and survival. *Nature* **493**: 679-683.

Eid W, Dauner K, Courtney KC, Gagnon A, Parks RJ, Sorisky A, Zha X. 2017. mTORC1 activates SREBP-2 by suppressing cholesterol trafficking to lysosomes in mammalian cells. *Proc Natl Acad Sci U S A* **114**: 7999-8004.

Gingras AC, Gygi SP, Raught B, Polakiewicz RD, Abraham RT, Hoekstra MF, Aebersold R, Sonenberg N. 1999. Regulation of 4E-BP1 phosphorylation: a novel two-step mechanism. *Genes Dev* **13**: 1422-1437.

Gong R, Li L, Liu Y, Wang P, Yang H, Wang L, Cheng J, Guan KL, Xu Y. 2011. Crystal structure of the Gtr1p-Gtr2p complex reveals new insights into the amino acid-induced TORC1 activation. *Genes Dev* **25**: 1668-1673.

Gonzalez A, Hall MN. 2017. Nutrient sensing and TOR signaling in yeast and mammals. *The EMBO journal* **36**: 397-408.
Grandison RC, Piper MD, Partridge L. 2009. Amino-acid imbalance explains extension of lifespan by dietary restriction in Drosophila. *Nature* **462**: 1061-1064.
Gu X, Orozco JM, Saxton RA, Condon KJ, Liu GY, Krawczyk PA, Scaria SM, Harper JW, Gygi SP, Sabatini DM. 2017. SAMTOR is an S-adenosylmethionine sensor for the mTORC1 pathway. *Science* **358**: 813-818.
Holz MK, Ballif BA, Gygi SP, Blenis J. 2005. mTOR and S6K1 mediate assembly of the translation preinitiation complex through dynamic protein interchange and ordered phosphorylation events. *Cell* **123**: 569-580.
Inoki K, Kim J, Guan KL. 2012. AMPK and mTOR in cellular energy homeostasis and drug targets. *Annu Rev Pharmacol Toxicol* **52**: 381-400.
Jezegou A, Llinares E, Anne C, Kieffer-Jaquinod S, O'Regan S, Aupetit J, Chabli A, Sagne C, Debacker C, Chadefaux-Vekemans B et al. 2012. Heptahelical protein PQLC2 is a lysosomal cationic amino acid exporter underlying the action of cysteamine in cystinosis therapy. *Proc Natl Acad Sci U S A* **109**: E3434-3443.
Kang SA, Pacold ME, Cervantes CL, Lim D, Lou HJ, Ottina K, Gray NS, Turk BE, Yaffe MB, Sabatini DM. 2013. mTORC1 phosphorylation sites encode their sensitivity to starvation and rapamycin. *Science* **341**: 1236566.
Kim E, Goraksha-Hicks P, Li L, Neufeld TP, Guan KL. 2008. Regulation of TORC1 by Rag GTPases in nutrient response. *Nat Cell Biol* **10**: 935-945.
Kogan K, Spear ED, Kaiser CA, Fass D. 2010. Structural conservation of components in the amino acid sensing branch of the TOR pathway in yeast and mammals. *Journal of molecular biology* **402**: 388-398.
Koshland DE, Jr. 2002. Special essay. The seven pillars of life. *Science* **295**: 2215-2216.
Lerman MI, Minna JD. 2000. The 630-kb lung cancer homozygous deletion region on human chromosome 3p21.3: identification and evaluation of the resident candidate tumor suppressor genes. The International Lung Cancer Chromosome 3p21.3 Tumor Suppressor Gene Consortium. *Cancer Res* **60**: 6116-6133.
Levine TP, Daniels RD, Wong LH, Gatta AT, Gerondopoulos A, Barr FA. 2013. Discovery of new Longin and Roadblock domains that form platforms for small GTPases in Ragulator and TRAPP-II. *Small GTPases* **4**: 62-69.
Levivier E, Goud B, Souchet M, Calmels TP, Mornon JP, Callebaut I. 2001. uDENN, DENN, and dDENN: indissociable domains in Rab and MAP kinases signaling pathways. *Biochem Biophys Res Commun* **287**: 688-695.
Li SC, Kane PM. 2009. The yeast lysosome-like vacuole: endpoint and crossroads. *Biochim Biophys Acta* **1793**: 650-663.
Liu B, Du H, Rutkowski R, Gartner A, Wang X. 2012. LAAT-1 is the lysosomal lysine/arginine transporter that maintains amino acid homeostasis. *Science* **337**: 351-354.
Marat AL, Dokainish H, McPherson PS. 2011. DENN domain proteins: regulators of Rab GTPases. *J Biol Chem* **286**: 13791-13800.

Meng J, Ferguson SM. 2018. GATOR1-dependent recruitment of FLCN-FNIP to lysosomes coordinates Rag GTPase heterodimer nucleotide status in response to amino acids. *J Cell Biol*.

Nakashima N, Noguchi E, Nishimoto T. 1999. Saccharomyces cerevisiae putative G protein, Gtr1p, which forms complexes with itself and a novel protein designated as Gtr2p, negatively regulates the Ran/Gsp1p G protein cycle through Gtr2p. *Genetics* **152**: 853-867.

Otani S, Takeda S, Yamada S, Sakakima Y, Sugimoto H, Nomoto S, Kasuya H, Kanazumi N, Nagasaka T, Nakao A. 2009. The tumor suppressor NPRL2 in hepatocellular carcinoma plays an important role in progression and can be served as an independent prognostic factor. *J Surg Oncol* **100**: 358-363.

Pacitto A, Ascher DB, Wong LH, Blaszczyk BK, Nookala RK, Zhang N, Dokudovskaya S, Levine TP, Blundell TL. 2015. Lst4, the yeast Fnip1/2 orthologue, is a DENN-family protein. *Open Biol* **5**: 150174.

Panchaud N, Peli-Gulli MP, De Virgilio C. 2013. Amino acid deprivation inhibits TORC1 through a GTPase-activating protein complex for the Rag family GTPase Gtr1. *Science signaling* **6**: ra42.

Peli-Gulli MP, Raucci S, Hu Z, Dengjel J, De Virgilio C. 2017. Feedback Inhibition of the Rag GTPase GAP Complex Lst4-Lst7 Safeguards TORC1 from Hyperactivation by Amino Acid Signals. *Cell Rep* **20**: 281-288.

Peli-Gulli MP, Sardu A, Panchaud N, Raucci S, De Virgilio C. 2015. Amino Acids Stimulate TORC1 through Lst4-Lst7, a GTPase-Activating Protein Complex for the Rag Family GTPase Gtr2. *Cell Rep* **13**: 1-7.

Peng M, Yin N, Li MO. 2017. SZT2 dictates GATOR control of mTORC1 signalling. *Nature* **543**: 433-437.

Perera RM, Zoncu R. 2016. The Lysosome as a Regulatory Hub. *Annu Rev Cell Dev Biol* **32**: 223-253.

Peterson TR, Sengupta SS, Harris TE, Carmack AE, Kang SA, Balderas E, Guertin DA, Madden KL, Carpenter AE, Finck BN et al. 2011. mTOR complex 1 regulates lipin 1 localization to control the SREBP pathway. *Cell* **146**: 408-420.

Petit CS, Roczniak-Ferguson A, Ferguson SM. 2013. Recruitment of folliculin to lysosomes supports the amino acid-dependent activation of Rag GTPases. *J Cell Biol* **202**: 1107-1122.

Polishchuk EV, Concilli M, Iacobacci S, Chesi G, Pastore N, Piccolo P, Paladino S, Baldantoni D, van ISC, Chan J et al. 2014. Wilson disease protein ATP7B utilizes lysosomal exocytosis to maintain copper homeostasis. *Dev Cell* **29**: 686-700.

Powis K, Zhang T, Panchaud N, Wang R, De Virgilio C, Ding J. 2015. Crystal structure of the Ego1-Ego2-Ego3 complex and its role in promoting Rag GTPase-dependent TORC1 signaling. *Cell Res* **25**: 1043-1059.

Prouteau M, Desfosses A, Sieben C, Bourgoint C, Lydia Mozaffari N, Demurtas D, Mitra AK, Guichard P, Manley S, Loewith R. 2017. TORC1 organized in inhibited domains (TOROIDs) regulate TORC1 activity. *Nature* **550**: 265-269.

Rebsamen M, Pochini L, Stasyk T, de Araujo ME, Galluccio M, Kandasamy RK, Snijder B, Fauster A, Rudashevskaya EL, Bruckner M et al. 2015. SLC38A9 is a

component of the lysosomal amino acid sensing machinery that controls mTORC1. *Nature* **519**: 477-481.
Rong Y, McPhee CK, Deng S, Huang L, Chen L, Liu M, Tracy K, Baehrecke EH, Yu L, Lenardo MJ. 2011. Spinster is required for autophagic lysosome reformation and mTOR reactivation following starvation. *Proceedings of the National Academy of Sciences of the United States of America* **108**: 7826-7831.
Russnak R, Konczal D, McIntire SL. 2001. A family of yeast proteins mediating bidirectional vacuolar amino acid transport. *J Biol Chem* **276**: 23849-23857.
Sabatini DM. 2017. Twenty-five years of mTOR: Uncovering the link from nutrients to growth. *Proc Natl Acad Sci U S A* **114**: 11818-11825.
Sagne C, Agulhon C, Ravassard P, Darmon M, Hamon M, El Mestikawy S, Gasnier B, Giros B. 2001. Identification and characterization of a lysosomal transporter for small neutral amino acids. *Proc Natl Acad Sci U S A* **98**: 7206-7211.
Sancak Y, Bar-Peled L, Zoncu R, Markhard AL, Nada S, Sabatini DM. 2010. Ragulator-Rag complex targets mTORC1 to the lysosomal surface and is necessary for its activation by amino acids. *Cell* **141**: 290-303.
Sancak Y, Peterson TR, Shaul YD, Lindquist RA, Thoreen CC, Bar-Peled L, Sabatini DM. 2008. The Rag GTPases bind raptor and mediate amino acid signaling to mTORC1. *Science* **320**: 1496-1501.
Saxton RA, Chantranupong L, Knockenhauer KE, Schwartz TU, Sabatini DM. 2016a. Mechanism of arginine sensing by CASTOR1 upstream of mTORC1. *Nature* **536**: 229-233.
Saxton RA, Knockenhauer KE, Wolfson RL, Chantranupong L, Pacold ME, Wang T, Schwartz TU, Sabatini DM. 2016b. Structural basis for leucine sensing by the Sestrin2-mTORC1 pathway. *Science* **351**: 53-58.
Saxton RA, Sabatini DM. 2017. mTOR Signaling in Growth, Metabolism, and Disease. *Cell* **169**: 361-371.
Settembre C, Fraldi A, Medina DL, Ballabio A. 2013. Signals from the lysosome: a control centre for cellular clearance and energy metabolism. *Nature reviews Molecular cell biology* **14**: 283-296.
Stracka D, Jozefczuk S, Rudroff F, Sauer U, Hall MN. 2014. Nitrogen source activates TOR (target of rapamycin) complex 1 via glutamine and independently of Gtr/Rag proteins. *J Biol Chem* **289**: 25010-25020.
Su MY, Morris KL, Kim DJ, Fu Y, Lawrence R, Stjepanovic G, Zoncu R, Hurley JH. 2017. Hybrid Structure of the RagA/C-Ragulator mTORC1 Activation Complex. *Molecular cell* **68**: 835-846 e833.
Sullivan A, Wallace RL, Wellington R, Luo X, Capaldi AP. 2019. Multilayered regulation of TORC1-body formation in budding yeast. *Mol Biol Cell* **30**: 400-410.
Sutter BM, Wu X, Laxman S, Tu BP. 2013. Methionine inhibits autophagy and promotes growth by inducing the SAM-responsive methylation of PP2A. *Cell* **154**: 403-415.
Tsun ZY, Bar-Peled L, Chantranupong L, Zoncu R, Wang T, Kim C, Spooner E, Sabatini DM. 2013. The Folliculin Tumor Suppressor Is a GAP for the RagC/D GTPases That Signal Amino Acid Levels to mTORC1. *Molecular cell*.

Valvezan AJ, Manning BD. 2019. Molecular logic of mTORC1 signalling as a metabolic rheostat. *Nature Metabolism* **1**.

Verdon Q, Boonen M, Ribes C, Jadot M, Gasnier B, Sagne C. 2017. SNAT7 is the primary lysosomal glutamine exporter required for extracellular protein-dependent growth of cancer cells. *Proc Natl Acad Sci U S A* **114**: E3602-E3611.

Wang S, Tsun ZY, Wolfson RL, Shen K, Wyant GA, Plovanich ME, Yuan ED, Jones TD, Chantranupong L, Comb W et al. 2015. Metabolism. Lysosomal amino acid transporter SLC38A9 signals arginine sufficiency to mTORC1. *Science* **347**: 188-194.

Wolfson RL, Chantranupong L, Saxton RA, Shen K, Scaria SM, Cantor JR, Sabatini DM. 2016. Sestrin2 is a leucine sensor for the mTORC1 pathway. *Science* **351**: 43-48.

Wolfson RL, Chantranupong L, Wyant GA, Gu X, Orozco JM, Shen K, Condon KJ, Petri S, Kedir J, Scaria SM et al. 2017. KICSTOR recruits GATOR1 to the lysosome and is necessary for nutrients to regulate mTORC1. *Nature* **543**: 438-442.

Wyant GA, Abu-Remaileh M, Wolfson RL, Chen WW, Freinkman E, Danai LV, Vander Heiden MG, Sabatini DM. 2017. mTORC1 Activator SLC38A9 Is Required to Efflux Essential Amino Acids from Lysosomes and Use Protein as a Nutrient. *Cell* **171**: 642-654 e612.

Yang H, Jiang X, Li B, Yang HJ, Miller M, Yang A, Dhar A, Pavletich NP. 2017. Mechanisms of mTORC1 activation by RHEB and inhibition by PRAS40. *Nature*.

Yang H, Rudge DG, Koos JD, Vaidialingam B, Yang HJ, Pavletich NP. 2013. mTOR kinase structure, mechanism and regulation. *Nature* **497**: 217-223.

Yip V, Mete M, Topaloglu U, Kockara S. 2010. Concept Discovery for Pathology Reports using an N-gram Model. *Summit Transl Bioinform* **2010**: 43-47.

Zhang CS, Jiang B, Li M, Zhu M, Peng Y, Zhang YL, Wu YQ, Li TY, Liang Y, Lu Z et al. 2014. The lysosomal v-ATPase-Ragulator complex is a common activator for AMPK and mTORC1, acting as a switch between catabolism and anabolism. *Cell Metab* **20**: 526-540.

Zhang T, Peli-Gulli MP, Yang H, De Virgilio C, Ding J. 2012. Ego3 functions as a homodimer to mediate the interaction between Gtr1-Gtr2 and Ego1 in the ego complex to activate TORC1. *Structure* **20**: 2151-2160.

Zhao J, Benlekbir S, Rubinstein JL. 2015. Electron cryomicroscopy observation of rotational states in a eukaryotic V-ATPase. *Nature* **521**: 241-245.

Zoncu R, Bar-Peled L, Efeyan A, Wang S, Sancak Y, Sabatini DM. 2011. mTORC1 senses lysosomal amino acids through an inside-out mechanism that requires the vacuolar H(+)-ATPase. *Science* **334**: 678-683.

Chapter 2

Spatial cycling of Rag GTPases attenuates mTORC1 activity

Chapter Summary

A key step in nutrient sensing is the activation of the master growth regulator, mTORC1 kinase, on the surface of lysosomes. Nutrients enable mTORC1 scaffolding by a complex composed of the Rag GTPases (Rags) and Ragulator, but the underlying mechanism of mTORC1 capture is poorly understood. Combining dynamic imaging in cells and reconstituted systems, we uncover an affinity switch that controls mTORC1 lifetime and activation at the lysosome. Nutrients destabilize the Rag-Ragulator interface, causing cycling of the Rags between lysosome-bound Ragulator and the cytoplasm, and rendering mTORC1 capture contingent on simultaneous engagement of two Rag-binding interfaces. Rag GTPase domains trigger cycling by coordinately weakening binding of the C-terminal domains to Ragulator in a nucleotide-controlled manner. Cancer-specific Rag mutants override release from Ragulator and enhance mTORC1 recruitment and signaling output. Cycling in the active state sets the Rags apart from most signaling GTPases, and provides a mechanism to attenuate mTORC1 signaling.

A portion of the content presented in this chapter has been previously published as part of the following research article: Lawrence, R. E., Cho, K. F., Rappold, R., Thrun, A., Tofaute, M., Kim, D. J., Hurley, J.H., and Zoncu, R. (2018). A nutrient-induced affinity switch controls mTORC1 activation by its Rag GTPase–Ragulator lysosomal scaffold. *Nature Cell Biology*, *20*(9), 1052–1063.

R.E.L. and R.Z. conceived of the study. R.E.L., K.F.C., J.H.H. and R.Z. designed experiments. K.F.C. developed and performed in vitro FRAP and single molecule experiments, along with R.L., R.R., A.F.T., and M.T. K.F.C. performed Rag truncation immunoprecipitation experiments, and R.Z. performed FLAG-Raptor-Rheb15 fractionation experiments. R.L. performed all other experiments. R.L. and K.F.C. performed quantitative analysis of results. D.J.K. generated reagents. R.E.L. and R.Z. wrote the manuscript. All authors reviewed and edited the manuscript.

2.1 Background

A key event in nutrient-dependent signal transduction is the recruitment of the master growth regulator, mechanistic Target of Rapamycin Complex 1 (mTORC1) kinase, to the surface of lysosomes. mTORC1 integrates signals from nutrients, growth factors and energy to drive cellular mass accumulation and proliferation, while simultaneously inhibiting nutrient scavenging and quality-control (Perera and Zoncu 2016; Saxton and Sabatini 2017). Due to its extensive actions on cellular metabolism, dysregulated mTORC1 signaling is a driving force in diseases ranging from cancer to type-2 diabetes to neurodegeneration(Perera and Zoncu 2016; Saxton and Sabatini 2017).

Nutrients, including amino acids, glucose and lipids, drive the recruitment of mTORC1 to the lysosomal surface via the Rag Guanosine Triphosphatases (GTPases) (Kim et al. 2008; Sancak et al. 2008; Binda et al. 2009; Sancak et al. 2010; Efeyan et al. 2013; Castellano et al. 2017). The Rags are heterodimers of functionally equivalent Rag A or B in complex with functionally equivalent Rag C or D(Kim et al. 2008; Sancak et al. 2008). A second GTPase, Rheb, downstream of the insulin-PhosphatidylInositol 3-Kinase (PI3K) pathway(Perera and Zoncu 2016; Saxton and Sabatini 2017), unlocks mTORC1 kinase activity and enables phosphorylation of mTORC1 substrates(Sancak et al. 2008; Sancak et al. 2010; Demetriades et al. 2014; Menon et al. 2014). Current evidence suggests that, similar to other small GTPase-regulated kinases, mTORC1 must be bound to the lysosomal membrane surface and in physical contact with Rheb in order to be active (Pacold et al. 2000; Sancak et al. 2010; Demetriades et al. 2014; Menon et al. 2014; Yang et al. 2017). Thus, factors regulating the residence time of mTORC1 at the lysosomal surface should play critical roles in regulating mTORC1 signaling strength, as suggested by the recent identification of oncogenic mutations or deletions in several of these factors(Bar-Peled et al. 2013; Okosun et al. 2016; Ying et al. 2016).

The Rags are scaffolded to the lysosomal surface by the pentameric Ragulator complex, composed of p18, p14, MP1, c7orf59 and HBXIP (also known as Lamtor1-5, respectively)(Teis et al. 2002; Sancak et al. 2010; Bar-Peled et al. 2012). Ragulator is specifically targeted to the lysosome via myristoyl and palmitoyl modifications of the N-terminal region of its p18/Lamtor1 subunit(Nada et al. 2009; Sancak et al. 2010). The fact that the Rags are not directly lapidated separates them from most membrane-associated GTPases(Peurois et al. 2019). It is tempting to speculate that the architectural features of the Rag-Ragulator mTORC1 scaffold confer specific properties to the assembled mTORC1 complex at the lysosome. For example, does relieving the Rag GTPase scaffold of direct, stable lipidation motifs enable increased dynamics? Furthermore, the Ragulator complex has been reported to act as a GEF to the Rag GTPases. In what ways does Ragulator's role as a scaffold and its roles in regulating Rag GTPase nucleotide binding interact?

We dissected the lysosomal mTORC1 capture process using dynamic imaging both in cells and in minimal reconstituted systems. These studies reveal an affinity switch that enables Rag-mTORC1 binding, while destabilizing Rag GTPase binding to

Ragulator. This mechanism renders mTORC1 recruitment dependent on the simultaneous engagement of two highly dynamic interfaces on the Rag GTPases, a feature that prevents mTORC1 hyperaccumulation and oncogenic activity.

2.2 Results

2.2.1 A fraction of mTORC1 relocalizes to lysosomes upon nutrient repletion

To determine the efficiency of mTORC1 lysosomal capture, we quantitated the fraction of lysosome-localized mTORC1 from z-stacks of U2OS cells stained for endogenous mTOR and LAMP2. We found that the percent of mTOR signal that colocalized with lysosomes in nutrient-stimulated cells was only around 50% when normalized to a lysosome-resident protein (LAMP2) (Figure 2.1a-c). We obtained similar results in HAP-1 cells in which the endogenous Raptor gene is tagged with GFP (Raptor:GFP) (Manifava et al. 2016) (Figure 2.1a-c). This finding is especially surprising given that Rags and Ragulator are not limiting for mTORC1, as each of their subunits is estimated to be in excess of Raptor with stoichiometries ranging between 4:1 and 25:1(Kulak et al. 2014). Thus, mTORC1 lysosomal binding is not saturated in nutrient-replete conditions.

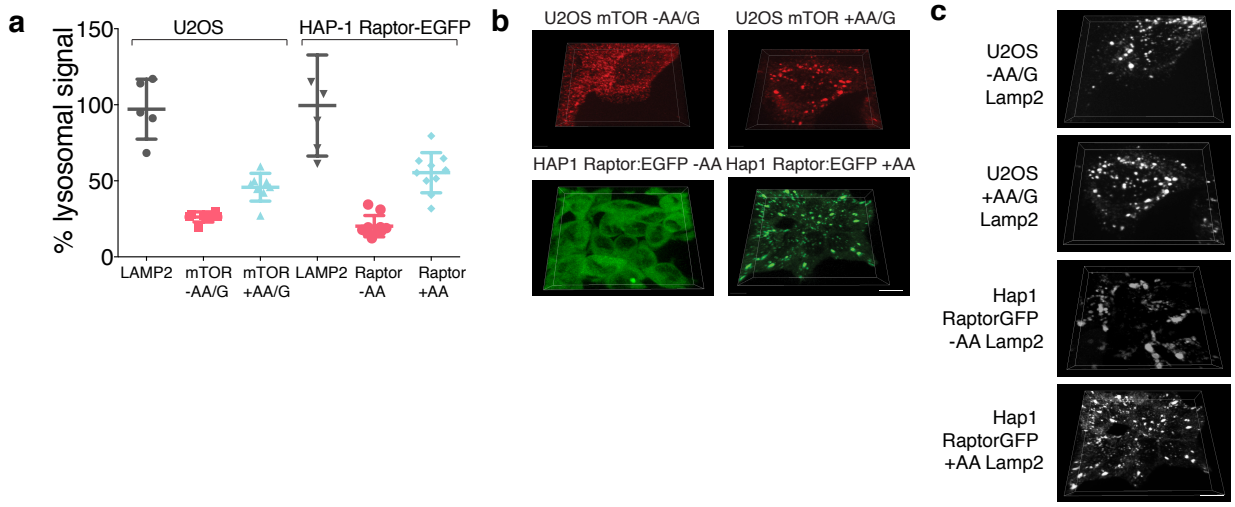

Figure 2.1 mTORC1 only partially relocalizes to lysosome in response to amino acids. *(a)* *Quantitation of lysosome-localized mTOR or Raptor:EGFP from U2OS or genome edited HAP-1 Raptor:GFP cells, respectively. U2OS cells were starved for amino acids and glucose (-AA/G) or starved and restimulated (+AA/G), and HAP-1 Raptor:EGFP cells were starved for amino acids (-AA) or starved and restimulated (+AA) followed by 3-D volumetric analysis of z-stacks. (average ± Standard Deviation (SD).* ***(b)*** *(Top) Representative 3D images of mTOR stained U2OS cells analyzed as in* ***(a)****. (Bottom) Representative 3D images of Raptor:GFP signal for HAP-1 Raptor:EGFP cells analyzed as in* ***(a)****. Scale bar 10 μm****. (c)*** *Corresponding 3D images of endogenous LAMP2 staining from U2OS cells or Raptor:GFP signal from Hap1 Raptor:GFP cells presented in (****b****).*

2.2.2 Live cell FRAP uncovers Rag spatial cycling

These results were consistent with two possible scenarios. In the first, two distinct and stable populations of mTORC1, one lysosome-bound and one cytoplasmic,

coexist. Alternatively, mTORC1 molecules actively exchange between a lysosome-bound and a cytoplasmic pool. To distinguish between these possibilities, we performed Fluorescence Recovery After Photobleaching (FRAP) experiments, which reveal the rate of exchange between two populations(Sprague et al. 2004). We transiently expressed GFP-tagged Raptor, Rags or Ragulator in U2OS cells, photobleached selected GFP-positive lysosomes, and measured fluorescence recovery over five-minute periods (Figure 2.2a,b). To minimize measurement errors due to lysosomal motility, we briefly treated cells with nocodazole to disrupt microtubule-based transport prior to imaging. This treatment did not affect mTORC1 lysosomal localization or signaling output in response to nutrients (Figure 2.2d,e).

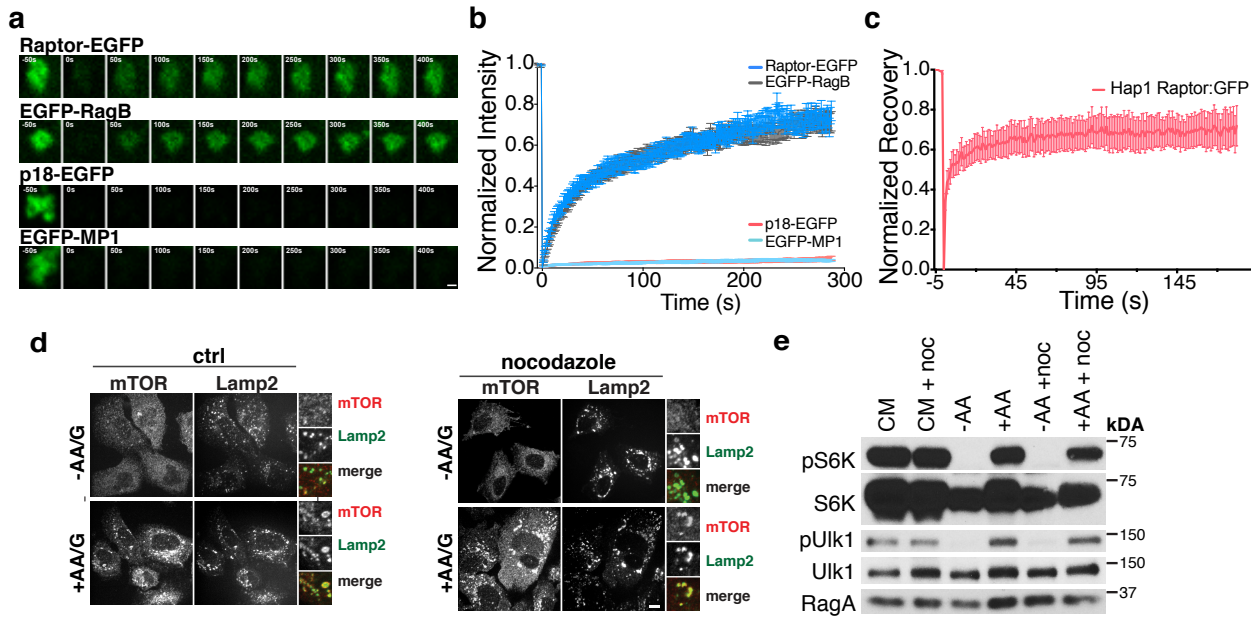

Figure 2.2 mTORC1 and Rags dynamically exchange between cytoplasmic and lysosomal pools. (a) *Time-lapse of Fluorescence Recovery After Photobleaching (FRAP) of single lysosomes in U2OS cells expressing the indicated EGFP-tagged mTORC1, Rag GTPase and Ragulator subunits. Scale bar 1 µm.* ***(b)*** *Fluorescence over time curves from FRAP experiments in U2OS cells expressing the indicated constructs. Each curve is the average ± S.E.M..* ***(c)*** *Fluorescence recovery over time curves from FRAP experiments in Raptor:GFP edited HAP-1 cells. Curve is the average ± S.E.M.* ***(d)*** *mTOR localization in U2OS cells is not affected by incubation in nocodazole. U2OS cells were starved for amino acids and glucose, or starved and restimulated, and 2.5 µg/mL nocodazole was added for the last 20 minutes where indicated. Cells were fixed and subjected to immunofluorescence for mTOR and LAMP2. Scale bar 10 µm.* ***(e)*** *mTOR signaling in U2OS cells is not affected by nocodazole treatment. U2OS cells were starved for amino acids and glucose, or starved and restimulated, and 2.5 µg/mL nocodazole was added for the last 20 minutes where indicated. Cells were lysed, followed by immunoblotting for the indicated proteins and phosphor-proteins.*

In nutrient replete cells, Raptor:GFP fluorescence recovered to 70-80% of pre-bleach intensity, with halftimes on the order of 30 seconds (Figure 2.2a,b). This indicates that mTORC1 actively exchanges between a lysosome-bound and a cytoplasmic pool in high nutrients. Similar results were obtained with Raptor:GFP genome-edited HAP-1 cells, suggesting that the observed exchange is not due to overexpression artifacts (Figure 2.2c). Two Ragulator components, p18 and MP1, showed minimal fluorescence recovery, indicating stable binding to the lysosomal surface (Figure 2.2a,b). Surprisingly, both GFP-tagged Rags actively exchanged between the lysosomal surface and the cytoplasm, with kinetics nearly identical to Raptor:GFP (Figure 2.2a,b).

2.2.3 Rag spatial cycling controls mTORC1 accumulation at the lysosome

The active cycling of the Rag GTPases between the lysosomal surface and the cytoplasm in full nutrients could limit lysosomal accumulation of mTORC1. To directly test this possibility, we engineered a system to lock the Rags to the lysosomal surface in an inducible and controlled manner, via heterodimerization of the FKBP and FRB protein domains(Inoue et al. 2005; Zoncu et al. 2009). We fused a mutated FRB domain to RagA or RagC, and coexpressed it along with a lysosomal transmembrane protein, TMEM192 (Schroder et al. 2010; Abu-Remaileh et al. 2017), fused to FKBP (TMEM192-FKBP) (Figure 2.3a). Addition of a rapamycin-like molecule (rapalogue) which does not bind to the FRB domain of endogenous mTORC1(Liberles et al. 1997) induced dimerization of FRB-RagC with TMEM192 FKBP as shown by loss of fluorescence recovery in FRAP experiments (Figure 2.3d).

Locking the Rags to the lysosome strongly increased mTORC1 lysosomal recruitment compared to non-rapalogue-treated cells, or to rapalogue-treated cells expressing TMEM192 without the FKBP domain (Figure 2.3b,c). Thus, suppressing Rag dissociation from lysosomes increases mTORC1 capture efficiency. Notably, in cells in which the Rags had been dimerized to TMEM192-FKBP, mTORC1 did not release from lysosomes upon nutrient withdrawal (Figure 2.1b,c). This suggests that release of Rags from the lysosome may facilitate their inactivation and subsequent dissociation from mTORC1 as nutrient levels fall.

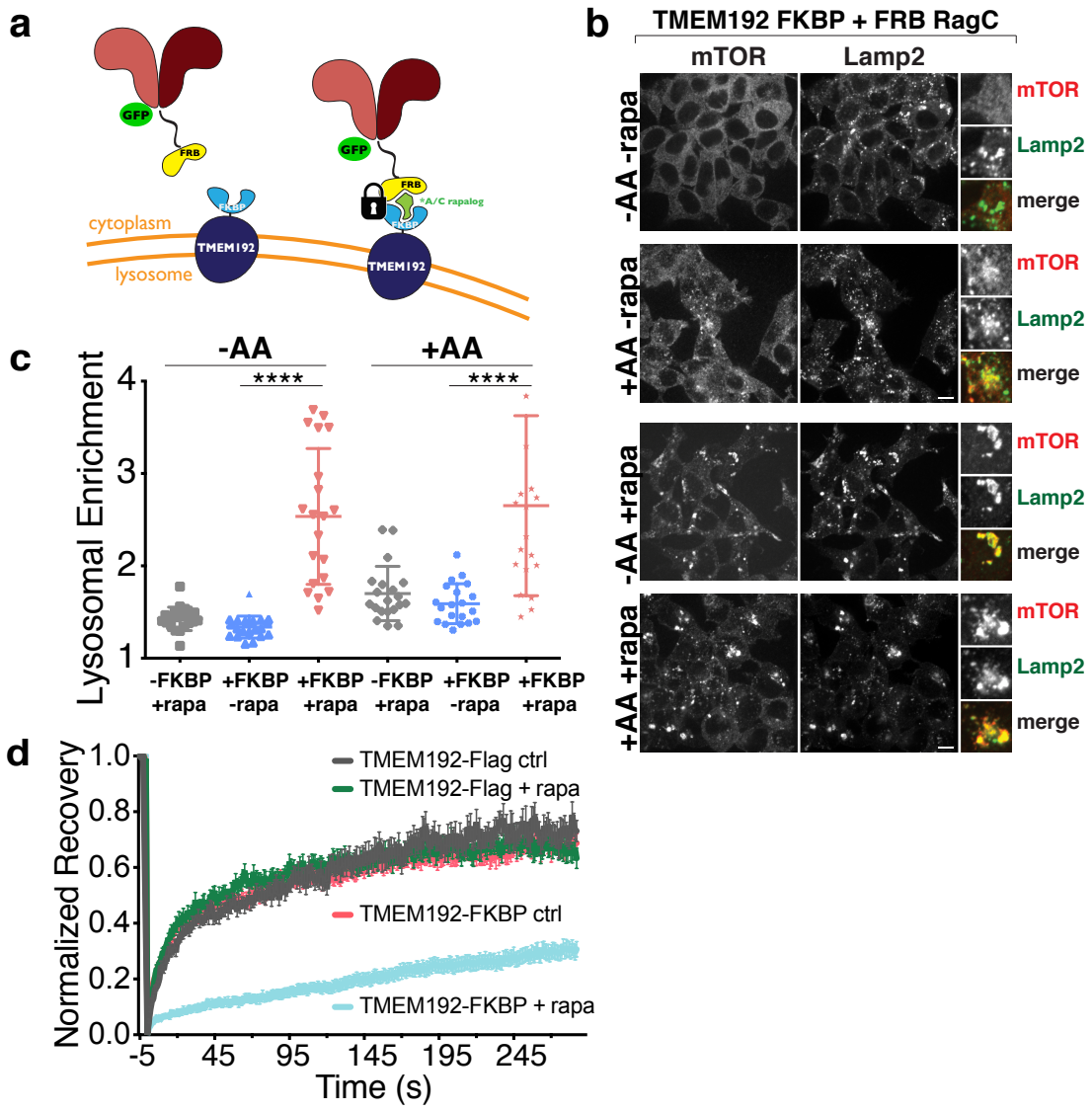

Figure 2.3 mTORC1 association with the lysosome is transient and is regulated by Rag GTPases. (a) *Schematic of in vivo induced dimerization assay for locking Rags to the lysosomal surface via rapalogue-mediated FRB/FKBP induced dimerization to the TMEM192 lysosomal resident protein.* ***(b)*** *Immunofluorescence images of 293T cells expressing the indicated constructs that have been starved of amino acids for 1 hour ('-AA') or starved for 50 minutes then restimulated with amino acids for 10 minutes ('+AA'). For conditions treated with 50 nM rapalogue (rapa), the drug was added for 20 minutes prior to starvation and was maintained in the media throughout starvation. Scale bar 10 μm.* ***(c)*** *Quantitation of mTOR Lysosomal Enrichment Score for immunofluorescence images in* ***(b)*** *(mean ± S.D).* ***(d)*** *Fluorescence recovery over time curves from FRAP experiments in U2OS cells stably expressing the indicated TMEM192 complex along with FRB-myc RagC and GFP-RagB. Cells were treated with the indicated concentration of rapalogue (rapa) for 30 minutes prior to imaging. Each curve is the average ± S.E.M.*

To determine whether the Rags and mTORC1 could stabilize each other at the lysosomal surface, we fractionated cells expressing a membrane-anchored Raptor isoform (Raptor-Rheb15) (Sancak et al. 2010). Larger amounts of RagC and RagA were recovered in membrane fractions from cells expressing Raptor-Rheb15 than in control Raptor-expressing cells (Figure 2.4a). Consistently, in cells expressing Raptor-Rheb15, both RagA and RagC were strongly clustered on lysosomes to a much greater extent than in control cells (Figure 2.4b,c). Thus, the transient Rag-mTORC1 complex can be stabilized when either partner is more securely attached to the lysosomal membrane.

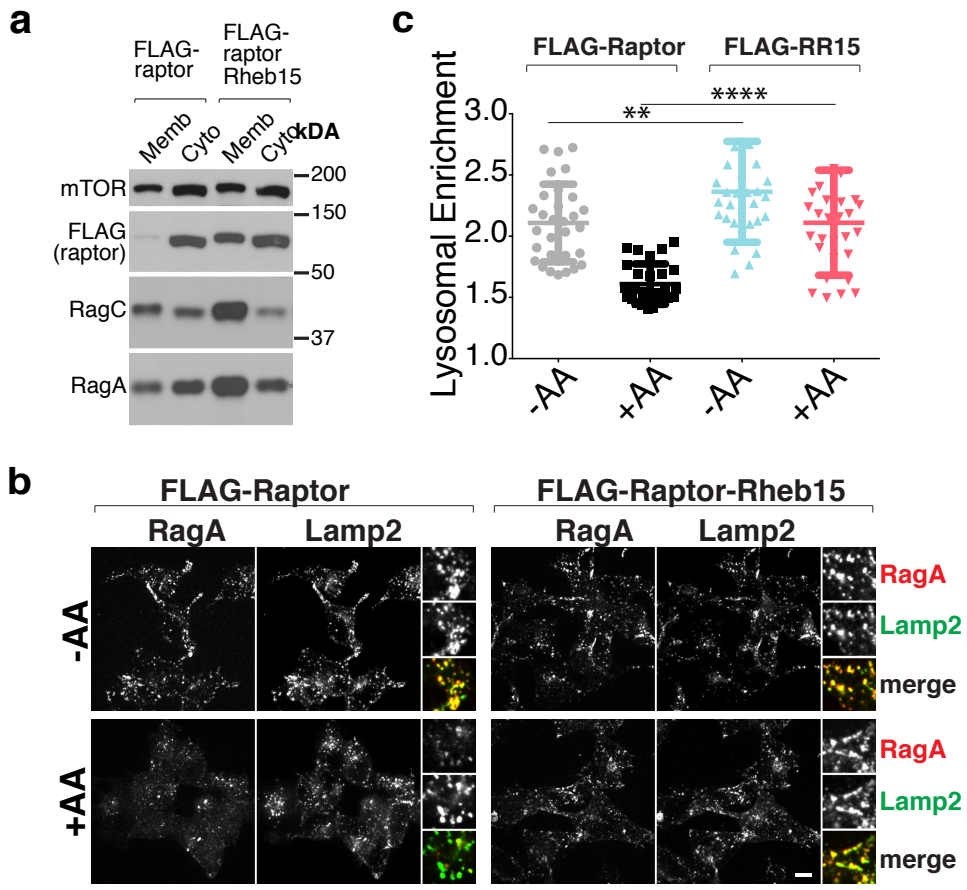

Figure 2.4 The Rag-mTORC1 complex is transient and can be stabilized by membrane-anchoring either component. (a) *HEK-293T cells stably expressing FLAG-Raptor or FLAG-Raptor-Rheb15 were starved of amino acids for 1 hour, or starved for 50 minutes then restimulated with amino acids for 10 minutes, followed by fractionation and collection of light membrane and cytoplasm fractions. Fractions were immunoblotted for the indicated proteins.* ***(b)*** *HEK- 293T cells expressing FLAG-Raptor or FLAG-Raptor-Rheb15 were starved of amino acids for 1 hour, or starved for 50 minutes then restimulated with amino acids for 10 minutes, followed by immunostaining for the indicated proteins. Scale bar 10 μm.* ***(c)*** *Quantitation of RagA Lysosomal Enrichment Score for IF images in* ***(b)*** *(mean ± S.D.).*

2.2.4 Rag spatial cycling is regulated by nutrients

Nutrients are thought to switch the Rag GTPases to the 'active' nucleotide state, which enables their binding to mTORC1(Kim et al. 2008; Sancak et al. 2008). Thus, we asked whether nutrients and nucleotide state also control Rag cycling behavior. By quantifying colocalization between endogenous Rags and Lamp2 in immunofluorescence images, we noticed that the fraction of lysosome-bound RagA and RagC decreased in response to nutrient stimulation, whereas the lysosomal fraction of Ragulator subunit p18 was nutrient-independent (**Figure 2.5a,b**).

We confirmed these results by FRAP analysis. In high nutrients, Rags had a significantly higher recovery fraction than in starved conditions, indicating a more transient association with the lysosome (**Figure 2.5c-e**). We next performed FRAP experiments in cells in which RagA/B is expected to be constitutively GTP-loaded: those lacking the Nprl2 component of the Gator1 RagA GAP complex, and cells expressing the Q99L mutant of RagB, which is defective for nucleotide hydrolysis(Kim et al. 2008; Sancak et al. 2008; Bar-Peled et al. 2013; Panchaud et al. 2013). In Nprl2-deficient cells, GFP-RagB exhibited high fluorescence recovery independent of nutrient status, whereas re-expressing Nprl2 was sufficient to re-establish suppression of RagB cycling by nutrient withdrawal (**Figure 2.5f**). Similarly, GTP-locked GFP-RagB^{Q99L} was highly dynamic irrespective of nutrient condition (**Figure 2.5g**). In contrast, in cells lacking FLCN, the GAP for RagC/D, Rag GTPase cycling was indistinguishable from wild-type cells and fully responsive to nutrient status (**Figure 2.5h**).

Unlike the Rags, Ragulator remained stably bound to the lysosomal surface irrespective of nutrient status (**Figure 2.5i**). Also, the lysosome-associated GTPase Rab7, which is not thought to be directly nutrient-regulated, displayed nearly identical recovery fractions in nutrient starved and replete conditions (**Figure 2.5i**). Thus, by controlling the nucleotide state of RagA/B, nutrients specifically trigger the cycling of Rags between the lysosomal and the cytoplasmic pools.

Taken together, these data indicate that nutrient-driven mTORC1 recruitment to the lysosome is intrinsically inefficient. Nutrients enable the Rag GTPases to bind to mTORC1, but also trigger their dissociation from the lysosomal surface. In turn, as indicated by our heterodimerization experiments, Rag cycling places a limit on the amount of mTORC1 that is bound to lysosomes.

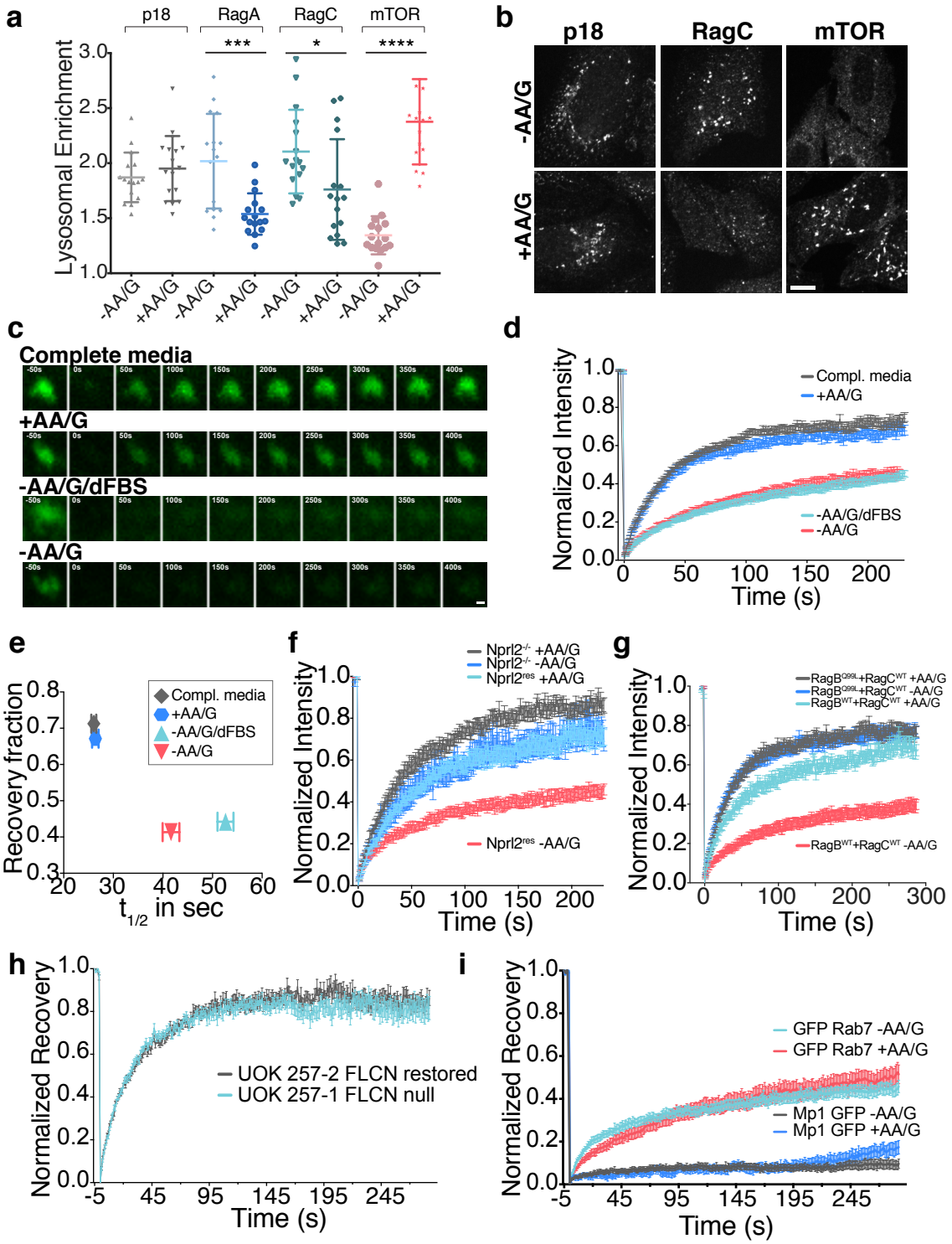

Figure 2.5 The Rag GTPases cycle between the lysosome and the cytoplasm in a nutrient-controlled manner. (a) *Quantitation of Lysosomal Enrichment Score for p18, RagA, RagC and mTOR based on endogenous LAMP2 staining in U2OS cells that were starved for amino acids and glucose for 2h ('-AA/G'), or starved for 1.5h and restimulated for amino acids and glucose for 30 min ('+AA/G') (mean ± S.D).* ***(b)*** *Representative immunofluorescence images analyzed in* ***(a).*** *Scale bar 10 µm.* ***(c)***

FRAP time-lapse of single lysosomes in U2OS cells expressing GFP-RagB + FLAG-RagC and subjected to the indicated nutrient conditions. "Compl. Media" indicates that cells were kept continuously in complete media, whereas "+AA/G" cells were starved of amino acids and glucose for 1.5hr then restimulated with amino acids and glucose for 30 min. "-AA/G/dFBS" indicates that cells were deprived of dialyzed FBS during starvation whereas –AA/G were starved in the presence of dialyzed FBS. Scale bar 1 µm. ***(d)*** *Fluorescence over time curves from FRAP experiments in* ***(c).*** *Each curve is the average ± S.E.M.* ***(e)*** *Plot showing inverse correlation between recovery fraction and halftime ($t_{1/2}$) from the curves in* ***(d).*** *Shown are best fit values with 95% confidence intervals.* ***(f)*** *Fluorescence over time curves from FRAP experiments on SW780 Nprl2$^{-/-}$ cells and SW780 Nprl2 rescue (Nprl2^{res}) cells expressing GFP-RagB that were either starved or restimulated for amino acids and glucose. Each curve is the average ± S.E.M.* ***(g)*** *Fluorescence over time curves from FRAP experiments on U2OS cells coexpressing GFP-RagB^{Q99L} (nucleotide hydrolysis deficient mutant) or GFP-RagB^{WT} along with FLAG-RagC, which were either starved or restimulated for amino acids and glucose. Each curve is the average ± S.E.M.* ***(h)*** *MP1 and Rab7 FRAP is independent of nutrient conditions. Fluorescence recovery over time curves from FRAP experiments in U2OS cells expressing GFP-tagged MP1 or Rab7. Cells were either starved or restimulated for amino acids and glucose. Each curve is the average ± S.E.M.*

2.2.5 Rag spatial cycling is regulated by nucleotide binding state

To dissect nutrient-regulated Rag cycling in mechanistic detail, we engineered a minimal reconstituted system that enables dynamic analysis of Ragulator-Rag interactions via FRAP *in vitro* (**Figure 2.6a**) (Vink et al. 2006; Fracchiolla et al. 2016; Young et al. 2016). GST-tagged Ragulator was purified from HEK-293T cells and immobilized to glutathione beads. Subsequently, purified GFP-tagged Rag heterodimers were added to the beads. After a short incubation, Ragulator-coated beads (but not beads coated with a control protein, GST-Metap2) acquired a uniform green fluorescent signal, indicating Rag binding to Ragulator (**Figure 2.6b**).

Figure 2.6 (below) GTP-loading of RagA/B destabilizes Ragulator-Rag GTPase interaction (a) *Schematic of the fluorescence in vitro binding assay for interaction of soluble, GFP-tagged Rag GTPases with non-fluorescent, bead-bound Ragulator. Excess GFP-Rags in solution allow fluorescence recovery upon photobleaching of a bead section.* ***(b)*** *Confocal images of glutathione beads coated with GST-Metap2 (left) or pentameric GST-Ragulator (right) and incubated with an excess of GFP-RagB + FLAG-RagC. Scale bar 100 µm.* ***(c)*** *In vitro FRAP experiment in which Ragulator-coated beads were incubated with GFP-RagB + FLAG-RagC^{D181N} (X-mutant) and loaded with the indicated guanine nucleotide combinations. Each curve is the average ± S.E.M.* ***(d)*** *Plot of recovery fraction vs. halftime ($t_{1/2}$) from the fits in* ***(c).*** *Shown are best fit values with 95% confidence intervals.* ***(e)*** *FRAP time-lapse of single ROIs from Ragulator-coated beads incubated with excess GFP-RagB + FLAG-RagC^{D181N} (X-mutant) and loaded with the indicated guanine or xanthosine nucleotide combinations. Scale bar 10 µm.* ***(f)*** *FRAP time-lapse of single ROIs from Ragulator-coated beads*

incubated with excess GFP-RagB + FLAG-RagC^{D181N} (X-mutant) loaded with the indicated guanine nucleotide combinations and, where indicated, incubated with 1mM GTPγS or XTPγS. Scale bar 10 μm. ***(g)*** *FRAP curves related to the experiment in* ***(f).*** *Each curve is the average ± S.E.M.* ***(h)*** *Model displaying destabilization of Ragulator-Rag GTPase interaction upon GTP-loading of RagA/B. Interaction with Ragulator is minimally affected by the nucleotide state of Rag C/D.*

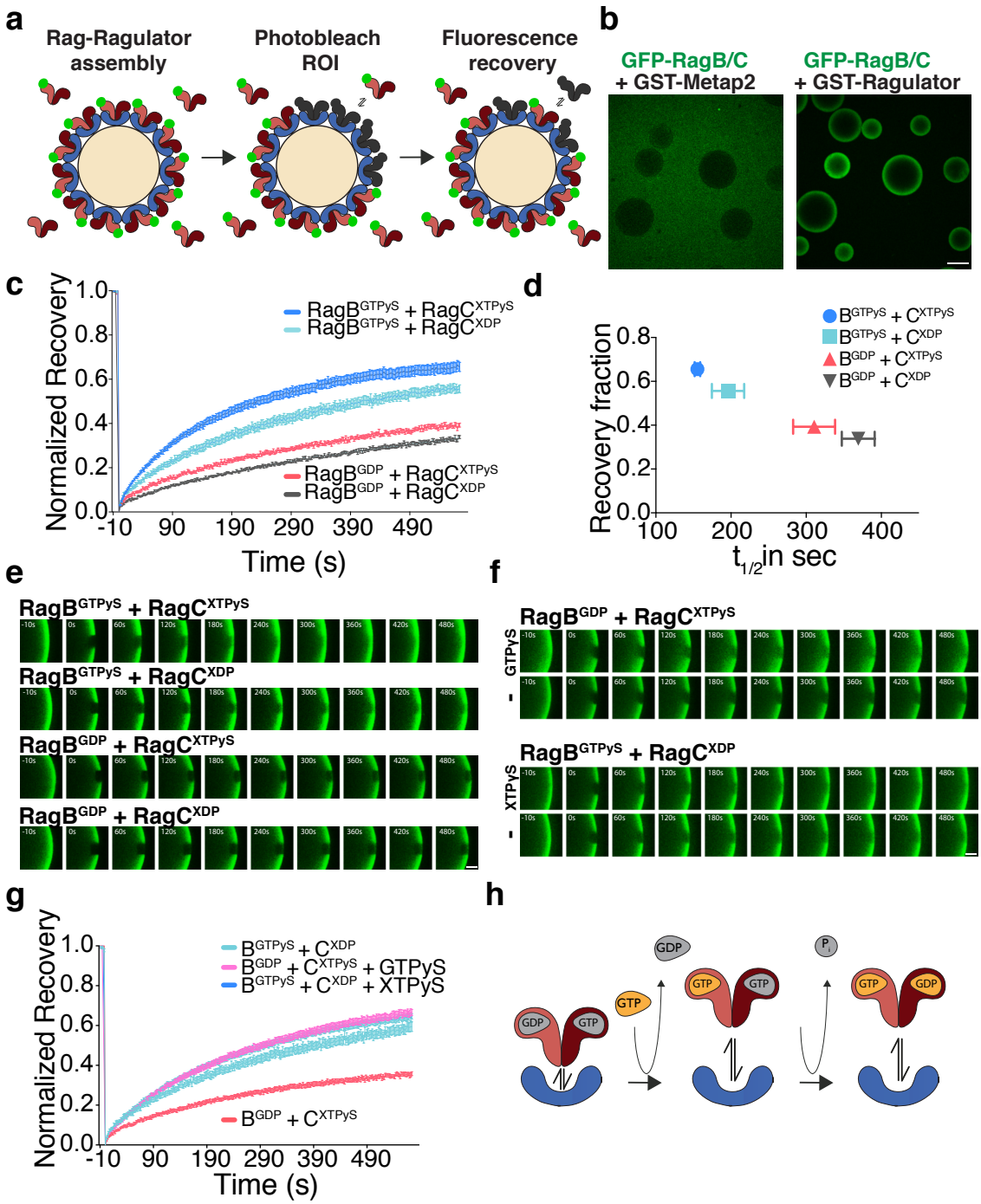

To test whether Rag cycling could be recapitulated on a minimal Ragulator scaffold, we photobleached a small region of the bead and monitored fluorescence recovery over time. When this experiment was performed in the presence of excess, unbound GFP-Rags, a large fraction of the initial fluorescence recovered. The recovery percentage and rate were independent of the concentration of excess GFP-Rags, which therefore were not rate-limiting (**Figure 2.7a-c**). However, when the experiment was performed without an excess of unbound GFP-Rags, no fluorescence recovery occurred in the photobleached area, indicating absence of lateral mobility of Ragulator-Rag complexes on the bead surface (**Figure 2.7d,e**). Furthermore, no fluorescence recovery was observed for bead-bound GST-RagB + GFP-RagC (without Ragulator) incubated in the presence of excess FLAG-RagB + GFP-RagC, indicating that Rag heterodimers are stable and do not exchange individual Rag subunits (**Figure 2.7 f,g**).

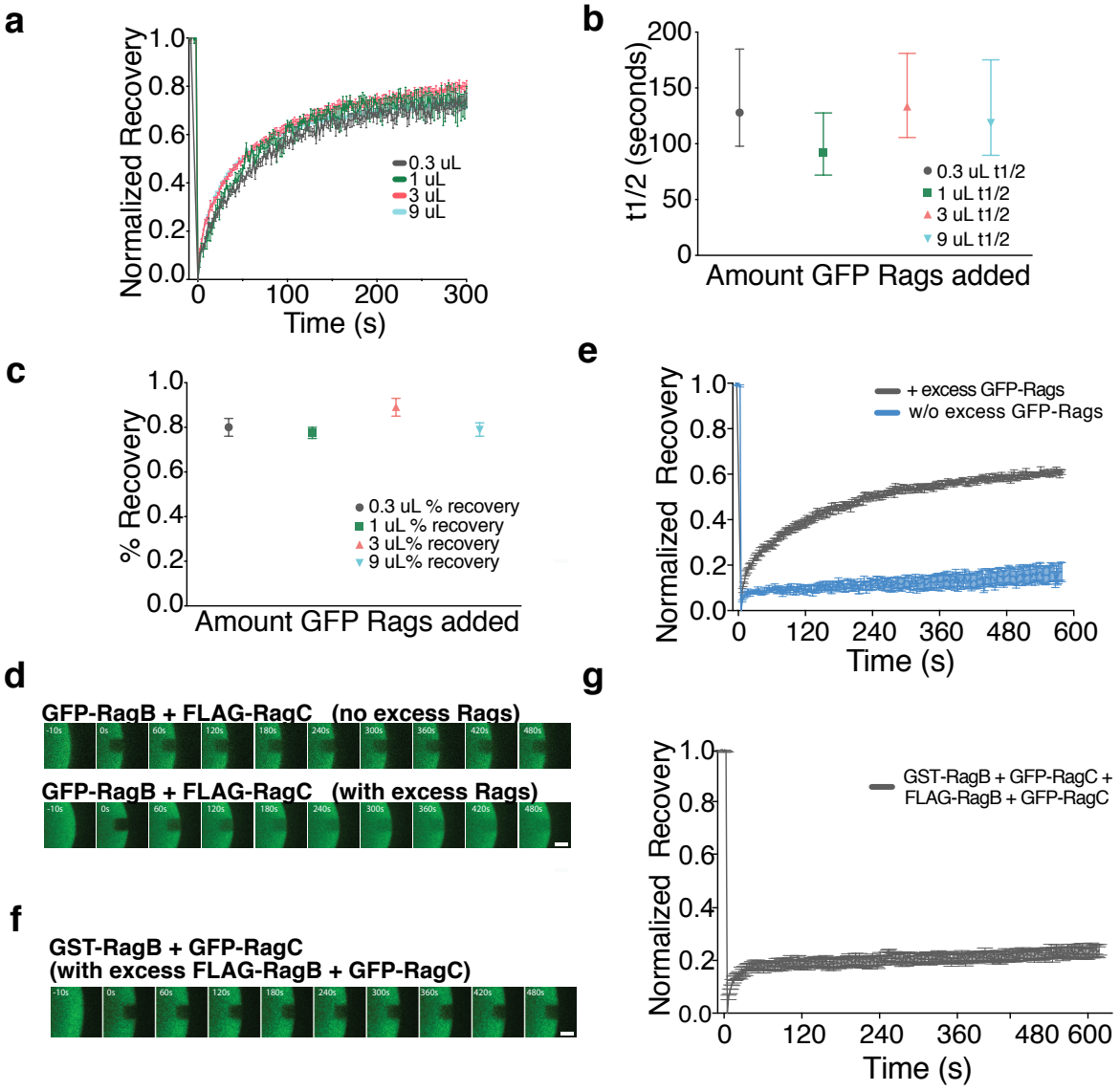

Figure 2.7 c. a) *In vitro FRAP experiment in which Ragulator-coated beads were incubated with increasing amounts of GFP-RagB + Flag RagC. Each curve is the average ± S.E.M.* ***(b)*** *Halftime ($t_{1/2}$) calculations on single exponential fits of FRAP recovery curves in* ***(a)****. Shown are best fit values with 95% confidence intervals.* ***(c)*** *Recovery fraction calculations on single exponential fits of FRAP recovery curves in* ***(a)*** *the presence of increasing concentrations of soluble GFP-tagged Rag GTPases. Shown are best fit values with 95% confidence intervals.* ***(d)*** *Montages showing fluorescence recovery over time for in vitro FRAP experiment of GFP-labeled Rag GTPases bound to GST-tagged Ragulator on beads, either in the presence or absence of excess GFP-labeled Rag GTPase heterodimers. Scale bar 10 µm.* ***(e)*** *Fluorescence recovery over time curves for* ***(d)****. Fluorescence recovery occurs only when excess GFP-Rag heterodimers are present, indicating absence of lateral diffusion of the bead-bound Ragulator-Rag complexes into the bleached area. Each curve is the average ± S.E.M. of [+excess GFP-Rags N=12, w/o excess GFP Rags N=9] bead regions.* ***(f)*** *Montages showing fluorescence recovery over time for in vitro FRAP experiment of bead-bound GST-RagB + GFP-RagC in the presence of excess FLAG-RagB + GFP-RagC. Scale bar 10 µm.* ***(g)*** *Fluorescence recovery over time curves for* ***(f).*** *No fluorescence recovery occurs, indicating that Rag heterodimers are stable and that no GFP-RagC exchanges between bead-bound GST-RagB and soluble FLAG-RagB. Curve is the average ± S.E.M. of N=12 bead regions.*

Next, we tested whether Rag cycling off Ragulator *in vitro* is governed by Rag nucleotide state, as suggested by our results in cells. To load the two Rags independently with nucleotides, we utilized a RagC mutant that binds preferentially to xanthosine over guanosine nucleotides ($RagC^{X}$)(Schmidt et al. 1996; Bar-Peled et al. 2012). $RagA^{WT}$ and $RagC^{X}$ were co-expressed, co-purified, and independently loaded with nucleotides *in vitro*. Using FRAP, we established that the 'inactive-loaded' GFP-tagged $RagB^{GDP}$ + $RagC^{XTP\gamma S}$ heterodimer (which is thought to occur in nutrient starved conditions) bound to Ragulator on the beads more stably than the 'active-loaded' $RagB^{GTP\gamma S}$ + $RagC^{XDP}$ heterodimer (which is thought to occur in nutrient stimulated conditions) (**Figure 2.6c-e**). Interestingly, the 'double-GTP' heterodimer ($RagB^{GTP\gamma S}$ + $RagC^{XTP}$), which likely represents a transition state, exhibited slightly higher fluorescence recovery than the active-loaded Rags. Conversely, $RagB^{GDP}$ + $RagC^{XDP}$ was the least mobile.

When inactive-loaded $RagB^{GDP}$ + $RagC^{XTP\gamma S}$ were provided with excess GTPγS, they transitioned to the high cycling state, consistent with RagB exchanging GDP with GTPγS (**Figure 2.6f,g**). However, supplementing active-loaded Rags ($RagB^{GTP\gamma S}$ + $RagC^{XDP}$) with XTPγS increased the rate of cycling only subtly over the already mobile active-loaded Rags. Taken together, these results demonstrate that nutrient-dependent Rag cycling can be fully recapitulated on a Ragulator scaffold *in vitro* without additional factors. Moreover, consistent with the observations in cells, the cycling is largely determined by the nucleotide state of RagA/B (**Figure 2.6h**).

2.2.6 Rag spatial cycling regulates mTORC1 residence time at the lysosome

FRAP recovery curves represent the combined contributions of both on-rates and off-rates, and thus they cannot unambiguously reveal the lifetime of a protein-protein interaction, which is determined by the off-rate (Sprague et al. 2004). Moreover, the FRAP-based system was not suitable to characterize the interaction of mTORC1 with Rag GTPases *in vitro*. While we could detect binding of GFP-tagged Raptor (co-purified with mTOR and mLST8) to bead-bound Rags set to the active state, this interaction was too weak to allow robust FRAP measurements (**Figure 2.8a**). To overcome these limitations, we developed a more sensitive *in vitro* system that allows direct measurement of single molecule lifetimes. We fused RagB to a Halo tag, which enables covalent labeling with tetramethylrhodamine (TMR) dyes that are bright enough for single molecule visualization(Chen et al. 2014; Knight et al. 2015; Hansen et al. 2017). We imaged TMR-labeled Rags via near-Total Internal Reflection Fluorescence microscopy with a relatively shallow angle that captures a significant cross-section of the Ragulator-coated beads while minimizing background from freely diffusing, unbound fluorophores (**Figure 2.8b,c**). Single Halo^{TMR} –Rag heterodimers were imaged with long exposure times (300 ms) to motion blur freely diffusing molecules and specifically detect bound molecules(Chen et al. 2014; Knight et al. 2015; Hansen et al. 2017). Binding events were tracked using a custom-written single particle-tracking algorithm and were displayed as survival probability plots (**Figure 2.8d,e**). Survival probability plots were best fit with double exponential functions, in which the fast component likely represents short-lived nonspecific collisions (also present in the Metap2 control sample) and the slow component reflects Rag-Ragulator binding lifetimes. Half lives were estimated after correcting the slow component for photobleaching (**Figure 2.8f**).

In agreement with bulk FRAP measurements, inactive-loaded Halo^{TMR}-tagged RagB^{GDP} + RagC$^{XTP\gamma S}$ displayed two-fold longer residence times on Ragulator than active-loaded RagB$^{GTP\gamma S}$ + RagC^{XDP} (7.0 ± 0.5s vs 3.5 ± 0.2s) (**Figure 2.8f**). Furthermore, when GTPγS was added to inactive-loaded Rags, their half-lives decreased to match those of active-loaded Rags, whereas adding XTPγS to active-loaded RagB$^{GTP\gamma S}$ + RagC^{XDP} did not significantly affect the half-life (Figure 4e). Thus, both FRAP and single molecule analysis support a model in which GTP-loading of RagA/B destabilizes the interaction with Ragulator, resulting in decreased residence times.

To determine how a destabilized interface between Rags and Ragulator influences mTORC1 residence time on its Rag-Ragulator scaffold, we re-engineered our single molecule assay to track a three-component system (**Figure 2.8g**). Specifically, we measured the residence times of Raptor-Halo^{TMR} (co-purified with mTOR and mLST8) on glutathione beads bearing GST-Ragulator pre-incubated with GFP-tagged active-loaded Rag heterodimers and calculated an average residence time of 3.1 ± 0.2 seconds (**Figure 2.8i**).

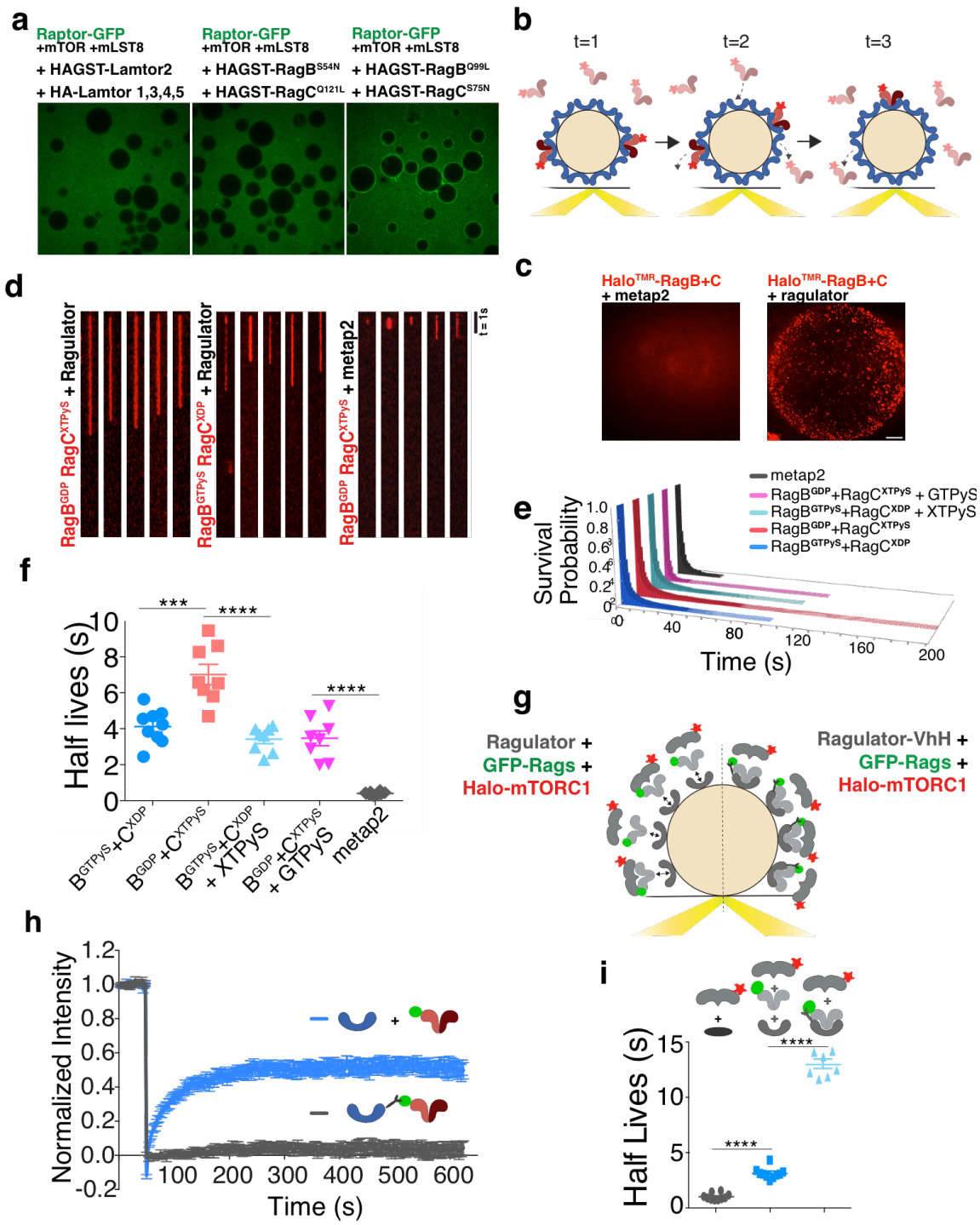

Figure 2.8 Rag release from Ragulator requires both G-domains. (a) *Confocal images of glutathione beads coated with GST-Ragulator (left) or GST-inactive-loaded Rags (middle) or GST-active-loaded Rags (right) and incubated with an excess of GFP-Raptor (co-expressed along with mTOR and mLST8). Notice binding of GFP-Raptor to the surface of beads bearing active Rags, but not inactive Rags or Ragulator. Scale bar 100 µm.* ***(b)*** *Single molecule in vitro binding assay. Recombinant, Halo-tagged Rag*

GTPases bound to tetramethylrhodamine (TMR) are combined with Ragulator-coated beads. Binding events are visualized using near-Total Internal Reflection Fluorescence (TIRF). ***(c)*** *Kymographs of single Halo^{TMR}-RagB + FLAG-RagC^{X} molecules loaded with the indicated guanine and xanthosine nucleotides, binding to Ragulator-coated or to Metap2-coated beads. Scale bar 1s.* ***(d)*** *Survival probability plots of Halo^{TMR}-RagB + FLAG-RagC^{X} molecules loaded with the indicated combination of guanine and xanthosine nucleotides, binding to Ragulator-coated or to Metap2-coated beads.* ***(e)*** *Comparison of the slow $t_{1/2}$ values, following photobleaching correction, for the residence time of the indicated Rag nucleotide states on Ragulator. Residence times from three biological replicates were pooled, divided into 10 randomly determined sets. Survival probabilities were fitted to single exponentials. Displayed is mean ± S.E.M.; *** p=0.0004, **** p<0.0001, two-sided unpaired t-tests.* ***(f)*** *Integrated time-lapse image of Halo^{TMR}-RagB + FLAG-RagC binding to a Ragulator-coated bead (right) or to a Metap2-coated bead (left). Scale bar 10 µm.* ***(g)*** *Three-component binding assay. TMR-labeled mTORC1 is combined with Ragulator-coated beads and free, active GFP-tagged Rags (left) or with beads coated with stable Ragulator-VhH + GFP-Rag complexes (right). Binding events are visualized using near-TIRF.* ***(h)*** *Fluorescence recovery over time curves from FRAP experiments in U2OS cells expressing p18-VhH (p18 fused with a GFP nanobody) or p18 alone along with GFP-tagged Rag GTPases. Each curve is the average ± S.E.M.* ***(i)*** *Photobleaching-corrected halflives ($t_{1/2}$) values for binding of Raptor-Halo^{TMR} molecules to beads coated with Metap2 or with the indicated Ragulator-Rag GTPase combinations. Single molecule residence time data from three biological replicates were pooled and divided into 10 randomly determined sets. Half-lives were calculated from single exponential fits of each set. Displayed is mean ± S.E.M.; **** p<0.0001, two-sided unpaired t-tests.*

To measure the contribution of Rag-Ragulator dissociation to mTORC1 residence time, we repeated the experiment using GST-Ragulator in which the p18 subunit was fused to VhH^{GFP}, a nanobody that binds to GFP with nanomolar affinity (p18-VhH^{GFP})(Caussinus et al. 2011), in the presence of GFP-tagged, active-loaded Rag heterodimers. Due to the high affinity of the VhH-GFP interaction, GFP-Rag heterodimers were virtually locked to p18-VhH^{GFP}, as shown by near absence of fluorescence recovery in FRAP experiments (**Figure 2.8h**). Locking the Rags to Ragulator via p18-VhH^{GFP} increased the residence times of mTORC1-Halo^{TMR} four-fold, from 3.1 ± 0.2 to 13.2 ± 0.4 seconds (**Figure 2.8i**). This result indicates that stabilizing the Rag-Ragulator interface decreases the probability of mTORC1 dissociation from its lysosomal scaffold.

2.2.7 Rag release from ragulator requires both G-domains

We next dissected the mechanisms through which GTP-loading of RagA/B destabilizes binding to Ragulator. The Rags are each composed of a canonical G-Domain (GD) and a C-Terminal Domain (CTD) that has a roadblock fold(Kurzbauer et al. 2004; Gong et al. 2011; Zhang et al. 2012; Powis et al. 2015). Structural studies

show that the Rag CTDs make direct contact with the p14 and MP1 subunits of Ragulator, which also have roadblock folds (de Araujo et al. 2017; Su et al. 2017; Yonehara et al. 2017; Zhang et al. 2017). Moreover, by interacting with each other, the CTDs mediate heterodimerization of RagA/B with Rag C/D (Gong et al. 2011; Jeong et al. 2012).

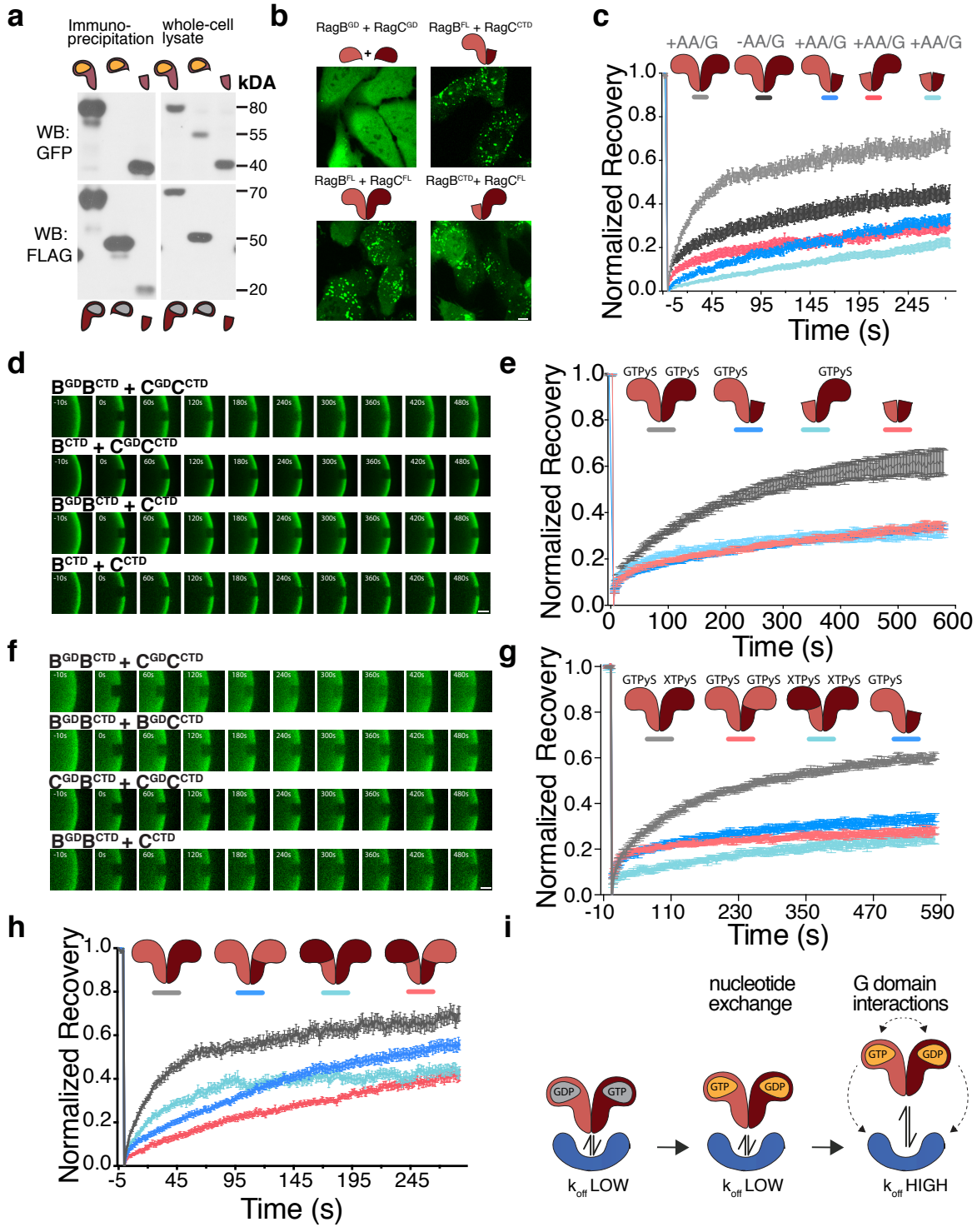

Figure 2.9 Both G-domains are required for dynamic Rag GTPase dissociation from Ragulator. (a) *HEK-293T cells were transiently transfected with FLAG-tagged full-length or truncated RagB, along with GFP-tagged, full-length or truncated RagC. Cells were subjected to lysis and FLAG immunoprecipitation, followed by western blotting for FLAG and GFP.* ***(b)*** *Subcellular localization of the indicated full length or truncated GFP-RagB + FLAG-RagC heterodimers in U2OS cells. Scale bar 10 μm. Experiment repeated 3x.* ***(c)*** *Both G-domains are required for dynamic Rag GTPase association to lysosomes. Fluorescence recovery over time curves for nutrient starved (-AA/G) and nutrient restimulated (+AA/G) GFP-tagged Rag GTPase heterodimers as well as indicated truncation constructs. Each curve is the average ± S.E.M.* ***(d)*** *Two Rag G-domains are required for dynamic binding to Ragulator in vitro. FRAP time-lapse of single ROIs from Ragulator-coated beads incubated with excess GFP-tagged Rag full length and truncation constructs that were loaded with GTPγS. Scale bar 10 μm.* ***(e)*** *Fluorescence Recovery curves for the experiment shown in (d). Each curve is the average ± S.E.M.* ***(f)*** *Chimeric Rag heterodimers containing two of the same G domains release less efficiently from Ragulator than wild-type Rag heterodimers. FRAP time-lapse of single ROIs from Ragulator-coated beads incubated with excess GFP-tagged, wild-type and chimeric Rag heterodimers that were loaded with GTPγS. Scale bar 10 μm.* ***(g)*** *FRAP recovery curves for the experiment shown in* ***(f)****. Each curve is the average ± S.E.M.* ***(h)*** *Fluorescence recovery curves from FRAP experiments in U2OS cells expressing the indicated GFP-tagged wildtype and chimera Rag constructs. Each curve is the average ± S.E.M.* ***(i)*** *Model displaying how, upon loading of Rag A/B with GTP, the presence of both G-domains is required to destabilize Ragulator-Rag GTPase interaction.*

We engineered GFP-tagged Rag CTD heterodimers ($RagB^{CTD}$ + $RagC^{CTD}$) and confirmed their binding to each other by co-immunoprecipitation (**Figure 2.9a**). When expressed in cells, $RagB^{CTD}$ + $RagC^{CTD}$ localized to lysosomes, as previously shown(Gong et al. 2011). In contrast, GFP-tagged G domains of RagB and C ($RagB^{GD}$ + $RagC^{GD}$) did not heterodimerize when coexpressed, nor localize to lysosomes (**Figure 2.9b**). Heterodimers composed of one full-length Rag and one G domain-deleted Rag ($RagB^{FL}$ + $RagC^{CTD}$ or $RagB^{CTD}$ + C^{FL}) localized to the lysosome (**Figure 2.9b**). Thus Rag CTDs are necessary and sufficient for Rag binding to lysosomes(Gong et al. 2011).

Surprisingly, in nutrient-replete cells both $RagB^{CTD}$ + $RagC^{CTD}$ and the single-G domain $RagB^{FL}$ + $RagC^{CTD}$ and $RagB^{CTD}$ + $RagC^{FL}$ heterodimers exhibited minimal fluorescence recovery, even lower than full-length Rag heterodimers in starved cells (**Figure 2.9c**). Thus, both G-domains are required to induce Rag separation from Ragulator in response to nutrients.

Moreover, absence of the RagC/D G-domain suppressed cycling induced by GTP-loading of the RagA/B G-domain. Consistent with the results in cells, *in vitro* FRAP experiments of GFP-labeled $RagB^{FL\text{-}GTP\gamma S}$ + $RagC^{CTD}$ on Ragulator-coated affinitiy beads uncovered a defect in cycling despite the presence of GTPγS in the G-domain of RagB (**Figure 2.9d,e**). $RagB^{CTD}$ + $RagC^{FL\text{-}GTP\gamma S}$ also showed little FRAP recovery on

Ragulator-coated beads. Thus, lack of RagC G-domain overrides cycling induced by GTP-loading of RagB.

The previous result suggests that the two Rag G-domains must cooperate to trigger active release from Ragulator. To test the requirement for inter-G-domain communication, we constructed chimeras in which the G-domain of RagC was replaced with that of RagB ($RagB^{GD}B^{CTD}$ + $RagB^{GD}C^{CTD}$) or, conversely, chimeras bearing two RagC G-domains ($RagC^{GD}B^{CTD}$ + $RagC^{GD}C^{CTD}$). Despite loading with GTPγS, both chimeras were stably bound to Ragulator (**Figure 2.9f,g**). Similarly, $RagB^{GD}B^{CTD}$ + $RagB^{GD}C^{CTD}$ and $RagC^{GD}B^{CTD}$ + $RagC^{GD}C^{CTD}$ chimeras exhibited reduced cycling in nutrient-replete cells (**Figure 2.9h**). Thus, upon GTP loading of RagA/B, the two G-domains cooperate to trigger the release of the CTDs from Ragulator (**Figure 2.9i**).

2.2.8 Oncogenic mutations block Rag spatial cycling and promote mTORC1 lysosomal accumulation and activity

We demonstrated above that Rag cycling limits the fraction of lysosome-bound mTORC1. We wondered whether disrupting Rag cycling may contribute to aberrant mTORC1 activation in disease settings. Recently, recurrent mutations in the G-domain of RagC were identified in Follicular Lymphoma (FL)(Okosun et al. 2016; Ying et al. 2016). These mutations were shown to alter the affinity of RagC for guanine nucleotides *in vitro*, increase RagC binding to Raptor in cells, and to render mTORC1 signaling resistant to leucine starvation.

We stably expressed RagC constructs harboring FL hotspot mutations Thr90Asn and Trp115Arg, along with wild-type RagC and the previously characterized, 'activating' Ser75Asn, which behaves similarly to Ser75 RagC mutants found in FL (Tsun et al. 2013; Okosun et al. 2016; Ying et al. 2016). All of the mutants increased the lysosome-bound fraction of endogenous mTORC1 compared to U2OS cells expressing wild-type RagC, both under amino acid-starved and replete conditions (**Figure 2.10a,b**).

In light of these results, we next asked whether increased recruitment of mTORC1 to the lysosome might be due to altered cycling behavior of the FL RagC mutants. Strikingly, when FL RagC mutants were coexpressed with wild-type RagB in nutrient replete U2OS cells, they showed decreased FRAP recovery relative to control Rag GTPase heterodimers (**Figure 2.10c,d**). We confirmed this behavior in our *in vitro* assay, where FL RagC mutant-containing heterodimers displayed dramatically reduced cycling on Ragulator-coated beads (**Figure 2.10e,f**). Importantly, decreased Rag cycling *in vitro* occurred irrespective of the nucleotide state: FL RagC containing heterodimers displayed stable binding to Ragulator even when they were loaded with GTPγS. These results were confirmed at the single molecule level; the residence times of Halo-tagged RagB + FL RagC heterodimers on Ragulator were increased 2 to 3-fold compared to wild-type RagC (**Figure 2.10g,h**).

Thus, we propose that the FL RagC mutants lead to increased lysosomal mTORC1 capture in part by stabilizing the Rag-Ragulator interface. Consistent with our results with rapalogue-mediated tethering, stabilized binding of FL-mutant Rags to

Ragulator may also prevent mTORC1 dissociation from the lysosome in response to nutrient depletion.

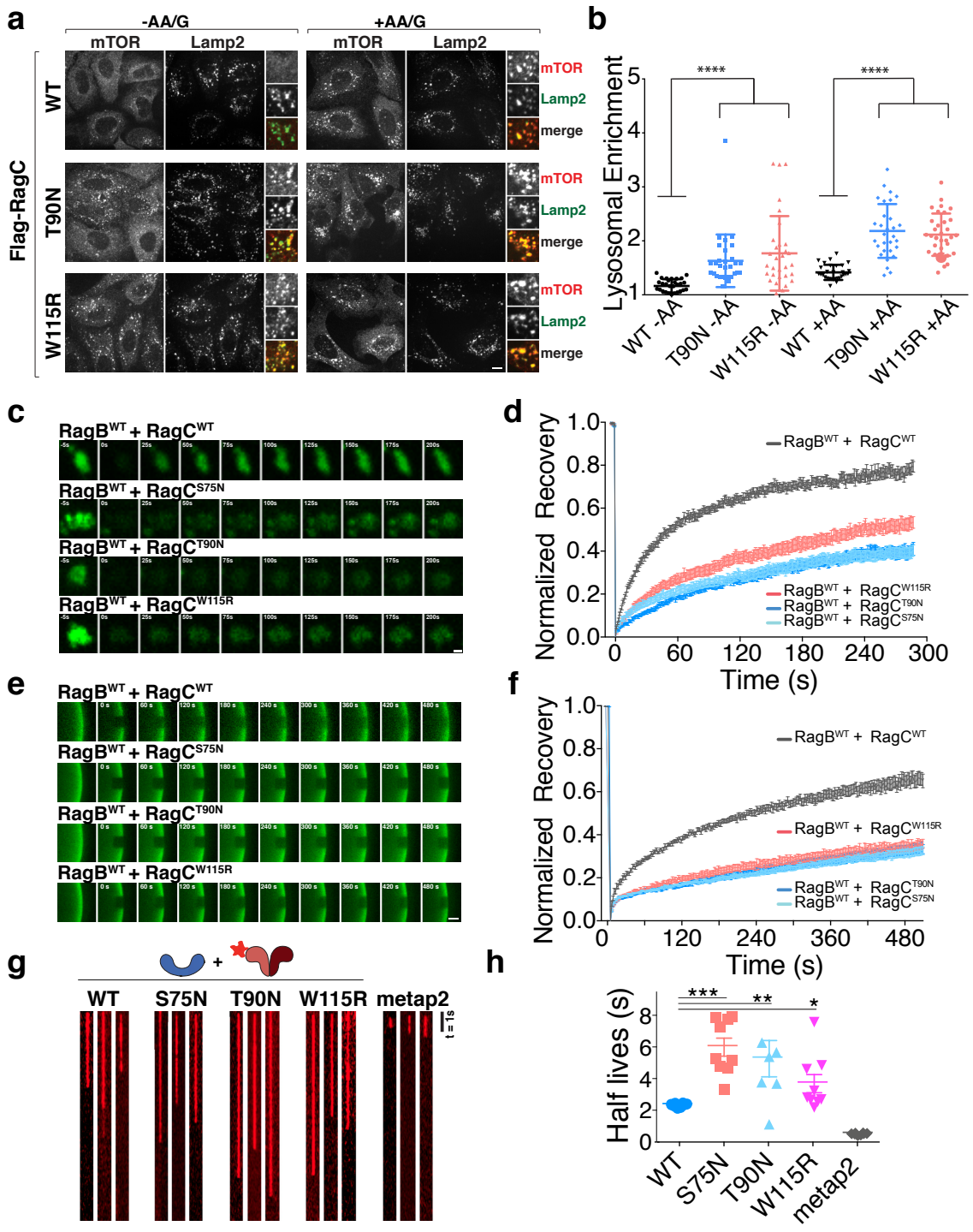

Figure 2.10 Cancer-specific Rag GTPase mutants stabilize mTORC1 at the lysosome by overriding dynamic dissociation from Ragulator. (a) *Immunofluorescence images of endogenous mTOR and LAMP2 in U2OS cells stably*

expressing the indicated wild-type and mutant FLAG-RagC constructs and maintained for 2h in the indicated nutrient conditions. Scale bar 10 μm. ***(b)*** *Quantitation of mTOR Lysosomal Enrichment Score for immunofluorescence images in* ***(a)*** *(mean ± S.D, **** p<.0001, two-sided unpaired t-tests).* ***(c)*** *Time-lapse of fluorescence recovery after photobleaching (FRAP) of single lysosomes in U2OS cells expressing the indicated GFP-tagged Rag GTPase heterodimer containing the indicated RagC mutation. Scale bar 1 μm.* ***(d)*** *Fluorescence recovery over time curves from FRAP experiments in U2OS cells expressing the indicated GFP-tagged Rag GTPase heterodimer. Each curve is the average ± S.E.M.* ***(e)*** *FRAP time-lapse of single ROIs from Ragulator-coated beads incubated with excess GFP-tagged Rag heterodimers containing the indicated wild-type and mutant RagC constructs. Scale bar 10 μm.* ***(f)*** *FRAP recovery curves for the experiment shown in* ***(e).*** *Each curve is the average ± S.E.M.* ***(g)*** *Kymographs of single Halo^{TMR}-RagB co-purfied with the indicated wild-type and mutant FLAG-RagC constructs, binding to Ragulator-coated or to Metap2-coated beads. Scale bar 1s.* ***(h)*** *Photobleach-corrected half-life ($t_{1/2}$) values for the residence time of the indicated Halo^{TMR}-RagB + FLAG-RagC constructs on Ragulator beads. Metap2 is included as negative control. Single molecule residence time data from three biological replicates were pooled and divided into 10 randomly determined sets. Half-lives were calculated from single exponential fits of each set. Displayed is mean ± S.E.M, **** p<0.0001, ** p=0.0074; *p=0.0238, two-sided unpaired t-tests.*

2.2.9 mTORC1 activity is limited by Rag spatial cycling

We next investigated the effects of the FL-RagC mutants on mTORC1 signaling output. Stable expression of the S75N, T90N and W115R mutants caused a strong boost in S6K1, ULK1 and 4E-BP1 phosphorylation over wild-type RagC expressed at similar levels (**Figure 2.11a**). These mutants also conferred resistance to starvation to varying degrees, consistent with previous reports (Okosun et al. 2016; Ying et al. 2016).

Enhanced signaling by the FL-RagC mutants impacted autophagy, a canonical readout of mTORC1 signaling. In cells stably expressing the FL-RagC mutants, autophagic flux was significantly inhibited over wild type RagC-expressing cells, as shown by decreased accumulation of cleaved LC3b upon treatment of cells with Bafilomycin A (BafA) (**Figure 2.11b**). Immunofluorescence-based quantification of LC3b puncta in BafA-treated cells supported this conclusion (**Figure 2.11c,d**). Thus, stabilizing the Ragulator-Rag interface increases the amount of lysosome-bound mTORC1, leading to enhanced signaling output.

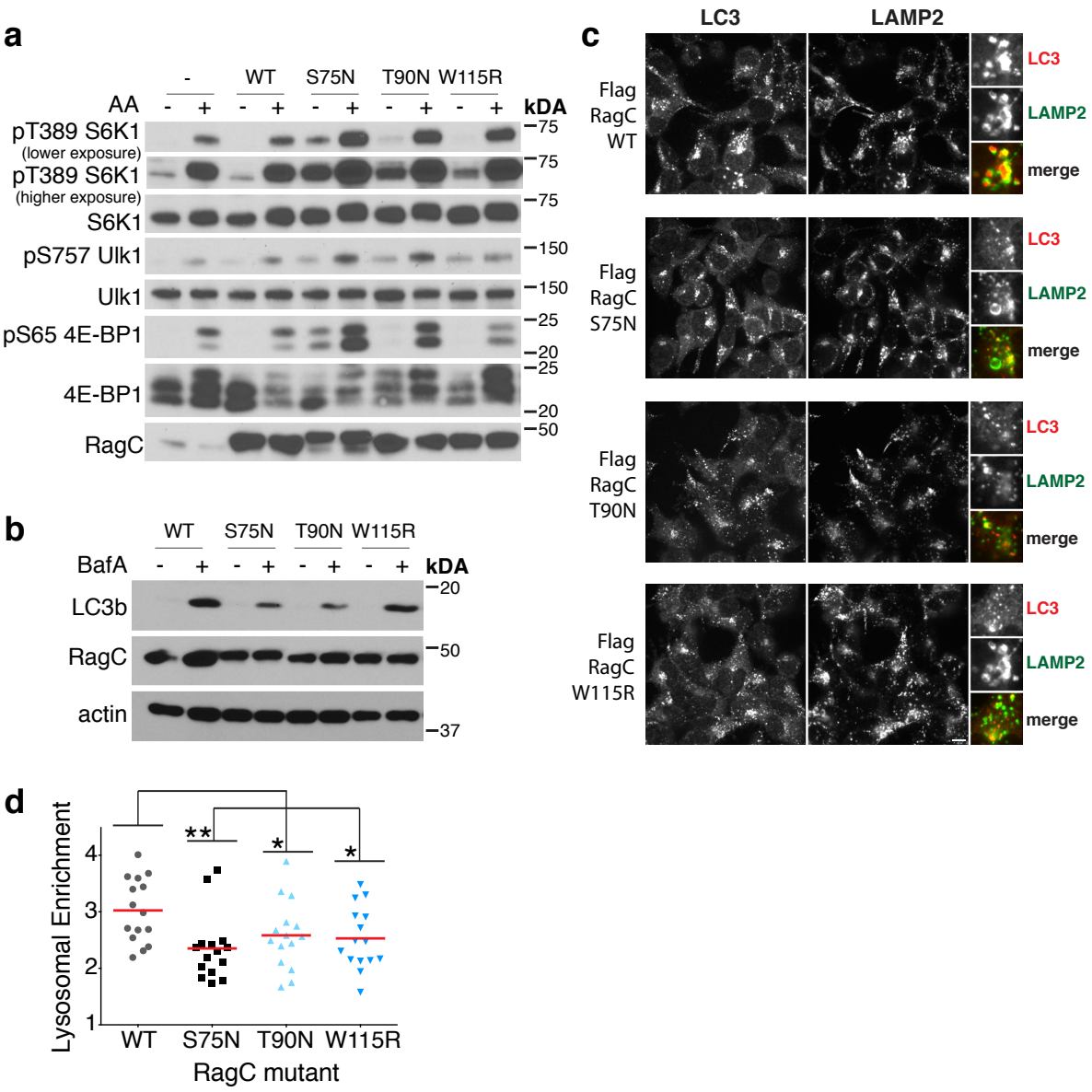

Figure 2.11 Rag cycling limits mTORC1 activity. (a) *HEK-293T cells stably expressing Flag-RagC harboring the indicated mutations were starved for amino acids for 50 min or starved and restimulated for 10 min, lysed, and immunoblotted for the indicated proteins and phosphor-proteins.* ***(b)*** *HEK-293T cells stably expressing Flag-RagC containing the indicated mutations were treated with vehicle or BafA for 2h, then lysed and immunoblotted for the indicated proteins.* ***(c)*** *HEK-293T cells stably expressing Flag-RagC containing the indicated mutations were treated with BafA for 2h, fixed and immunostained for LC3 and LAMP2. Scale bar 10 µm.* ***(d)*** *Quantitation of the Lysosomal Enrichment Score of LC3 signal at LAMP2-positive lysosomes versus cytoplasmic LC3 signal for cells pictured in* ***(c)*** *(mean ± S.D., **p = .0036, (T90N) *p = 0.0498, (W115R) *p = 0.0230, two-sided unpaired t-tests).*

2.2.10 mTORC1 activity is confined to the lysosomal surface

These data suggest that mTORC1 phosphorylates its substrates while bound to the lysosomal surface and disfavor an alternative model in which, following its activation at the lysosomal surface, mTORC1 could diffuse and phosphorylate its substrates in the cytoplasm. To further test these alternatives, we suppressed the ability of active mTORC1 to diffuse in the cytoplasm by fusing Raptor and Rheb to the mitochondrial transmembrane domain of outer membrane protein 25 (OMP25) (**Figure 2.12c,d**). Co-targeting Raptor and Rheb (but not either protein individually) to mitochondria resulted in both resistance to amino acid withdrawal and enhanced signaling in the presence of amino acids (**Figure 2.12b**), supporting the conclusion that mTORC1 does not need to release from a membrane to phosphorylate its substrates.

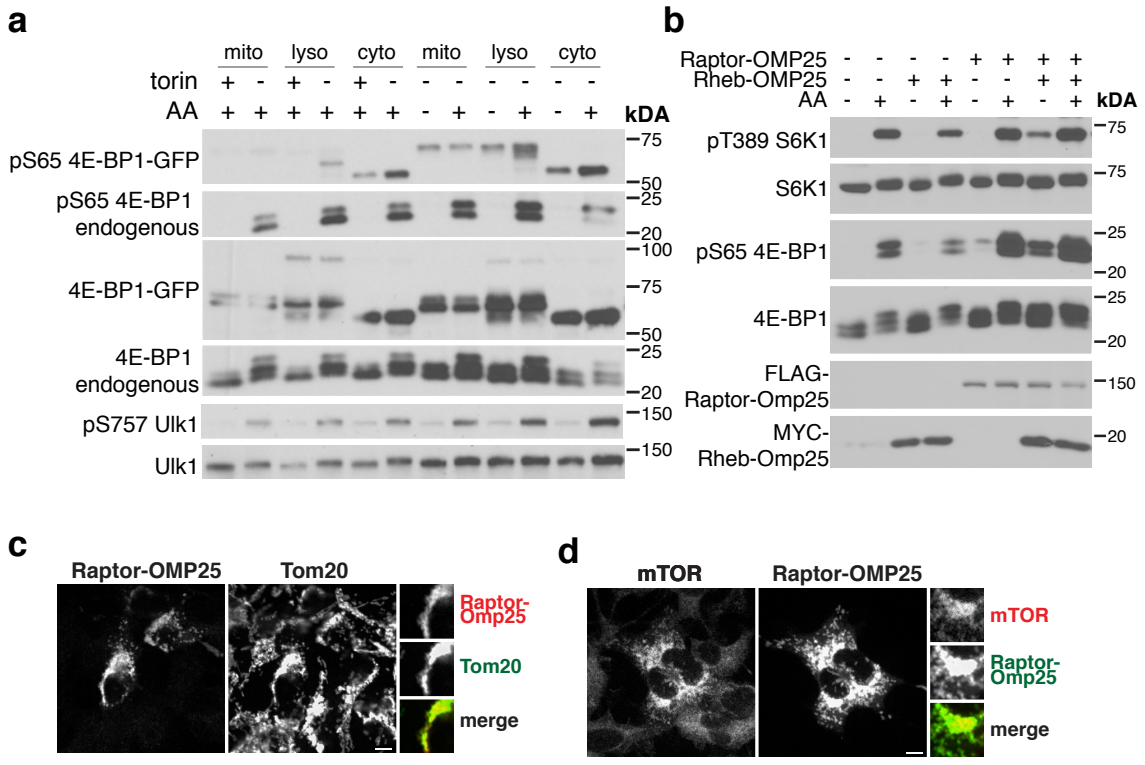

Figure 2.12 The primary site of mTORC1 activity is the lysosomal surface. (a) *HEK-293T cells stably expressing GFP-4E-BP1-OMP25 (mito), GFP-4E-BP1-Rheb15 (lyso) or GFP-4E-BP1-Rheb15-CAAX mutant (cyto) were treated with torin overnight or with torin overnight followed by a 2-hour torin washout (lanes 1-6), or were starved of amino acids for two hours or starved then restimulated for 10 minutes (lanes 7-12), followed by cell lysis and immunoblotting for the indicated proteins and phosphor-proteins.* ***(b)*** *U2OS cells transiently overexpressing FLAG-Raptor-Omp25 (Raptor-OMP25) and/or MYC-Rheb-Omp25 (Rheb-OMP25) were starved for amino acids for 50 min, or starved and restimulated for 10 min, followed by cell lysis and immunoblotting for the indicated proteins and phosphor-proteins.* ***(c)*** *Immunofluorescence images of*

HEK-293T cells expressing FLAG-Raptor-Omp25 stained for FLAG and for the TOM20 mitochondrial marker. Scale bar 10 µm. ***(d)*** *Immunofluorescence images of HEK-293T cells expressing Flag-Raptor-Omp25 (Raptor-OMP25) stained for endogenous mTOR and for FLAG (Raptor-OMP25). Scale bar 10 µm.*

To further test the idea that mTORC1 kinase activity is confined to the lysosomal surface, we targeted 4EBP1 to the mitochondrial surface and monitored the efficiency of its phosphorylation by endogenous mTORC1, comparing it to freely diffusing and lysosome-anchored 4EBP1 isoforms. Upon stimulation with amino acids, mTORC1 activity was not observed on mitochondria-anchored 4E-BP1, whereas mTORC1 efficiently phosphorylated both lysosome-anchored and freely diffusing 4E-BP1 constructs (**Figure 2.12a**). Thus, mTORC1 kinase activity away from the lysosome is strongly reduced, further supporting the conclusion that release of mTORC1 from the lysosomal surface by Rag cycling limits mTORC1 signaling output.

2.4 Discussion

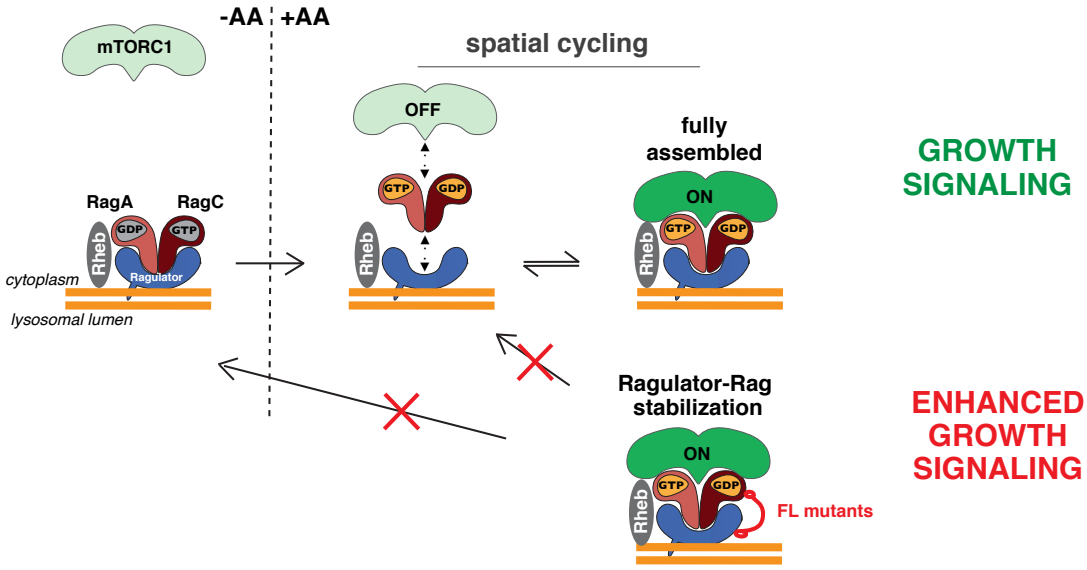

Figure 2.13 Model for nutrient-induced mTORC1 capture to the lysosome. *In low-nutrient states, Rag heterodimers loaded with the inactive nucleotide combinations are stably bound to Ragulator on the lysosomal surface. Nutrients cause the switch of the Rags to the active nucleotide state, while destabilizing Rag interaction with Ragulator. Consequently, both Rag GTPases and mTORC1 undergo spatial cycling, which limits the pool of mTORC1 activated by Rheb at the lysosomal surface. Cancer-specific RagC mutants decrease the off-rate of the Rag-Ragulator interaction and stabilize mTORC1 at the lysosome, resulting in increased signaling. Stabilization of the Rag-Ragulator interaction may also prevent Rag inactivation as nutrient levels decrease, maintaining mTORC1 in a constitutively active state.*

Our results reveal a nutrient-activated mechanism that modulates Rag-Ragulator affinity and ultimately limits mTORC1 lysosomal recruitment and activity. Specifically, as nutrients activate a Rag-mTORC1 binding interface, they also cause the Rag-Ragulator binding interface to become destabilized, leading to mTORC1 release and inactivation (**Figure 2.13**).

We also clarify the question of where in the cell mTORC1 encounters its substrates (Sancak et al. 2010; Roczniak-Ferguson et al. 2012; Settembre et al. 2012; Martina and Puertollano 2013; Menon et al. 2014; Zhou et al. 2015; Manifava et al. 2016). While our data cannot rule out that a subset of mTORC1 molecules may retain activity as they diffuse in the cytoplasm, direct comparison of membrane-immobilized and freely diffusing 4E-BP1 indicates that most of the kinase activity occurs at the lysosomal membrane, where mTORC1 may directly contact Rheb. Recent structural work supports this model by demonstrating that Rheb activates mTORC1 by physically binding to it and allosterically displacing an auto-inhibitory intramolecular interaction ('FAT-clamp') that would otherwise prevent substrate phosphorylation (Yang et al. 2017).

Recent structural work provides hints of possible mechanisms for Rag GTPase release from Ragulator. Rag-Ragulator structures indicate that a primary interacting surface is provided by the Rag CTDs binding to the Lamtor2-3 (p14-MP1) dimer (de Araujo et al. 2017; Su et al. 2017; Yonehara et al. 2017; Zhang et al. 2017). In addition, Lamtor1/p18, which wraps around the Ragulator ordered core, contributes additional binding elements that stabilize the Ragulator-Rag interaction (de Araujo et al. 2017; Su et al. 2017; Yonehara et al. 2017; Zhang et al. 2017). It is conceivable that displacement of one or more of these elements upon GTP loading of RagA/B may weaken the interaction and trigger Rag cycling.

The fact that the active form of the Rag GTPases does not optimize for maximal mTORC1 lysosomal accumulation places the Rags in a distinct category from most signaling GTPases, which rely on feed-forward mechanisms to recruit their effectors to membranes. For example, a pioneer pool of activated Rab5 molecules activate the Rab5 GEF, Rabex, leading to increased Rab5 activation and establishment of patches of amplified effector recruitment and activity on endosomal membranes(Horiuchi et al. 1997; Lippe et al. 2001; Cherfils and Zeghouf 2013). Ras activation proceeds similarly (Gureasko et al. 2008; Groves and Kuriyan 2010). In contrast, rather than evolving to maximize effector recruitment, Rag activation is tuned to oppose hyperaccumulation and activation of mTORC1 on the lysosomal membrane. Accordingly, RagC mutations found in follicular lymphoma override this attenuator mechanism, at least in part, by stabilizing Rag binding to Ragulator and suppressing Rag spatial cycling.

Strikingly, we show that Ragulator and the inactivating Rags exist as a more stable lysosomal complex than do the activating Rags with Ragulator, which actually act as the mTORC1 scaffold. This observation prompts the question of whether Ragulator and Rags in their “inactivating” conformation toward mTORC1 (RagA/B^{GDP}:RagC/D^{GTP}) may have as-yet-uncharacterized functions, perhaps scaffolding auxiliary mTORC1 regulatory machinery or participating in other lysosomal pathways. In Chapter three, I will discuss follow-up work on this topic that identified a new interacting partner for the inactive Rags—the FLCN:FNIP2 complex.

In summary, we demonstrate that the Rag GTPases undergo spatial cycling between lysosomal and cytosolic pools while in their mTORC1-activating nucleotide binding conformation. A likely function of Rag spatial cycling is to attenuate mTORC1 signaling by decreasing the amount of time that mTORC1 spends in direct contact with Rheb at the lysosomal surface. Consistently, expression of FL-associated RagC mutants, which stabilize both the Rag-Ragulator and the Rag-Raptor interfaces (Okosun et al. 2016; Ying et al. 2016), results in increased lysosomal mTORC1 recruitment and enhanced substrate phosphorylation.

Future studies will determine how other components of the mTORC1-scaffolding machinery may modulate the stability of the Rag-Ragulator interface (Zoncu et al. 2011; Wang et al. 2015; Castellano et al. 2017; Filipek et al. 2017; Pu et al. 2017; Wolfson et al. 2017). Furthermore, additional mutations recently identified in human cancers, such as those targeting the mTOR gene(Grabiner et al. 2014; Rodrik-Outmezguine et al. 2016), could affect signaling outputs by altering the lifetime of these scaffolding interactions.

2.5 Methods

Cell lines and Culture Conditions

Biochemical experiments were performed in HEK293T human-derived cell lines. Live imaging experiments were performed in the U2OS, UOK257-1, UOK257-2, SW780, and SW780-1 human-derived cell lines. Immunofluorescence experiments were performed in HEK293T, HAP-1 Raptor:GFP, and U2OS cell lines. Purified proteins in Visual IP assay were purified from adherent HEK293T human tissue culture cells. HEK293T, UOK257-1, and UOK257-2 cells were cultured in DMEM (Thermo Fisher) supplemented with 10 % FBS + 5 % penicillin-streptomycin at 37°C and 5% CO_2. SW780-1 and SW780-2 cell lines were cultured in IMDM (Thermo Fisher) supplemented 10% FBS and 5% penicillin-streptomycin at 37°C and 5% CO_2.U2OS cells were cultured in McCoy's 5A media (GE Healthcare) lacking phenol red supplemented with 5% FBS and 5% penicillin-streptomycin at 37°C and 5% CO_2.HAP-1 Raptor:GFP cell lines were cultured in IMDM (Thermo Fisher) supplemented 10% FBS and 5% penicillin-streptomycin at 37°C and 5% CO_2.

Microscopy

All images were collected on a Nikon Ti-E inverted microscope (Nikon Instruments, Melville, NY) equipped with a Plan Apo 40x Air/1.21, 60x or 100x/1.49 Oil objective, and a Perfect Focus System. All live imaging was acquired using an electron-multiplying charge-coupled device camera (iXon ULTRA 897BV; Andor Technology). All immunofluorescence imaging was acquired using a Zyla 5.5 sCMOS camera (Andor Technology). All data was acquired using iQ3 acquisition software (Andor Technology).

Immunofluorescence

HEK-293T or HAP-1 cells were plated on fibronectin-coated glass coverslips in 6-well plates (35mm diameter/well), at 300,000-500,000 cells/well. U2OS were plated directly onto glass coverslips in 6- well plates at 150,000 cells/well. 12-16 hours later, cells were subjected to amino acid depletion/restimulation (see below) and fixed in 4% paraformaldehyde (in PBS) for 15 min at RT. The coverslips were rinsed twice with PBS and cells were permeabilized with 0.1% (w/v) saponin in PBS for 10 min. After rinsing twice with PBS, the slides were incubated with primary antibody in 5% normal donkey serum for 1 hour at room temperature, rinsed four times with PBS, and incubated with fluorophore-conjugated secondary antibodies produced in goat or donkey (Life Technologies, diluted 1:1000 in 5% normal donkey serum) for 45 min at room temperature in the dark, washed four times with PBS. Coverslips were mounted on glass slides using Vectashield and imaged on a spinning disk confocal system as indicated above.

Acquisition of Z-stacks for 3D Colocalization

U2OS or HAP-1 Raptor:GFP cells were fixed and stained for mTOR/LAMP2 (U2OS) or LAMP2 (HAP-1), and mounted in media containing DAPI stain for nuclei. At least 8 Z-stacks containing at least 4 U2OS cells or at least 10 HAP-1 cells were acquired

covering a 8-10 μm range (depending on cell volume) acquired at 0.33 μm intervals for U2OS an 0.5 μm intervals for HAP-1 cells.

Nucleofection of U2OS and SW780 cells for Live Imaging

For each condition, 1.2 million U2OS or SW780 cells were combined with 350 ng DNA for fluorescently labeled complex components and 700 ng DNA for non-fluorescently labeled components and transfected using a Lonza Nucleofector T-2b machine, resuspended using Nucleofector Kit R and pulsed with protocol X-001. Each transfection was divided and plated onto two chambered culture dishes with a glass coverslip bottom. Cells were treated and imaged the following day.

Fluorescence Recovery After Photobleaching

Fluorescence Recovery After Photobleaching (FRAP) experiments were performed on U2OS cells nucleofected with desired constructs as described above one day prior to imaging. For forty minutes prior to the experiment, U2OS cells were incubated in imaging buffer (10 mM HEPES, 136 mM NaCl, 2.5 mM KCl, 2 mM $CaCl_2$, 1.2 mM $MgCl_2$, pH 7.4) supplemented with 5 mM glucose, 1% dialysed FBS (dFBS), and amino acids (Sancak et al., 2008), 2.5 μg/mL nocodazole, and the indicated concentration A/C rapalog if indicated, for forty minutes. FRAP movies for nutrient depleted conditions were acquired in imaging buffer lacking supplemented nutrients. FRAP movies were acquired by taking five frames at one second intervals, applying a photobleach calibrated to bleach lysosome to background fluorescence levels using a dual galvanometer laser beam delivery system (Andor FRAPPA), then acquiring images at one second intervals for five minutes.

Live Cell Treatments

HEK293T and HAP-1 cells were plated in culture dishes or on glass coverslips and rinsed and incubated in amino acid-free RPMI for 50 minutes and restimulated with a 10X solution of amino acids or leucine for 10 minutes. Amino acid solutions were prepared from powders and the final concentration of amino acids in the media was the same as in commercial RPMI. For A/C rapalog (rapa) treatments, cells were pre-incubated for 20 minutes in complete media with 5 nM A/C rapalog for signaling experiments and 50 nM A/C rapalog for immunofluorescence experiments. Cells were then starved as above with the amino acid-free RPMI supplemented with 5 nM or 50 nM rapalog for signaling and immunofluorescence experiments, respectively. U2OS and SW780 cells were treated as above except that starvation media lacked glucose and was supplemented with 5% dialyzed Fetal Bovine Serum (dFBS), and the starvation duration was two hours while the restimulation duration was 30 min. Nutrient starvation treatments were adjusted based on determining conditions that maximally disperse mTORC1 from lysosomes in each cell type. Torin treatments of 293T cells were applied as overnight (16 hour) treatment in 250 nM Torin in standard culture media, followed by washout (2 media replacements) with standard culture media. Bafilomycin treatments of 293T cells were applied as 2 hour treatments with 100 nM bafilomycin.

Visual IP Sample Preparation

HEK293T cells were plated on 15 cm plates at 10 million cells per plate. 24 hours later, the cells were transfected using 500 uL OptiMEM transfection media, 60 uL polyethyleneimine (PEI, Sigma) and 10 ug total DNA. The transfection mix was incubated for 15 minutes and then added directly to the cell media. 48 hours later, the media was removed, and the cells were washed three times with PBS. The cells were scraped from the plate and collected in 10 mL PBS. The samples were centrifuged for 5 minutes at 1500g at 4°C. The cell pellets were then resuspended in 1 mL Triton lysis buffer (1% Triton X-100, 130 mM NaCl, 2mM EGTA, 2.5 mM $MgCl_2$, 25 mM HEPES, pH 7.4, 10% glycerol, protease inhibitor (Pierce)), and allowed to rotate at 4°C for 20 minutes. The samples were then centrifuged at 13000g for 2 minutes, and the supernatant was separated for immunoprecipitation. 50 uL of washed anti-FLAG affinity beads (Sigma) were added to the supernatant and the sample was rotated at 4°C for 2 hours. After immunoprecipitation, the samples were washed twice in Triton lysis buffer, once in high salt (500 mM NaCl) lyso sucrose buffer, and once in normal salt lyso sucrose buffer (250 mM sucrose, 10 mM KCl, 2 mM EGTA, 2.5 mM $MgCl_2$, 25 mM HEPES, pH 7.4, 10% glycerol, protease inhibitor (Pierce)). Each wash consisted of rotating with the wash buffer for 5 minutes at 4°C and subsequent centrifugation at 2000g for 1 minute. For elution off FLAG beads, 3x- FLAG peptide in Phosphate Buffered Saline (PBS) was added to the sample, [RL2] and the sample was allowed to rotate overnight at 4°C. The sample was then centrifuged at 3000g for 3 minutes and the proteins used for subsequent experiments were present in the supernatant fraction.

Cytosol Preparation

HEK293T cells were grown to confluence on 15 cm plates. The media was removed, and the cells were washed three times with PBS. The samples were centrifuged for 5 minutes at 1500g at 4°C, and the pellet was resuspended in 500 uL lyso sucrose buffer (250 mM sucrose, 10 mM KCl, 2 mM EGTA, 2.5 mM $MgCl_2$, 25 mM HEPES, pH 7.4, 10% glycerol, protease inhibitor (Pierce)). The resuspended cells were passaged through a 25g needle syringe three times, and then centrifuged for 10 minutes at 2700g at 4°C. The supernatant was extracted and further centrifuged for 2 minutes at 13000g at 4°C; the supernatant fraction of the final centrifugation step was the cytosol fraction.

Rag GTPase Nucleotide Loading

For nucleotide loading of Rag GTPases that are bound to affinity beads, EDTA was added to lyso buffer to a concentration of 20 mM and beads were allowed to rotate for 1 hour at 4°C. The sample was washed in lyso sucrose buffer twice and the corresponding nucleotides for loading (XTPγS/XDP/GTPγS/GDP) were added to a final concentration of 25 uM each. The sample was allowed to rotate for 30 minutes at 4°C. $MgCl_2$ was added to the sample to a final concentration of 50 mM, and the sample was rotated for 1 hour at 4°C. The sample was washed twice before use in subsequent experiments. If the Rag GTPases were used as the soluble partner in the assay, they were eluted in 0.5 mg/mL 3x-Flag peptide.

Visual IP FRAP
Samples were assembled with 10 uL bead suspension with bound protein 1, 15 uL cytosol preparation, 20 uL lyso sucrose buffer, and 3 uL FLAG elution of protein 2. Ragulator and Rags were incubated at room temperature for 15 minutes. 20 uL of the sample was mounted onto a glass slide, and the coverslip was sealed with nail polish. FRAP movies were acquired by taking five frames at two second intervals, applying photobleach using a dual galvanometer laser beam delivery system (Andor FRAPPA), and then imaging at two second intervals for 10 minutes.

Visual IP Single-Molecule
For single-molecule experiments, samples were prepared as previously described with minor adjustments. Expressed Halo-tagged proteins were tagged in cells directly by adding tetramethylrhodamine (TMR) ligand to the media at a final concentration of 1 nM, and incubated for 15 minutes at 37°C. After protein purification, samples were assembled with 20 uL bead suspension with bound protein 1, 20 uL cytosol preparation, 5 uL FLAG elution of protein 2, 20 uL 5x concentration lyso sucrose buffer, 35 uL Trolox/dextrose solution (10 mg/mL Trolox, and 0.8% w/v D- glucose), and 1 uL glucose oxidase/catalase solution (34 U/uL glucose oxidase, 520 U/uL catalase in 50 mM Tris, pH 8). The samples were imaged using near-TIRF and images were acquired using 300 msec exposures, at 1 second intervals for 15 minutes.

Lentiviral infection
Lentivirus was generated using the Calcium Phosphate packaging method. Briefly, 20 ug of a lentiviral vector (desired construct in pLJM1-PURO) was combined with 15 ug of psPax2 and 5 ug VSVG viral packaging plasmids in 500 uL ddH2O supplemented with a final concentration of 500 uM CaCl2, pH 7. This DNA solution was combined dropwise with 500 uL HEBS buffer (280 mM NaCl, 50 mM HEPES, 1.5 mM Na_2PO_4, pH 7) while maintaining bubbles in the HEBS buffer during DNA addition. This solution was incubated at room temperature for 15 minutes, then added to a 10 cm dish containing 7 million recently plated 293T cells. 16 hours later, media was exchanged for Complete Media. 24 hours after that, media containing virus was collected from cells, spun down at 1300 x g for 5 minutes to remove cell debris, and then concentrated using Lenti-X Concentrator (Takara) and resuspended in 500 uL of complete media per 10 cm dish. For FRB-FKBP experiments, 20 uL of TMEM192-Flag-FKBP or TMEM192-Flag concentrated virus was co-infected with 5 uL of FRB-myc-RagA or FRB-myc-RagC frozen virus on day 1. For Raptor:GFP + F.L. RagC mutant experiments, 5 uL of Raptor:GFP frozen virus was co-infected with 10 uL of the corresponding Flag-RagC frozen virus. On day 2, media was replaced with media containing 1 ng/mL Puromycin. On day 3 cells were plated onto fibronectin-coated coverslips or split into multiple wells of a 6-well plate for signaling experiments.

Cell lysis, Immunoprecipitation, and Western Blot
HEK-293T cells stably expressing FLAG-tagged and myc-tagged proteins were lysed in ice- cold lysis buffer (150mM NaCl, 20 mM HEPES [pH 7.4], 2 mM EDTA, 0.3% CHAPS

or 1% Triton X-100, and one tablet of EDTA-free protease inhibitors per 50 ml). Cell lysates were cleared by centrifugation at 13,000 rpm for 10 minutes in a microfuge. For immunoprecipitations, 30 µl of a 50% slurry of anti-FLAG affinity gel (Sigma) were added to each lysate and incubated with rotation for 2-3 hours at 4°C. Immunoprecipitates were washed three times with lysis buffer. Immunoprecipitated proteins were denatured by the addition of 50 µl of sample urea buffer and heating to 37°C for 15 minutes. For western blots without immunoprecipitation, samples were normalized to a total concentration of 1 mg/mL protein and combined with protein sample buffer, then boiled for 5 minutes at 95C. Samples were loaded onto 10% or 12% SDS-Page gels, and analyzed by immunoblotting. For antibody information see Supplementary Table 2.

Cell Fractionation

Confluent HEK-293T cells stably expressing FLAG-Raptor or FLAG-Raptor-Rheb15, plated in 2x15cm dishes, were rinsed once in cold PBS, then scraped, spun down and resuspended in 750ul of fractionation buffer: 140mM KCl, 1mM EGTA, 2.5mM MgCl2, 50mM Sucrose, 20mM HEPES, pH 7.4, supplemented with protease inhibitors. Cells were mechanically broken by spraying 4-5 times through a 23G needle attached to a 1ml syringe, then spun down at 2000g for 10min, yielding a post nuclear supernatant (PNS). The PNS was further spun at max speed for 15 min in a tabletop refrigerated centrifuge, thus separating the cytosol (the supernatant) from the light organellar fraction (the pellet), which contains the FLAG-Raptor or FLAG-Raptor-Rheb15-expressing lysosome. The light organelle fraction was resuspended in 50/50 Laemmli/fractionation buffer, bringing it to an equal volume to the Laemmli-supplemented cytosol. Equal volumes of each fraction were gel-loaded and subjected to immunoblotting. For antibody information see Supplementary Table 2.

Quantitation of FRAP data

FRAP data analysis was performed using custom-built MATLAB (Mathworks) scripts modified from those written by Lana Bosanac of the Xavier Darzacq lab (Knight et al., Science, 2016). Lysosomes that did not move substantially within the five minute movie were manually selected. Data was bleach corrected on a cell-by-cell basis by normalizing lysosomal intensities to the total cellular intensity. The contribution of diffusion of GFP-tagged molecules into the FRAPPed region was corrected for by FRAPPing several non-lysosomal spots of equal area and directly substracting the mean intensities of FRAPPed non-lysosomal areas from the FRAPPed lysosomal area. Bleach-corrected and photobleach-corrected recovery curves were assigned Normalized Intensity values based on a linear 0 to 1 scale between the post-bleach and the mean of 5 pre-bleach values, respectively. For each condition, between twenty and thirty individual FRAP traces from lysosomes from at least three different movies and five different cells were averaged and reported as a mean value with error bars representing Standard Error of the Mean (S.E.M.). Bleach- and diffusion-corrected FRAP curves were fitted using a single-component exponential.

Quantitation of Single-Molecule Assays

Single-molecule data was analyzed using a home-built MATLAB (Mathworks) script that localizes single molecule binding events by automatically determining local maxima, and tracks particles through the entire time lapse. Single-molecule binding events from three imaging experiments were pooled together. Ten sets of residence times were generated by randomly selecting ten percent of total binding events from the original pool. Each set was fitted with a double exponential binding curve, and the slow components were used for calculation of photobleach-corrected half-lives. Individual slow kinetic components were corrected for photobleaching using the formula $k_{actual} = k_{empirical} - k_{photobleaching}$. $k_{photobleaching}$ was determined by fitting taking the mean value of the slow component from 2-component exponential fits of 10 Halo-GST survival probability plots prepared from 10 randomly generated subsets of residence times, as above. Half lives were calculated using $t_{1/2} = \ln 2/k$, and mean values and Standard Error of the Mean (S.E.M.) were calculated.

3D Quantitation of mTORC1 lysosomal localization (fraction lysosomal mTOR)
3-channel Z-stacks were processed using Imaris software (Bitplane, Oxford Instruments). First, total cell voxels were segmented using the inbuilt “cell segmentation” algorithm, using the DAPI channel to detect nuclei and building out total cell volume using the mTOR or Raptor:GFP channel for U2OS and HAP-1 cells, respectively. The mTOR or Raptor:GFP channel was masked to exclude extracellular voxels. Total cellular intensity and total cellular volume (in voxels) was exported. Next, lysosomes were detected using the inbuilt “surfaces” algorithm,: the LAMP2 channel was masked to exclude voxels outside of the segmented lysosome surface, and filtered to remove objects that were smaller than 5 voxels. Total lysosomal intensity and total lysosomal volume (in voxels) measurements were exported. Finally, a control volume was generated manually in the mTOR or Raptor:GFP channel in a volume that did not include cells. The mTOR or Raptor:GFP channels were masked to exclude voxels outside of the control surface. Total control intensity and total control volume (in voxels) was exported. For both U2OS and HAP-1 cells, the LAMP2 channel was segmented three times to exclude voxels outside of the total cell volume, lysosome volume, and control volumes created above. Total intensity and volume (in voxels) measurements were exported for the corresponding LAMP2 channels.
The percent of mTOR or Raptor:GFP signal that colocalized with lysosomes was determined using intensity and voxel values measured in the mTORC1 or LAMP2 channel. Lysosomal Intensities and Totalcell Intensities were corrected for background by subtracting the total background intensity predicted for the corresponding volume based on the mean voxel intensity of the control region as follows:

*Background-Corrected Lysosomal Intensity = Lysosomal Intensity - (Control Intensity/Control Volume) * Lysosomal Volume*

*Background-Corrected Totalcell intensity = Totalcell Intensity - (Control Intensity/Control Volume) * Totalcell Volume*

The Raw Percent Lysosomal Intensity was calculated:

Raw Percent Lysosomal Intensity = (Background-Corrected Lysosomal Intensity) / (Background- Corrected Totalcell Intensity)

The same calculations were performed for the LAMP2 channel to determine the Percent Lysosomal Intensity for LAMP2. LAMP2 is a transmembrane protein and is a marker for the expected value of a 100% lysosome-localized protein. We normalized all Background-Corrected Percent Lysosomal Intensity values and Background-Corrected Percent Lysosomal Intensity values to the corresponding mean LAMP2 Background-Corrected Percent Lysosomal Intensity value by performing the following operation:

Normalized mTORC1 Percent Lysosomal Intensity = (Raw mTORC1 Lysosomal Intensity) / (Raw Lamp2 Lysosomal Intensity)

These values are reported as "% lysosomal signal" in Figure 1a.

Quantitation of 2D Immunofluorescence data for Lysosomal Enrichment Score
For immunofluorescence datasets in which images were acquired for both LAMP2 stain (mouse) and mTOR, RagA, RagC, p18, mp1, or LC3 stain, a home-built Matlab script was used to determine the lysosomal enrichment of the non-Lamp stain. First, a single cell was manually selected in the lamp channel. The nucleus was also manually selected and excluded from further analysis. Then, an Otsu- based thresholding algorithm was applied to automatically segment cellular pixels into LAMP2 (lysosomal) or non-LAMP2 (cytosolic) pixels. This mask generated in the LAMP2 channel was then applied to the non-LAMP2 channel. The average intensity of pixels in the lysosomal region was determined (mean lysosomal intensity), as was the average intensity of the pixels in the cytosolic region (mean cytosolic intensity). The Lysosomal Enrichment Score was determined by dividing the mean lysosomal intensity by the cytosolic lysosomal intensity. For each condition, at least twenty cells were analyzed from at least three different multi-channel images.

2D Lyso:cyto ratio quantitation
For 2-dimensional immunofluorescence images of cells coexpressing Raptor:GFP along with Flag- tagged Rag GTPases, a lysosomal:cytosolic fluorescence ratio was calculated to assess the level of Raptor:GFP enrichment on lysosomes in different conditions. The lysosomal area was manually selected in ImageJ, and the mean lysosomal intensity was determined by determining the mean intensity of pixels in this region. The mean cytosolic intensity was then calculated in an identically shaped region adjacent to the lysosome. Finally, the "lyso:cyto ratio" was determined by dividing the mean lysosomal intensity by the mean cytosolic intensity. For each condition, at least 30 individual measurements were made in at least five different cells.

2.6 References

Abu-Remaileh M, Wyant GA, Kim C, Laqtom NN, Abbasi M, Chan SH, Freinkman E, Sabatini DM. 2017. Lysosomal metabolomics reveals V-ATPase- and mTOR-dependent regulation of amino acid efflux from lysosomes. *Science* **358**: 807-813.

Bar-Peled L, Chantranupong L, Cherniack AD, Chen WW, Ottina KA, Grabiner BC, Spear ED, Carter SL, Meyerson M, Sabatini DM. 2013. A Tumor suppressor complex with GAP activity for the Rag GTPases that signal amino acid sufficiency to mTORC1. *Science* **340**: 1100-1106.

Bar-Peled L, Schweitzer LD, Zoncu R, Sabatini DM. 2012. Ragulator is a GEF for the rag GTPases that signal amino acid levels to mTORC1. *Cell* **150**: 1196-1208.

Binda M, Peli-Gulli MP, Bonfils G, Panchaud N, Urban J, Sturgill TW, Loewith R, De Virgilio C. 2009. The Vam6 GEF controls TORC1 by activating the EGO complex. *Mol Cell* **35**: 563-573.

Castellano BM, Thelen AM, Moldavski O, Feltes M, van der Welle RE, Mydock-McGrane L, Jiang X, van Eijkeren RJ, Davis OB, Louie SM et al. 2017. Lysosomal cholesterol activates mTORC1 via an SLC38A9-Niemann-Pick C1 signaling complex. *Science* **355**: 1306-1311.

Caussinus E, Kanca O, Affolter M. 2011. Fluorescent fusion protein knockout mediated by anti-GFP nanobody. *Nat Struct Mol Biol* **19**: 117-121.

Chen J, Zhang Z, Li L, Chen BC, Revyakin A, Hajj B, Legant W, Dahan M, Lionnet T, Betzig E et al. 2014. Single-molecule dynamics of enhanceosome assembly in embryonic stem cells. *Cell* **156**: 1274-1285.

Cherfils J, Zeghouf M. 2013. Regulation of small GTPases by GEFs, GAPs, and GDIs. *Physiol Rev* **93**: 269-309.

de Araujo MEG, Naschberger A, Furnrohr BG, Stasyk T, Dunzendorfer-Matt T, Lechner S, Welti S, Kremser L, Shivalingaiah G, Offterdinger M et al. 2017. Crystal structure of the human lysosomal mTORC1 scaffold complex and its impact on signaling. *Science* **358**: 377-381.

Demetriades C, Doumpas N, Teleman AA. 2014. Regulation of TORC1 in response to amino acid starvation via lysosomal recruitment of TSC2. *Cell* **156**: 786-799.

Efeyan A, Zoncu R, Chang S, Gumper I, Snitkin H, Wolfson RL, Kirak O, Sabatini DD, Sabatini DM. 2013. Regulation of mTORC1 by the Rag GTPases is necessary for neonatal autophagy and survival. *Nature* **493**: 679-683.

Filipek PA, de Araujo MEG, Vogel GF, De Smet CH, Eberharter D, Rebsamen M, Rudashevskaya EL, Kremser L, Yordanov T, Tschaikner P et al. 2017. LAMTOR/Ragulator is a negative regulator of Arl8b- and BORC-dependent late endosomal positioning. *J Cell Biol* **216**: 4199-4215.

Fracchiolla D, Sawa-Makarska J, Zens B, Ruiter A, Zaffagnini G, Brezovich A, Romanov J, Runggatscher K, Kraft C, Zagrovic B et al. 2016. Mechanism of cargo-directed Atg8 conjugation during selective autophagy. *Elife* **5**.

Gong R, Li L, Liu Y, Wang P, Yang H, Wang L, Cheng J, Guan KL, Xu Y. 2011. Crystal structure of the Gtr1p-Gtr2p complex reveals new insights into the amino acid-induced TORC1 activation. *Genes Dev* **25**: 1668-1673.

Grabiner BC, Nardi V, Birsoy K, Possemato R, Shen K, Sinha S, Jordan A, Beck AH, Sabatini DM. 2014. A diverse array of cancer-associated MTOR mutations are hyperactivating and can predict rapamycin sensitivity. *Cancer Discov* **4**: 554-563.

Groves JT, Kuriyan J. 2010. Molecular mechanisms in signal transduction at the membrane. *Nat Struct Mol Biol* **17**: 659-665.

Gureasko J, Galush WJ, Boykevisch S, Sondermann H, Bar-Sagi D, Groves JT, Kuriyan J. 2008. Membrane-dependent signal integration by the Ras activator Son of sevenless. *Nat Struct Mol Biol* **15**: 452-461.

Hansen AS, Pustova I, Cattoglio C, Tjian R, Darzacq X. 2017. CTCF and cohesin regulate chromatin loop stability with distinct dynamics. *Elife* **6**.

Horiuchi H, Lippe R, McBride HM, Rubino M, Woodman P, Stenmark H, Rybin V, Wilm M, Ashman K, Mann M et al. 1997. A novel Rab5 GDP/GTP exchange factor complexed to Rabaptin-5 links nucleotide exchange to effector recruitment and function. *Cell* **90**: 1149-1159.

Inoue T, Heo WD, Grimley JS, Wandless TJ, Meyer T. 2005. An inducible translocation strategy to rapidly activate and inhibit small GTPase signaling pathways. *Nat Methods* **2**: 415-418.

Jeong JH, Lee KH, Kim YM, Kim DH, Oh BH, Kim YG. 2012. Crystal structure of the Gtr1p(GTP)-Gtr2p(GDP) protein complex reveals large structural rearrangements triggered by GTP-to-GDP conversion. *J Biol Chem* **287**: 29648-29653.

Kim E, Goraksha-Hicks P, Li L, Neufeld TP, Guan KL. 2008. Regulation of TORC1 by Rag GTPases in nutrient response. *Nat Cell Biol* **10**: 935-945.

Knight SC, Xie L, Deng W, Guglielmi B, Witkowsky LB, Bosanac L, Zhang ET, El Beheiry M, Masson JB, Dahan M et al. 2015. Dynamics of CRISPR-Cas9 genome interrogation in living cells. *Science* **350**: 823-826.

Kulak NA, Pichler G, Paron I, Nagaraj N, Mann M. 2014. Minimal, encapsulated proteomic-sample processing applied to copy-number estimation in eukaryotic cells. *Nat Methods* **11**: 319-324.

Kurzbauer R, Teis D, de Araujo ME, Maurer-Stroh S, Eisenhaber F, Bourenkov GP, Bartunik HD, Hekman M, Rapp UR, Huber LA et al. 2004. Crystal structure of the p14/MP1 scaffolding complex: how a twin couple attaches mitogen-activated protein kinase signaling to late endosomes. *Proc Natl Acad Sci U S A* **101**: 10984-10989.

Liberles SD, Diver ST, Austin DJ, Schreiber SL. 1997. Inducible gene expression and protein translocation using nontoxic ligands identified by a mammalian three-hybrid screen. *Proc Natl Acad Sci U S A* **94**: 7825-7830.

Lippe R, Miaczynska M, Rybin V, Runge A, Zerial M. 2001. Functional synergy between Rab5 effector Rabaptin-5 and exchange factor Rabex-5 when physically associated in a complex. *Mol Biol Cell* **12**: 2219-2228.

Manifava M, Smith M, Rotondo S, Walker S, Niewczas I, Zoncu R, Clark J, Ktistakis NT. 2016. Dynamics of mTORC1 activation in response to amino acids. *Elife* **5**.

Martina JA, Puertollano R. 2013. Rag GTPases mediate amino acid-dependent recruitment of TFEB and MITF to lysosomes. *J Cell Biol* **200**: 475-491.
Menon S, Dibble CC, Talbott G, Hoxhaj G, Valvezan AJ, Takahashi H, Cantley LC, Manning BD. 2014. Spatial control of the TSC complex integrates insulin and nutrient regulation of mTORC1 at the lysosome. *Cell* **156**: 771-785.
Nada S, Hondo A, Kasai A, Koike M, Saito K, Uchiyama Y, Okada M. 2009. The novel lipid raft adaptor p18 controls endosome dynamics by anchoring the MEK-ERK pathway to late endosomes. *EMBO J* **28**: 477-489.
Okosun J, Wolfson RL, Wang J, Araf S, Wilkins L, Castellano BM, Escudero-Ibarz L, Al Seraihi AF, Richter J, Bernhart SH et al. 2016. Recurrent mTORC1-activating RRAGC mutations in follicular lymphoma. *Nat Genet* **48**: 183-188.
Pacold ME, Suire S, Perisic O, Lara-Gonzalez S, Davis CT, Walker EH, Hawkins PT, Stephens L, Eccleston JF, Williams RL. 2000. Crystal structure and functional analysis of Ras binding to its effector phosphoinositide 3-kinase gamma. *Cell* **103**: 931-943.
Panchaud N, Peli-Gulli MP, De Virgilio C. 2013. Amino acid deprivation inhibits TORC1 through a GTPase-activating protein complex for the Rag family GTPase Gtr1. *Sci Signal* **6**: ra42.
Perera RM, Zoncu R. 2016. The Lysosome as a Regulatory Hub. *Annu Rev Cell Dev Biol* **32**: 223-253.
Peurois F, Peyroche G, Cherfils J. 2019. Small GTPase peripheral binding to membranes: molecular determinants and supramolecular organization. *Biochem Soc Trans* **47**: 13-22.
Powis K, Zhang T, Panchaud N, Wang R, De Virgilio C, Ding J. 2015. Crystal structure of the Ego1-Ego2-Ego3 complex and its role in promoting Rag GTPase-dependent TORC1 signaling. *Cell Res* **25**: 1043-1059.
Pu J, Keren-Kaplan T, Bonifacino JS. 2017. A Ragulator-BORC interaction controls lysosome positioning in response to amino acid availability. *J Cell Biol* **216**: 4183-4197.
Roczniak-Ferguson A, Petit CS, Froehlich F, Qian S, Ky J, Angarola B, Walther TC, Ferguson SM. 2012. The transcription factor TFEB links mTORC1 signaling to transcriptional control of lysosome homeostasis. *Sci Signal* **5**: ra42.
Rodrik-Outmezguine VS, Okaniwa M, Yao Z, Novotny CJ, McWhirter C, Banaji A, Won H, Wong W, Berger M, de Stanchina E et al. 2016. Overcoming mTOR resistance mutations with a new-generation mTOR inhibitor. *Nature* **534**: 272-276.
Sancak Y, Bar-Peled L, Zoncu R, Markhard AL, Nada S, Sabatini DM. 2010. Ragulator-Rag complex targets mTORC1 to the lysosomal surface and is necessary for its activation by amino acids. *Cell* **141**: 290-303.
Sancak Y, Peterson TR, Shaul YD, Lindquist RA, Thoreen CC, Bar-Peled L, Sabatini DM. 2008. The Rag GTPases bind raptor and mediate amino acid signaling to mTORC1. *Science* **320**: 1496-1501.
Saxton RA, Sabatini DM. 2017. mTOR Signaling in Growth, Metabolism, and Disease. *Cell* **169**: 361-371.

Schmidt G, Lenzen C, Simon I, Deuter R, Cool RH, Goody RS, Wittinghofer A. 1996. Biochemical and biological consequences of changing the specificity of p21ras from guanosine to xanthosine nucleotides. *Oncogene* **12**: 87-96.

Schroder B, Wrocklage C, Hasilik A, Saftig P. 2010. Molecular characterisation of 'transmembrane protein 192' (TMEM192), a novel protein of the lysosomal membrane. *Biol Chem* **391**: 695-704.

Settembre C, Zoncu R, Medina DL, Vetrini F, Erdin S, Erdin S, Huynh T, Ferron M, Karsenty G, Vellard MC et al. 2012. A lysosome-to-nucleus signalling mechanism senses and regulates the lysosome via mTOR and TFEB. *EMBO J* **31**: 1095-1108.

Sprague BL, Pego RL, Stavreva DA, McNally JG. 2004. Analysis of binding reactions by fluorescence recovery after photobleaching. *Biophys J* **86**: 3473-3495.

Su MY, Morris KL, Kim DJ, Fu Y, Lawrence R, Stjepanovic G, Zoncu R, Hurley JH. 2017. Hybrid Structure of the RagA/C-Ragulator mTORC1 Activation Complex. *Mol Cell* **68**: 835-846 e833.

Teis D, Wunderlich W, Huber LA. 2002. Localization of the MP1-MAPK scaffold complex to endosomes is mediated by p14 and required for signal transduction. *Dev Cell* **3**: 803-814.

Tsun ZY, Bar-Peled L, Chantranupong L, Zoncu R, Wang T, Kim C, Spooner E, Sabatini DM. 2013. The Folliculin Tumor Suppressor Is a GAP for the RagC/D GTPases That Signal Amino Acid Levels to mTORC1. *Molecular cell*.

Vink M, Simonetta M, Transidico P, Ferrari K, Mapelli M, De Antoni A, Massimiliano L, Ciliberto A, Faretta M, Salmon ED et al. 2006. In vitro FRAP identifies the minimal requirements for Mad2 kinetochore dynamics. *Curr Biol* **16**: 755-766.

Wang S, Tsun ZY, Wolfson RL, Shen K, Wyant GA, Plovanich ME, Yuan ED, Jones TD, Chantranupong L, Comb W et al. 2015. Metabolism. Lysosomal amino acid transporter SLC38A9 signals arginine sufficiency to mTORC1. *Science* **347**: 188-194.

Wolfson RL, Chantranupong L, Wyant GA, Gu X, Orozco JM, Shen K, Condon KJ, Petri S, Kedir J, Scaria SM et al. 2017. KICSTOR recruits GATOR1 to the lysosome and is necessary for nutrients to regulate mTORC1. *Nature* **543**: 438-442.

Yang H, Jiang X, Li B, Yang HJ, Miller M, Yang A, Dhar A, Pavletich NP. 2017. Mechanisms of mTORC1 activation by RHEB and inhibition by PRAS40. *Nature*.

Ying ZX, Jin M, Peterson LF, Bernard D, Saiya-Cork K, Yildiz M, Wang S, Kaminski MS, Chang AE, Klionsky DJ et al. 2016. Recurrent Mutations in the MTOR Regulator RRAGC in Follicular Lymphoma. *Clin Cancer Res* **22**: 5383-5393.

Yonehara R, Nada S, Nakai T, Nakai M, Kitamura A, Ogawa A, Nakatsumi H, Nakayama KI, Li S, Standley DM et al. 2017. Structural basis for the assembly of the Ragulator-Rag GTPase complex. *Nat Commun* **8**: 1625.

Young LN, Cho K, Lawrence R, Zoncu R, Hurley JH. 2016. Dynamics and architecture of the NRBF2-containing phosphatidylinositol 3-kinase complex I of autophagy. *Proc Natl Acad Sci U S A* **113**: 8224-8229.

Zhang T, Peli-Gulli MP, Yang H, De Virgilio C, Ding J. 2012. Ego3 functions as a homodimer to mediate the interaction between Gtr1-Gtr2 and Ego1 in the ego complex to activate TORC1. *Structure* **20**: 2151-2160.

Zhang T, Wang R, Wang Z, Wang X, Wang F, Ding J. 2017. Structural basis for Ragulator functioning as a scaffold in membrane-anchoring of Rag GTPases and mTORC1. *Nat Commun* **8**: 1394.

Zhou X, Clister TL, Lowry PR, Seldin MM, Wong GW, Zhang J. 2015. Dynamic Visualization of mTORC1 Activity in Living Cells. *Cell Rep*.

Zoncu R, Bar-Peled L, Efeyan A, Wang S, Sancak Y, Sabatini DM. 2011. mTORC1 senses lysosomal amino acids through an inside-out mechanism that requires the vacuolar H(+)-ATPase. *Science* **334**: 678-683.

Zoncu R, Perera RM, Balkin DM, Pirruccello M, Toomre D, De Camilli P. 2009. A phosphoinositide switch controls the maturation and signaling properties of APPL endosomes. *Cell* **136**: 1110-1121.

Chapter 3

Rag GTPase Nucleotide states are interdependently gated by the FLCN:FNIP2 complex

Chapter Summary:

The tumor suppressor FLCN is required for nutrient-dependent activation of the mTORC1 kinase via its GTPase Activating Protein (GAP) activity toward RagC. Concomitant with mTORC1 inactivation by starvation, FLCN relocalizes from the cytosol to lysosomes. To determine the lysosomal function of FLCN, we reconstituted the stable lysosomal complex (LFC) containing FLCN, its partner FNIP2, the starved-state $RagA^{GDP}$:$RagC^{GTP}$ GTPases, and the lysosomal anchor Ragulator and determined its cryo-EM structure to 3.6Å. The FLCN catalytic Arg finger was identified and is not positioned to GAP RagC, explaining the inhibited RagC GTPase activity in the LFC. Within the LFC, FLCN:FNIP2 stabilizes starved-state $RagA^{GDP}$, blocking nucleotide exchange to GTP. Thus, FLCN:FNIP switches between inhibitory and activating modes toward the Rag dimer, implying a checkpoint role in lysosomal mTORC1 signaling.

A portion of the content presented in this chapter is currently under review as part of the following research article: Lawrence, R. E., Fromm, S. A., Fu, Y., Yokom, A. L., Kim, D.J., Thelen, A.T., Young, L.N., Hurley, J.H., and Zoncu, R. (2018). Structural Mechanism of Rag GTPase Gating by the Lysosomal Folliculin Complex**.** R.E.L and S.A.F. are designated as equal contributors, and J.H.H. and R.Z. are designated as co-corresponding authors.

Contributions are as follows: Conceptualization, R.E.L., S.A.F., J.H.H., R.Z.; Investigation, R.E.L., S.A.F., Y. F., A.L.Y., L.N.Y.; Resources, D.J.K., A.M.T.; Supervision, J.H.H., R.Z.; Writing- original draft, R.E.L. S.A.F., J.H.H., R.Z.; Writing- review and editing, all authors. Structural work was performed by S.A.F. and A.L.Y., with assistance from R.L., L.Y., A.T. and D.J.K. Functional assays were performed by R.L. and Y.F with assistance from S.F.

3.1 Background

The mechanistic Target of Rapamycin Complex 1 (mTORC1) kinase lies at the center of a complex biochemical network that relays information about the availability of nutrients, growth factors, oxygen and energy to downstream programs that drive growth and metabolism, while inhibiting catabolic pathways such as autophagy (Saxton and Sabatini 2017). Nutrients including amino acids, glucose and cholesterol activate mTORC1 by triggering its translocation from the cytosol to the lysosomal membrane, a step mediated by the heterodimeric Rag guanosine triphosphatases (GTPases)(Kim et al. 2008; Sancak et al. 2008; Sancak et al. 2010). Rag heterodimers consist of functionally equivalent RagA or RagB in complex with RagC or RagD (also functionally equivalent). Nutrients trigger the transition from the 'inactive' combination of guanosine diphosphate (GDP)-loaded Rag A/B and guanosine triphosphate (GTP)-loaded Rag C/D to the 'active' GTP-loaded RagA/B and GDP-loaded RagC/D, which interacts with mTORC1 and recruits it to the lysosome, enabling its subsequent activation (Kim et al. 2008; Sancak et al. 2008; Sancak et al. 2010).

The transition of the Rag GTPases between the inactive and active nucleotide states is central to mTORC1 signaling, yet the mechanisms controling this critical switch remain poorly understood. The GATOR1 complex, composed of DEPDC5, NPRL2 and NPRL3, is a RagA/B specific GTPase Activating Protein (GAP) that, by accelerating the intrinsically low GTP hydrolysis rate of RagA/B, promotes mTORC1 inactivation under low nutrients (Bar-Peled et al. 2013; Panchaud et al. 2013; Shen et al. 2018). Folliculin (FLCN), in complex with FLCN-interacting protein 1/2 (FNIP1/2) (Baba et al. 2006; Hasumi et al. 2008), functions as a RagC/D-specific GAP that converts RagC/D to the GDP-loaded, mTORC1-binding state when nutrients are high (Tsun et al. 2013). Knockdown of either FLCN or FNIP1/2 in cell culture impairs recruitment of mTORC1 to the lysosome induced by amino acids and leads to decreased mTORC1 signaling (Petit et al. 2013; Tsun et al. 2013).

Intriguingly FLCN is also the causative gene for Birt-Hogg-Dubé syndrome (BHD) (Nickerson et al. 2002). Experiments identifying FLCN truncations and deletions in many BHD patients led to the designation of FLCN as a classic tumor suppressor (Baba et al. 2006; Hong et al. 2010; Schmidt and Linehan 2018). Furthermore, homozygous deletion of *FLCN* in mice, which is embryonically lethal, is reported to upregulate mTORC1 (Hasumi et al. 2009). The tumor-suppressor and GAP roles point to a contradictory and context-dependent picture of FLCN function in the mTORC1 pathway.

Imaging suggests that FLCN:FNIP may exist in two distinct functional states. Under low nutrients in both human cells and yeast, the complex is localized to the lysosomal/vacuolar membrane, and is diffusely cytosolic in nutrient replete cells (Petit et al. 2013; Peli-Gulli et al. 2015). In Chapter 2, we reported similarly that the Rag GTPases are stably bound to their lysosomal scaffold under low nutrients, and are released to a lower affinity complex under high nutrients (Lawrence et al. 2018). The association of FLCN:FNIP with the lysosome is thus correlated with the nucleotide state of the Rags (Petit et al. 2013; Tsun et al. 2013; Meng and Ferguson 2018), but whether

and how the GAP activity of FLCN:FNIP is coordinated with, or regulated by, its separation from the lysosomal membrane is unclear.

Both FLCN and FNIP1/2 possess an N-terminal Longin domain and a C-terminal DENN domain, both of which are commonly found in guanine nucleotide exchange factors (GEFs) for GTPases of the Rab family (Levine et al. 2013). Except for crystal structures of the DENN domain of human FLCN (Nookala et al. 2012) and the Longin domain of the yeast FNIP1/2 orthologue, Lst4 (Pacitto et al. 2015), little is known about the architecture of FLCN:FNIP and nothing of its structural interaction with the Rag GTPases. Crucially, how FLCN and FNIP1/2 heterodimerize with each other, and which Longin or DENN domain of either protein mediates the RagC-GAP activity is unknown.

Here we combined biochemical reconstitution with cryo-EM to elucidate the architecture of the lysosomal FLCN:FNIP-Rag dimer-Ragulator supercomplex. The structure reveals how this stable complex blocks the RagC-GAP activity of FLCN:FNIP. We also identify the catalytic Arg finger of FLCN responsible for catalysis in the active state. These data reveal a two-state mode of regulation of FLCN:FNIP activity that highlights an unanticipated role for this complex as one of the central switches in the mTORC1 activation cycle.

3.2 Results

3.2.1 FLCN GAP activity depends on Rag-Ragulator substrate

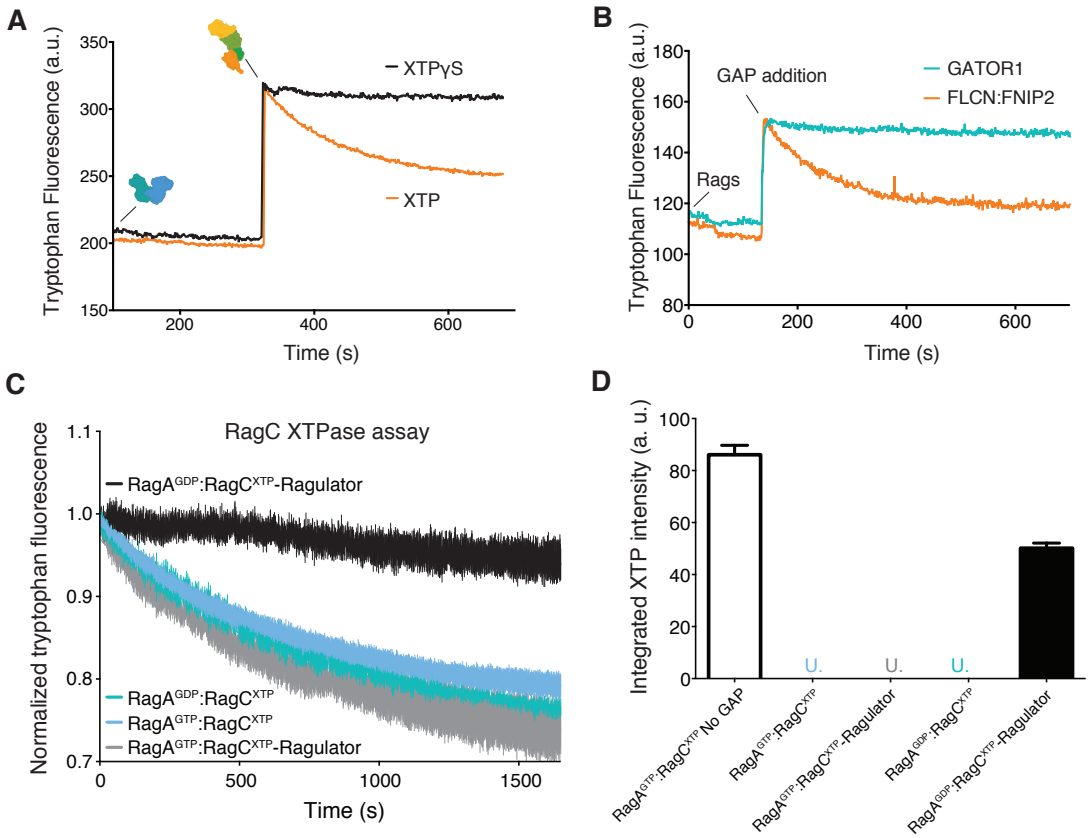

Figure 3.1 FLCN:FNIP2 GAP activity is substrate-dependent. *(**a**) Intrinsic tryptophan fluorescence signal was measured for $RagA^{GTP}$:$RagC^{XTP}$ (orange) or $RagA^{GTP}$:$RagC^{XTP\gamma S}$ (black) before and after addition of a FLCN:FNIP2 GAP at a molar ratio of 1:10 (GAP:Rags). One representative trace per condition is plotted. (**b**) RagA nucleotide hydrolysis cannot be visualized via intrinsic tryptophan fluorescence. Intrinsic tryptophan fluorescence signal is shown for $RagA^{GTP}$:$RagC^{XTP}$ before and after addition of a 1:10 GAP:Rag GTPases molar ratio of GATOR1 (cyan) or FLCN:FNIP2 (orange). One representative trace per condition is plotted. FLCN:FNIP2 RagC-GAP activity visualized by tryptophan fluorescence signal. Rags loaded in specified nucleotide-bound and ragulator-bound states (black: $RagA^{GDP}$:$RagC^{XTP}$ -Ragulator, grey: $RagA^{GDP}$:$RagC^{XTP}$, cyan: $RagA^{GTP}$:$RagC^{XTP}$, blue: $RagA^{GTP}$:$RagC^{XTP}$-Ragulator) were incubated with FLCN:FNIP2. GTPase reaction is visualized by tryptophan fluorescence signal decay. Mean and Standard Error of the Mean (SEM) are plotted. (**d**) HPLC-based GTPase assay comparing FLCN:FNIP2 RagC-GAP activity on the indicated Rag GTPase or Rag GTPase-Ragulator substrates. "No GAP" control was performed on a $RagA^{GTP}$:$RagC^{XTP}$ substrate. Mean and SD are plotted. "U." indicates that remaining XTP signal was undetectable by HPLC.*

To determine the function of lysosomal FLCN in starvation, we interrogated the FLCN:FNIP2 GAP reaction using *in vitro* RagA:RagC heterodimer GTPase assays. To selectively generate Rag heterodimers containing one diphosphate and one triphosphate nucleotide, we made use of the mutant $RagC^{D181N}$, which is specific for xanthine nucleotides (Bar-Peled et al. 2012; Tsun et al. 2013), and is henceforward referred to here simply as RagC. $RagA^{GTP}$:$RagC^{XTP}$ was incubated with a catalytic amount of the appropriate GAP complex (GATOR1 or FLCN:FNIP2) to generate a GTP:XDP or GDP:XTP bound heterodimer, and confirmed by HPLC (**Appendix 1**). An intrinsic tryptophan fluorescence GTPase assay (Ahmadian et al. 1999) was used to compare FLCN:FNIP2-catalyzed RagC-GTPase activity on Rag heterodimers containing a GDP- or GTP-loaded RagA, with or without the addition of stoichiometric amounts of Ragulator (**Figure 3.1a,b**). We observed similar FLCN:FNIP2 GAP activity for all tested substrate permutations, except that the $RagA^{GDP}$:$RagC^{XTP}$-Ragulator combination completely inhibited FLCN:FNIP2 GAP activity (**Figure 3.1c**). A HPLC-based GAP assay confirmed inhibition of FLCN:FNIP2 GAP activity in the presence of GDP-loaded RagA and Ragulator (**Figure 3.1d**).

3.2.2 Determining the components of a stable Lysosomal FLCN Complex (LFC)

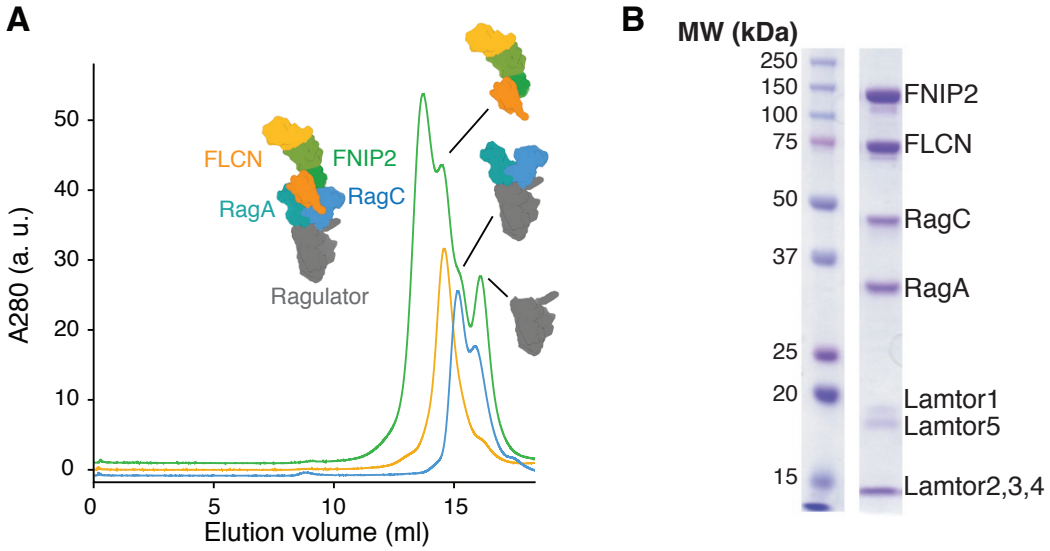

Figure 3.2 Purification of the LFC. (a) *Size Exclusion Chromatography (SEC) profile of $RagA^{GDP}$:$RagC^{XTP\gamma S}$-Ragulator (cyan), FLCN:FNIP2 (orange), or the full LFC containing $RagA^{GDP}$:$RagC^{XTP\gamma S}$-Ragulator-FLCN:FNIP2 (green). (**b**) Coomassie stain of eluted SEC fraction containing assembled LFC.*

Rag heterodimers containing GDP-loaded RagA form a tight complex with Ragulator at the lysosomal membrane (Lawrence et al. 2018). To determine whether $RagA^{GDP}$:$RagC^{XTP}$ and Ragulator form a larger complex that includes FLCN:FNIP2, we combined all three subcomplexes and subjected the mixture to size exclusion chromatography (SEC). We observed a unique early elution peak when all components

were combined, and confirmed that FLCN:FNIP2, RagA:RagC, and Ragulator co-eluted in this fraction (**Figure 3.2a,b**). Thus, FLCN:FNIP2 forms a stable complex with $RagA^{GDP}$:$RagC^{GTP}$-Ragulator, explaining the stable localization of FLCN on the lysosomal surface during starvation. Because this complex corresponds to all the properties expected of the lysosomal form of FLCN, we designate it the "Lysosomal FLCN Complex" (LFC).

3.2.3 Cryo-Electron Microscopy Structure of the LFC

We determined the structure of the LFC at a resolution of 3.6 Å by cryo-electron microscopy (cryo-EM) (**Figure 3.3a-c**). The complex adopts an elongated shape of 240 Å in the longest dimension. The reconstructed cryo-EM density was used to build an atomic coordinate model (**Figure 3.3c**) comprising about 60 % of the mass of the complex. The remainder of the molecular mass consists of flexible loops with no corresponding cryo-EM density visible (**Figure 3.3a**). Through known crystal structures (Nookala et al. 2012; Su et al. 2017), the Ragulator sub-complex and the FLCN DENN domain could be positioned at opposite tips of the complex. The Rag GTPase heterodimer was built on the basis of known structures (Gong et al. 2011; Shen et al. 2018), and their location was consistent with the crystallographically resolved interaction of their C-terminal roadblock domains with Ragulator (de Araujo et al. 2017). The atomic models of the remaining structural elements from FLCN and FNIP2 were built *de novo*.

Models for the FLCN and FNIP2 longin domains were based on the crystal structure of the Lst4 longin domain (Pacitto et al. 2015), the *S. cerevisiae* FNIP ortholog, and the FNIP2 DENN domain model was based on the FLCN DENN domain structure (Nookala et al. 2012). Through visual inspection of the unassigned density of the LFC, a recognizable α-helical interface could be identified, placing the FNIP2 DENN domain next to the FLCN DENN domain with an approximate rotation of 180˚ relative to each other (**Figure 3.3d**). The C-terminal α-helical portion of the FNIP2 DENN domain fit the density well, but the remainder required manual adjustments. The FNIP2 DENN domain carries additional α-helical elements compared to the FLCN DENN domain. Due to their structural similarity, the relative position of the two longin domains could not be assigned solely based on the homology models. The α1-helix of FLCN is predicted to be considerably larger than its counterpart in FNIP2, and FNIP2 lacks a linker between the longin and DENN domain. Thereby the position of both longin domains could be unambiguously defined.

FLCN and FNIP2 share a similar domain organization comprised of an N-terminal longin domain followed by a DENN domain. This domain architecture is referred to as a DENN module (Zhang et al. 2012). Structures of dimeric DENN module complexes have so far not been reported and the DENN interface between FLCN and FNIP2 thus constitutes a novel protein-protein interaction (**Figure 3.3d**). The only available structure of a full DENN module to date is that of DENND 1B (Wu et al. 2011), a Rab35 GEF which is not known to form complexes with other DENN proteins. The DENN module of FNIP2, in contrast, is sandwiched between the FLCN longin and DENN domain and has an architecture distinct to the one found in the Rab35 GEF DENND 1B (**Figure 3.3e**).

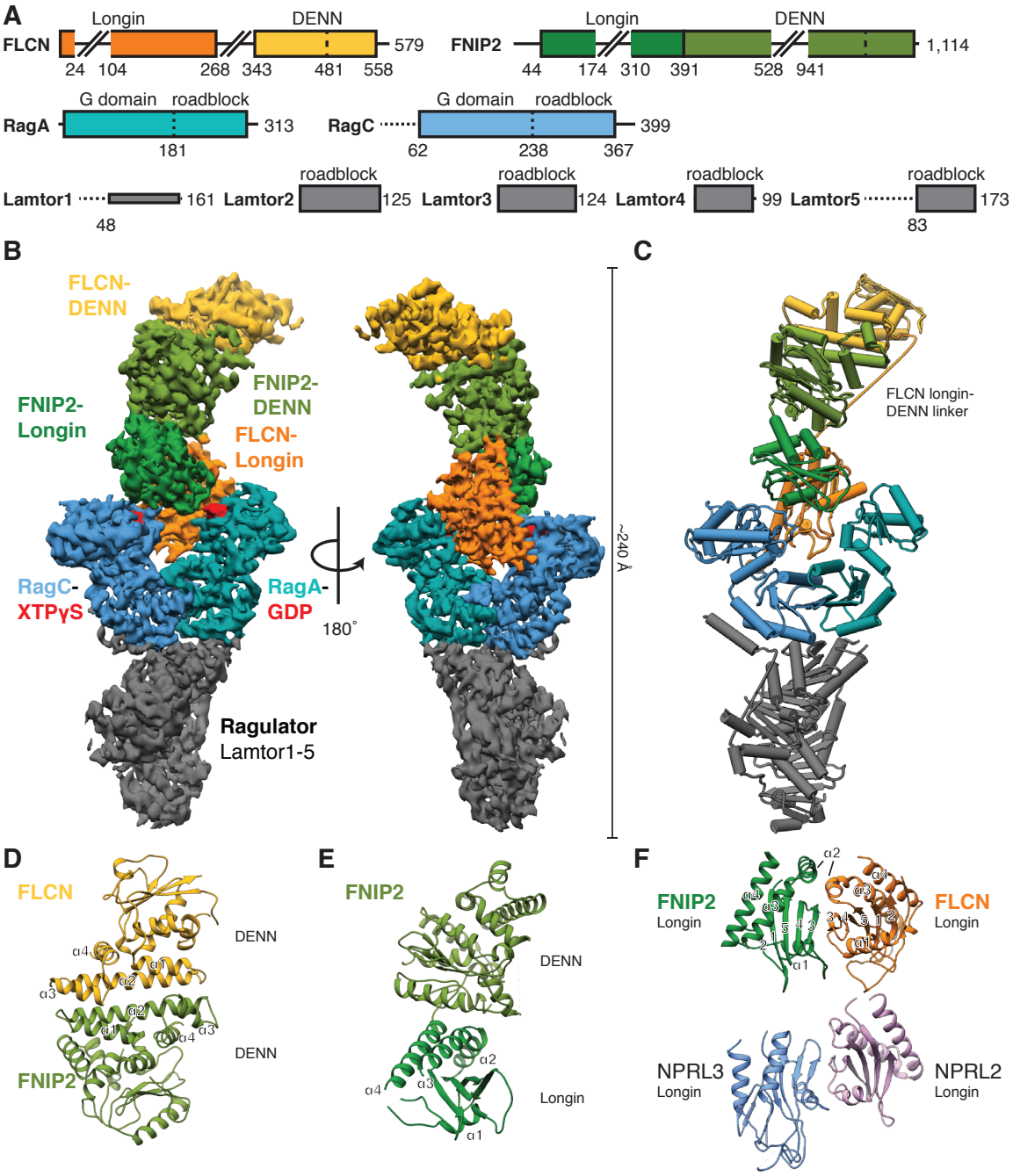

Figure 3.3 Cryo-EM structure of the LFC. *(**a**) Domain organization of the LFC proteins. Horizontal dashed lines indicate disordered regions. Extended loops in FLCN and FNIP2 are indicated by skewed lines. (**b**) Cryo-EM density map and (**c**) atomic model of the LFC. Color scheme as in (A). (**d** to **f**) Ribbon representation of FLCN:FNIP2 domain architecture. DENN-DENN interaction (D), FNIP2 DENN module arrangement (E) and longin-longin domain (F, top). The NPRL2-NPRL3 longin-longin domain from GATOR1 is displayed for comparison (F, bottom; pdb 6CES).*

The FLCN longin and DENN domain have no direct interaction interface (**Figure 3.3b**) and are only connected by a flexible linker (**Figure 3.3 a,c**) revealing a plasticity in DENN module domain arrangements consistent with the wide variety of their functions. The two longin domains of FLCN:FNIP2 form a heterodimer similar to the NPRL2-NPRL3 longin domains of the RagA GAP Gator1 (**Figure 3.3f**) (Shen et al. 2018). This longin-longin heterodimer is the only FLCN:FNIP2 element to directly interact with the RagA:RagC G domains.

3.2.4 R164A is the catalytic Arg for FLCN GAP activity

Within the LFC, the inactive-loaded RagA and RagC G domains show clear density for GDP and XTPγS bound to RagA and RagC, respectively (**Figures. 3.4Aa and 3.5a**). The switch 1 and switch 2 region of RagC are well defined and adopt the conformation expected for the GTP-bound state (**Figure 3.4a**). Consistent with the finding that FLCN:FNIP2 does not exert GAP activity in the LFC (**Figure 3.1c,d**), the interface between FLCN:FNIP2 and $RagC^{XTP\gamma S}$ lacks any Arg residue poised to function as the catalytic 'arginine finger' characteristic for most GAPs (Ahmadian et al. 1997) (**Figure 3.4a**). Recently, the arginine finger of the RagA GAP GATOR1 was identified as Arg78 in loop β4-β5 of the NPRL2 longin domain (Shen et al. 2019). The longin domains of FLCN and FNIP2 do contain an argine residue in loop β4-β5 as well, but only Arg164 of FLCN is highly conserved from yeast to human (**Figure 3.4b**). In the LFC, FLCN Arg164 is located more than 20 Å away from either nucleotide between the two G domains with no intersubunit contacts (**Figure 3.4c**). We found that $FLCN^{R164A}$ assembles into an LFC that migrates normally on SEC (**Figure 3.4d**), yet GAP activity is abolished (**Figure 3.4e,f**). These data establish the catalytic arginine required for canonical FLCN RagC-GAP activity and explain structurally why FLCN is not GAP-competent in the LFC.

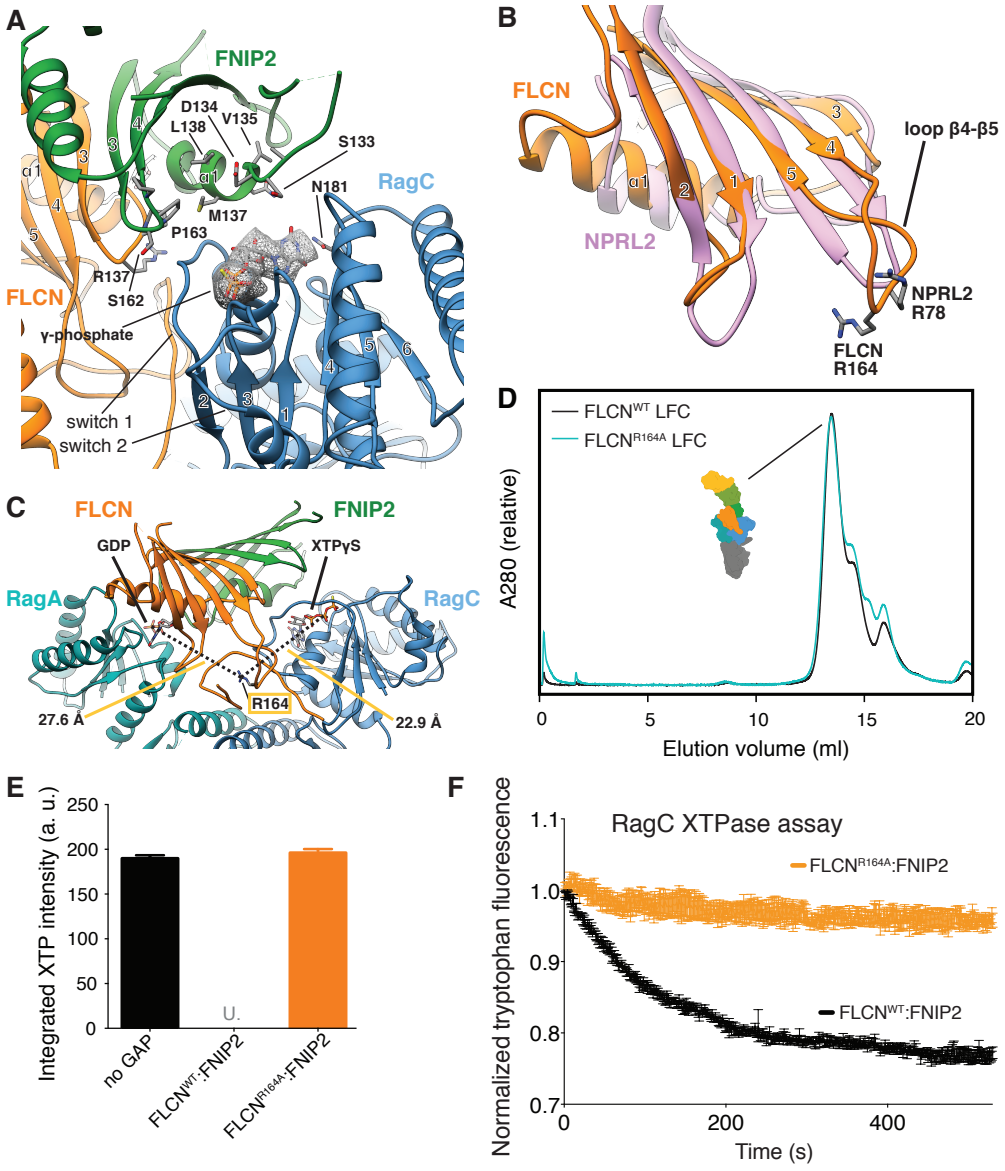

Figure 3.4 RagC-XTPγS binding pocket in the LFC. *(**a**) Nucleotide binding pockets and interaction with FLCN:FNIP2 (orange, green) of the RagC G domain (blue) in the LFC. XTPγS is highlighted by the according cryo-EM density and stick representation. FLCN:FNIP2 residues in the interface are labeled and side chains are shown as sticks. The γ-phosphate of XTPγS locking the switch 1 and switch 2 region of RagC is indicated. (**b**) Overlay of the FLCN (orange) and NPRL2 (rose) longin domains. α-helices α3 and α4 are omitted for clarity. NPRL2 arginine finger (R78) and FLCN R164 in loop β4-β5 are represented as sticks. (**c**) Position of FLCN R164 in the LFC. Distances to the β-phosphate of GDP (RagA) and XTPγS (RagC) are indicated. (**d**) SEC elution profile of LFC (Ragulator-RagA^{GDP}:RagC^{XTPγS}-FLCN:FNIP2) containing FLCN^{WT} (black) or mutant FLCN^{R164A} (cyan). (**e**) HPLC-based GTPase assay assessing GAP activity of FLCN^{WT}:FNIP2 or FLCN^{R164A}:FNIP2 on a RagA^{GTP}:RagC^{XTP} substrate by remaining XTP nucleotide. Mean and SD are plotted. "U." indicates that remaining XTP signal was undetectable by HPLC. (**f**) Tryptophan fluorescence XTPase assay with*

FLCN:FNIP2 mutants. RagA^{GTP}:RagC^{XTP} are incubated with FLCN^{WT}:FNIP2 (black), FLCN^{F118D}:FNIP2 (orange), or FLCN^{R164}:FNIP2 (cyan). Mean and Standard Error of the Mean (SEM) are plotted.

3.2.5 RagA has a low affinity for nucleotide, which is stabilized by Ragulator

In sharp contrast to RagC, much of the switch regions of RagA are not visible in the cryo-EM density, suggesting that this part of the RagA G domain is highly dynamic in the LFC (**Figure 3.5a**). This was observed for the GDP-bound state of yeast Gtr2 and distinguishes the Rag GTPases from other Ras-related GTPases (Jeong et al. 2012). Comparison of the direct interaction of FLCN:FNIP2 with GDP and XTPγS revealed that FLCN:FNIP2 interacts more extensively with the GDP molecule bound to RagA than with the XTPγS molecule bound to RagC (150 *vs.* 20 Å^2 buried surface area) (**Figures. 3.4a and 3.5a**). This prompted us to investigate whether FLCN:FNIP2 regulates nucleotide exchange on RagA.

We used a fluorescence-based assay to monitor RagA nucleotide exchange. The RagA:RagC dimer was first loaded with mantGTP and XTPγS, and incubated with GATOR1 to generate RagA^{mantGDP}:RagC$^{XTP\gamma S}$. GDP-GTP exchange was monitored as release of fluorescence from mantGDP-loaded RagA upon addition of unlabeled GTP. We observed rapid and complete replacement of mantGDP with GTP in the absence of other proteins. In contrast, the ER-associated small GTPase Sar1, which strictly depends on the GEF activity of Sec12 for nucleotide loading, showed negligible mantGDP release under identical conditions (**Figure 3.5b**) (Barlowe and Schekman 1993). These data suggest that, unlike almost all other small GTPases, RagA is able to exchange its guanine nucleotide without the assistance of a GEF. The addition of either Ragulator or FLCN:FNIP2 slowed the kinetics of mantGDP release (**Figure 3.5c**). Strikingly, when the entire LFC was assembled, RagA nucleotide exchange was barely detectable (**Figure 3.5c**), as confirmed by HPLC (**Figure 3.5d**).

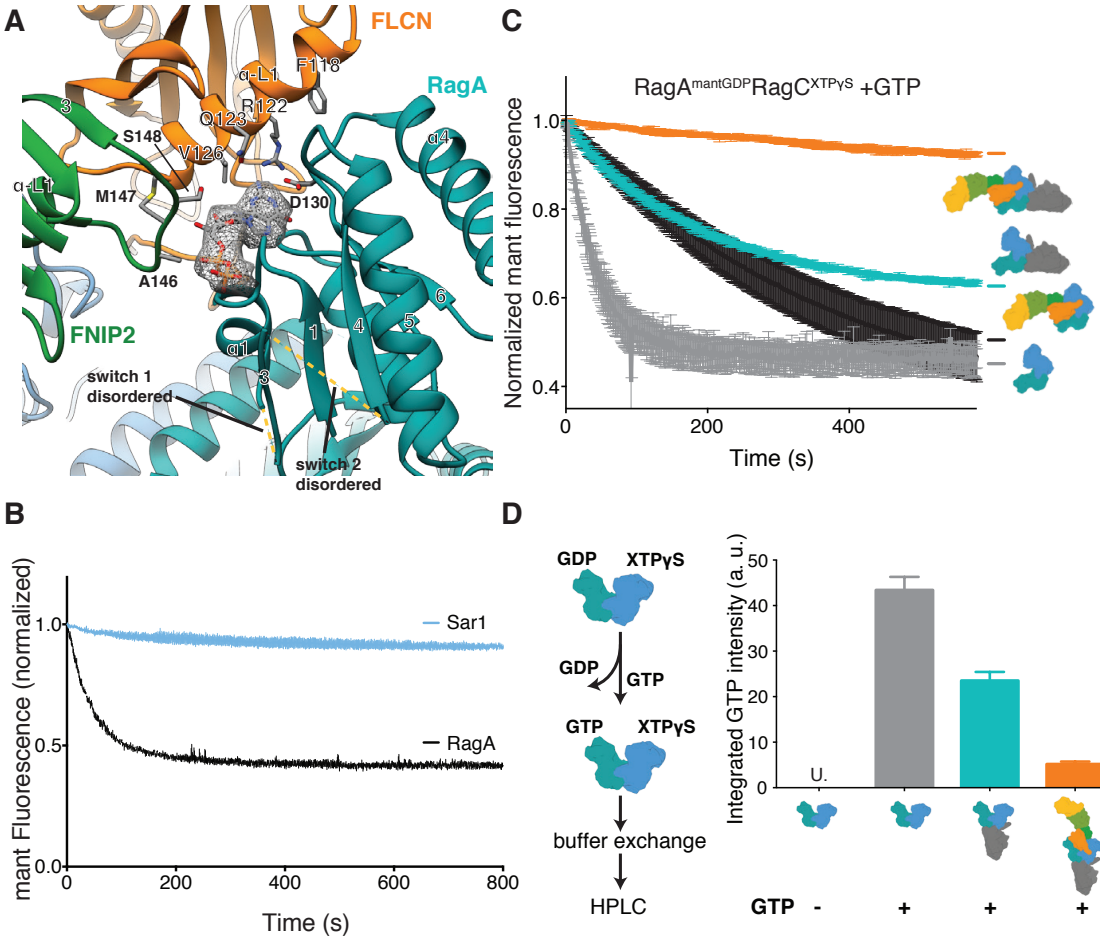

Figure 3.5 RagA has a low affinity for nucleotide. *(**a**) Nucleotide binding pocket and interaction with FLCN:FNIP2 (orange, green) of the RagA G domain (cyan) in the LFC. GDP is highlighted by the according cryo-EM density and stick representation. FLCN:FNIP2 residues in the interface are labeled and side chains are shown as sticks. Disordered switch 1 and switch 2 of RagA absent from the coordinate model are indicated by dashed lines. (**b**) Mant fluorescence intensity was recorded for $RagA^{mantGDP}$:$RagC^{XTPγS}$ (black) or $Sar1^{mantGDP}$ (blue) upon addition of unlabeled GTP at t=0. Mant signals were normalized to pre-GTP-addition intensity values. Mant fluorescence signal decays by approximately half upon release from GTPase active site. Mean and Standard Error of the Mean (SEM) are plotted. (**c**) RagA nucleotide exchange visualized by mant fluorescence. GTP replacement of mantGDP was monitored for $RagA^{mantGDP}$:$RagC^{XTPγS}$ alone (grey), in complex with Ragulator only (cyan), in complex with FLCN:FNIP2 only (black) or in the context of the assembled LFC (orange). Mean and Standard Error of the Mean (SEM) are plotted. (**d**) HPLC-based nucleotide exchange assay for RagA. GTP replacement of GDP for $RagA^{GDP}$:$RagC^{XTPγS}$ alone (grey), in complex with Ragulator (cyan), or in the full LFC (orange) is monitored by appearance of a GTP peak in HPLC elution profile. "U." indicates that GTP signal was undetectable for a control sample in which no GTP was added to the assay. Mean and Standard Deviation (SD) of integrated peak intensities from three replicates are plotted.*

3.2.6 The LFC gates RagA nucleotide exchange

We sought to disrupt the FLCN-RagA G domain binding interface responsible for inhibiting nucleotide exchange by introducing destabilizing amino acid substitutions. A FLCN:FNIP2 complex containing a FLCN^{F118D} mutation did not assemble into a stable LFC as judged by SEC (**Figure 3.6a,b**). Mant nucleotide exchange assays showed that FLCN^{F118D}:FNIP2 no longer inhibited RagA nucleotide exchange. This was true both for FLCN^{F118D}:FNIP2 alone, and in the context of the LFC (for RagA in the presence of both Ragulator and FLCN^{F118D}:FNIP2) (**Figure 3.6c**).

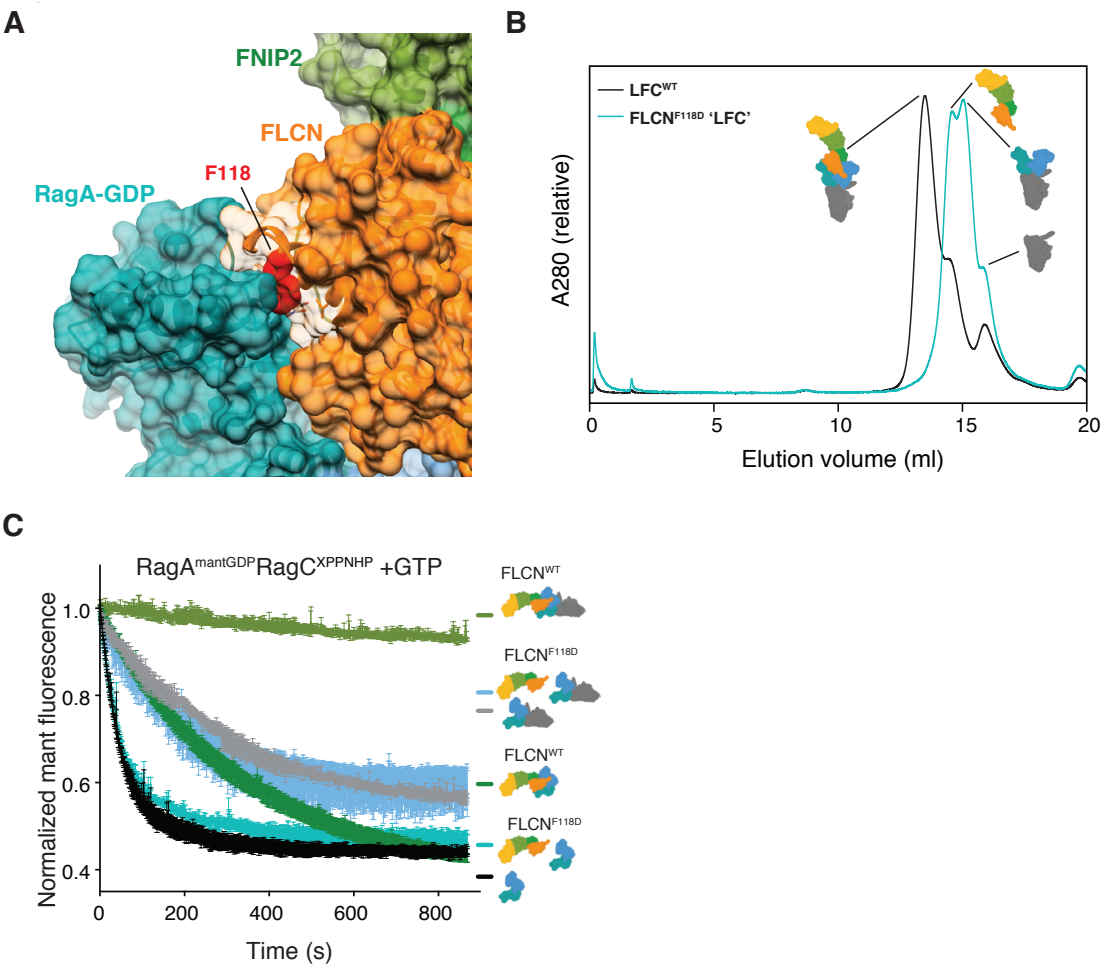

Figure 3.6 The LFC gates RagA nucleotide exchange. *(**a**) Surface representation of the LFC model with FLCN F118 (red) at in the RagA-FLCN interface highlighted. (**b**) SEC elution profile of Ragulator-RagA^{GDP}:RagC^{XPPNHP}-FLCN:FNIP2 containing FLCN^{WT} (black) or FLCN F118D (teal). Peak shift indicates the FLCN F118D-containing complex failed to assemble into a stable LFC. (**c**) RagA nucleotide exchange in response to addition of unlabeled GTP visualized by mant fluorescence for RagA^{mantGDP}:RagC^{XPPNHP} alone (black), in complex with Ragulator (grey), in complex with FLCN:FNIP2 (light*

green), Ragulator and FLCN:FNIP2 (dark green), FLCN^{F118D}:FNIP2 (cyan), or Ragulator and FLCN^{118D}:FNIP2 (blue). Mean and Standard Error of the Mean (SEM) are plotted.

3.2.7 FLCN:FNIP2 interacts with the Rags in two distinct orientations.

Importantly, FLCN^{F118D}:FNIP2 had unaltered RagC-GAP activity on a Rags-only substrate (**Figure 3.7a**). However, unlike FLCN^{WT}:FNIP2, FLCN^{F118D}:FNIP2 could perform GAP activity on a Ragulator-RagA^{GDP}:RagC^{XTP} substrate (**Figure 3.7b**). These data show that FLCN's activating role as a RagC-GAP is structurally separable from its gating role in the LFC. Notably, the RagC-GAP-incompetent FLCN^{R164A}:FNIP2 complex can assemble into an LFC and was capable of blocking RagA nucleotide exchange (**Figure 3.7c**). Our data show that the LFC stabilizes the inactive RagA^{GDP}:RagC^{GTP} dimer by two mechanisms: inhibition of FLCN:FNIP2 RagC-GAP activity needed to convert RagC^{GTP} to RagC^{GDP}, and inhibition of the exchange process that converts RagA^{GDP} to RagA^{GTP}. Collectively, this makes the LFC a robust and powerful checkpoint in the Rag activation cycle.

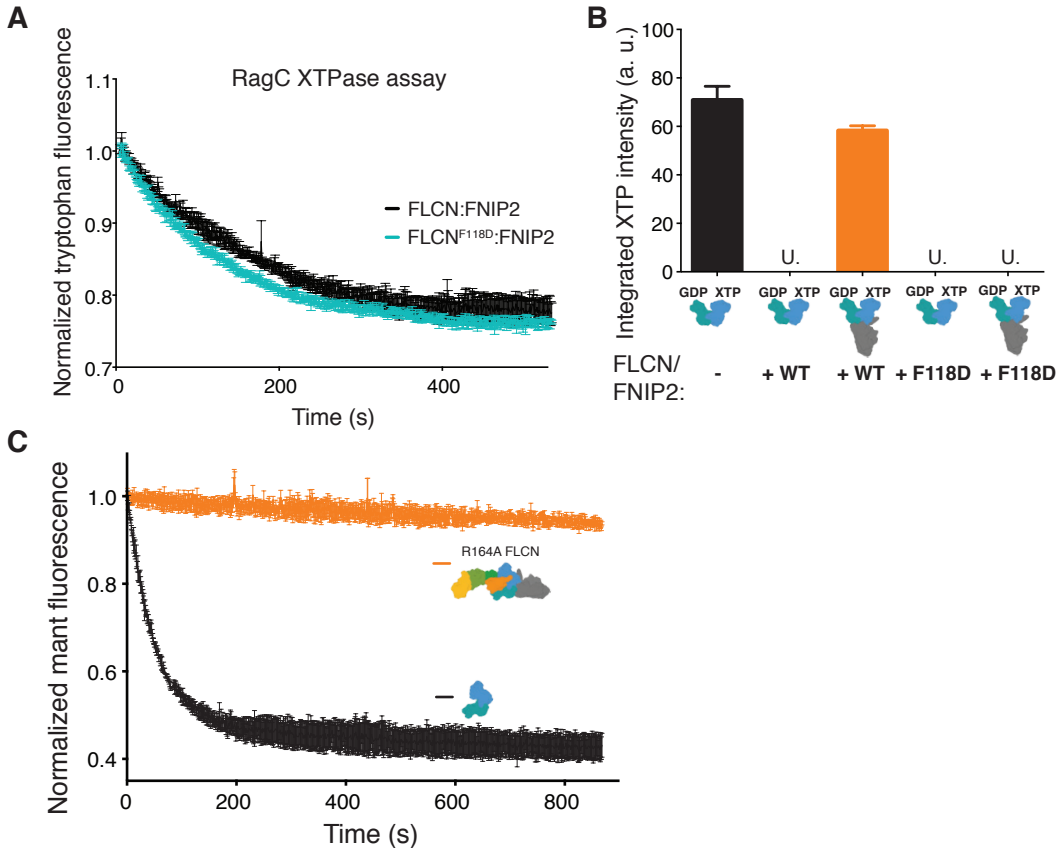

Figure 3.7 LFC functional mutations are orthogonal. *(**a**) Tryptophan fluorescence XTPase assay with FLCN:FNIP2 mutants. $RagA^{GTP}$:$RagC^{XTP}$ heterodimers were incubated with $FLCN^{WT}$:FNIP2 (black) or $FLCN^{F118D}$:FNIP2 (cyan). Mean and Standard Error of the Mean (SEM) are plotted. (**b**) Complex-disrupting $FLCN^{F118D}$ mutant overrides impairment of FLCN:FNIP2 GAP activity on $RagA^{GDP}$:$RagC^{XTP}$-Ragulator substrate. HPLC-based GTPase assay assessing GAP activity by remaining XTP nucleotide (left to right: no GAP control on $RagA^{GDP}$:$RagC^{XTP}$ substrate; $FLCN^{WT}$:FNIP2 on $RagA^{GDP}$:$RagC^{XTP}$ substrate; $FLCN^{WT}$:FNIP2 on $RagA^{GDP}$:$RagC^{XTP}$-Ragulator substrate; $FLCN^{F118D}$:FNIP2 on $RagA^{GDP}$:$RagC^{XTP}$ substrate; $FLCN^{F118D}$:FNIP2 on $RagA^{GDP}$:$RagC^{XTP}$-Ragulator substrate) "U." indicates that remaining XTP signal was undetectable by HPLC. Mean and SD are plotted. (**c**) Mant fluorescence intensity was recorded for $RagA^{mantGDP}$:$RagC^{XTP\gamma S}$ alone (black) or along with Ragulator and $FLCN^{R164A}$:FNIP2 (orange) upon addition of unlabeled GTP at t=0. Mant signals were normalized to pre-GTP-addition intensity values. Mant fluorescence signal decays by approximately half upon release from GTPase active site. Mean and Standard Error of the Mean (SEM) are plotted.*

3.3 Discussion

Our data provide a new perspective on how the transition of the Rag heterodimer from the inactive to the active nucleotide state is regulated. This is a crucial step in nutrient-dependent recruitment and activation of mTORC1 at the lysosome. Combining biochemical reconstitution with cryo-EM, we identify a physical complex of FLCN:FNIP2, inactive Rag GTPases and Ragulator, which we named the LFC. The LFC likely underlies the localization of FLCN observed at the lysosomal membrane under low nutrients (Petit et al. 2013; Tsun et al. 2013; Meng and Ferguson 2018). Moreover, our functional data strongly suggest that FLCN:FNIP2 is both a positive and negative regulator of the Rag heterodimer, and that it modulates the nucleotide states of both RagA and RagC. Thus, FLCN:FNIP2 is far more intimately and centrally involved in regulation of the Rag activation cycle than previously appreciated.

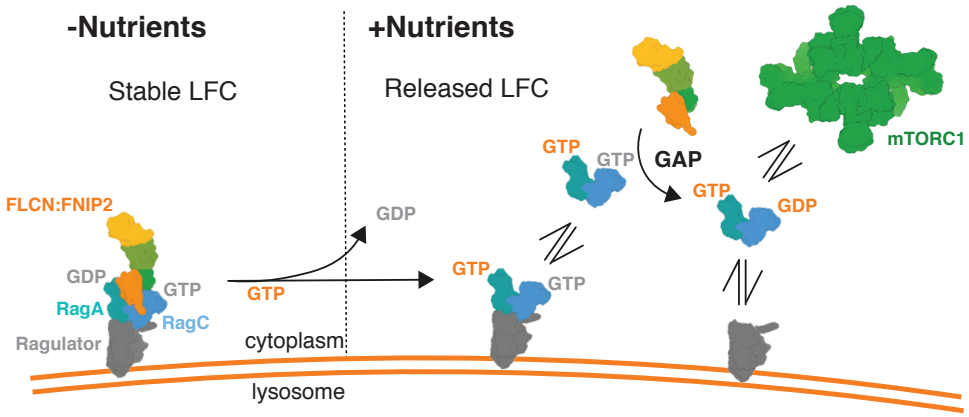

Figure 3.8 Model: The LFC gates Rag activation in response to nutrients. *In low nutrients, FLCN:FNIP2 binds stably to RagA^{GDP}:RagC^{XTP}–Ragulator at the lysosome to form the LFC. In the LFC, both RagA nucleotide exchange and FLCN:FNIP2 RagC-GAP activity are blocked. When nutrient levels reach sufficient levels to promote RagA nucleotide exchange, the LFC dissolves and FLCN:FNIP2 is liberated to perform GAP activity on RagC^{GTP}. Once the Rags are converted to the RagA^{GTP}:RagC^{GDP} state, mTORC1 can be recruited to the lysosome.*

Formation of the LFC critically depends upon the presence of GDP in the nucleotide-binding pocket of RagA, and on Rag dimer binding to Ragulator. Given that the well-resolved portions of FLCN:FNIP2 and Ragulator do not directly contact each other, the structural basis for how Ragulator exerts such a potent effect on the GAP activity of FLCN is unclear. One possibility is that internal loops of FLCN or FNIP2 or from the N-terminus of RagC that were not resolved in our structure could interact with the unresolved region of the Lamtor1 N-terminus. We compared the cryo-EM structures of inactive and active Rag dimers bound to Ragulator (this study) and previous structures of human Rag dimers (Shen et al. 2018) and their yeast orthologs (Gong et al. 2011; Jeong et al. 2012). The overall orientation of the Rag G domains is controlled by their nucleotide state, and appear to be unaffected at a gross level by the presence

of Ragulator. However, the nucleotide-binding P-loop (residues 13-28) of $RagA^{GDP}$ is driven into a low-mobility conformation by the presence of Ragulator, as shown by hydrogen-deuterium exchange (HDX) (Su et al. 2017). The previous HDX finding is supported by the well-ordered EM density for this region in the LFC. The C-terminus of the RagA P-loop region (helix α1) packs tightly against the FLCN longin domain, showing how the conformational dynamics of the P-loop could directly influence affinity for FLCN. A second possibility is thus that direct interaction between the RagA P-loop and FLCN mediates the Ragulator dependence of GAP inhibition and LFC formation.

The LFC appears to function as a checkpoint that makes the RagC-GAP activity of FLCN:FNIP2 contingent on RagA becoming loaded with GTP (**Figure 3.8**). Consistent with this model, our structure shows that, within the LFC, the newly-identified catalytic Arg164 of FLCN is far from the RagC nucleotide pocket and thus incompatible with GTP hydrolysis. This implies a hierarchical order of Rag activation, whereby nutrient-dependent loading of RagA with GTP unlocks the RagC-GAP activity of FLCN:FNIP.

How RagA exchanges its nucleotide remains to be fully determined. The RagA nucleotide-binding pocket is strikingly open in the GDP state in the absence of FLCN:FNIP2, consistent with our finding that RagA can spontaneously exchange GDP for GTP. FLCN:FNIP2 stabilizes the RagA GDP state by directly covering the guanosine portion of the nucleotide, as well as stabilizing RagA residues involved in guanosine binding. Thus, FLCN:FNIP2 could maintain the inactive Rag configuration until some external factor displaces it, allowing GTP loading into the RagA nucleotide pocket and breaking up the LFC. Candidates for this role include Rag-interacting proteins that are required for mTORC1 activation, such as SLC38A9 and the vacuolar H^+ATPase, as well as additional factors that remain to be identified (Zoncu et al. 2011; Rebsamen et al. 2015; Wang et al. 2015; Shen and Sabatini 2018).

Mutations in the *FLCN* tumor suppressor gene are responsible for BHD, which predisposes patients to kidney tumors (Schmidt and Linehan 2018). Numerous FLCN interactors have been postulated to function in tumor suppression, including FNIP1/2 and AMPK, while postulated downstream mediators include mTORC1 and the Rag GTPases, PGC1a, RhoA, and the TFEB/TFE3 transcription factors (Schmidt and Linehan 2018). Most FLCN mutations are nonsense mutations. Several missense mutations map to the surface of the DENN domain, however, and seem unlikely to disrupt protein stability. Our structure shows that these missense mutations are surface-exposed and distal to the FNIP2 contacts and to the Rag interfaces seen in the LFC. The residues of FNIP2 that contact FLCN are almost identically conserved in FNIP1, therefore the conclusions regarding FNIP2 can be extended to FNIP1. The mutations map, approximately, to a concave surface 40 Å wide and 50 Å across, formed by the extended, distal portions of the FLCN and FNIP2 DENN domains. The structure suggests that tumor-promoting mutations probably do not affect the inherent stability of the FLCN:FNIP complex or the LFC itself. This suggests that some critical regulatory factor binds to the DENN crescent and mediates anti-proliferative signals in some way. Conceivably, this factor might contribute to regulating the switch between the LFC and the active RagC-GAP form of FLCN. The identification of this factor, combined with

structural elucidation of the GAP-competent FLCN:FNIP2 in complex with the Rag heterodimer, will likely shed further light on the role of FLCN:FNIP2 in mTORC1 regulation as well as its elusive tumor suppressor role.

The ability of FLCN:FNIP to contact its client RagC in two states, the inactive, stable LFC and an active, GAP-compatible but transient interaction, is nearly unique among known GAPs, with the notable exception of GATOR1. The cryo-EM structure of Gator1 in complex with a Rag dimer revealed a stable, GAP-inhibited state in which the non-catalytic DEPDC5 subunit of GATOR1 makes direct contact with the G domain of RagA (Shen et al. 2018). Although there is still no structure of the GAP-competent GATOR1 complex, a dramatic rearrangement is thought to be essential for the catalytic NPRL2 and NPRL3 subunits to engage RagA. FLCN:FNIP is the mirror image of the GATOR1 complex in the sense that both contain a dual longin domain-based GAP and both complexes have dual positive and negative regulatory functions. This highlights that as compared to all other small GTPases, which are reciprocally governed by a GAP and a GEF, the Rag dimer appears to be governed principally by two different reciprocally acting GAP complexes.

3.4 Methods

Protein Purification

RagA:RagC^{D181N} GTPases and Ragulator were purified via Baculovirus SF9 insect cell expression as described in Su *et al (Su et al. 2017)* (Figure 3.9)

Codon-optimized DNAs coding for full-length human FLCN and FNIP2 were subcloned into pCAG-TWIN-STREP-FLAG and pCAG-GST vectors, respectively (Genscript). HEK-GNTI cells were transfected with a 2:1 FLCN:GST-FNIP2 DNA ratio, with 1 mg DNA and 3 mg P.E.I. per 1 liter of cells at 1E6 cells/ml. Cells were pelleted after 72 hours, and lysed via gentle shaking in triton lysis buffer (25 mM HEPES, 130 mM NaCl, 2.5 mM $MgCl_2$, 2 mM EGTA, 1% triton, pH 7.4) supplemented with Protease Inhibitor (Roche) and 0.5 mM TCEP for 20 minutes at 4°C. Lysate was clarified by centrifugation (18,000 x *g* for 60 minutes at 4°C). Supernatant was incubated with glutathione Sepharose 4B (GE Healthcare) in a gravity-flow column for two hours at 4˚C. The column was washed 1x in triton lysis buffer supplemented with 0.5 mM TCEP, 3x in triton lysis buffer supplemented with 0.5 mM TCEP and high salt (final 330 mM NaCl), then 3x in 0.5 mM TCEP-supplemented lysis buffer containing 0.1% CHAPS instead of 1% triton. The complex was eluted from the column via incubation with Tobacco Etch Virus (TEV) Protease overnight at 4˚C, which cleaved between GST and FNIP2. Eluted complexes were concentrated and purified to homogeneity by injection onto a Superose 6 (GE Healthcare) column equilibrated in Wash Buffer (25 mM HEPES, 130 mM Nacl, 2.5 mM $MgCl_2$, 2 mM EGTA, pH 7.4) supplemented with 0.5 mM TCEP (Figure 3.9).

Codon-optimized DNA coding for full-length GATOR1 components (NPRL2, NPRL3, and DEPDC5) were subcloned into pCAG (NPRL2 and NPRL3) or pCAG-GST (DEPDC5). HEK-GNTI cells were transfected with a 1:2:2 Depdc5:Nprl2:Nprl3 ratio, with 1 mg DNA and 3 mg P.E.I. per 1 liter of cells at 1E6 cells/ml. Cells were pelleted after 72 hours, and lysed via gentle shaking in triton lysis buffer (25 mM HEPES, 130 mM Nacl, 2.5 mM $MgCl_2$, 2 mM EGTA, 1% triton, pH 7.4) supplemented with Protease Inhibitor (Roche) and 0.5 mM TCEP for 20 minutes at 4°C. Lysate was then clarified by centrifugation (18,000 x *g* for 60 minutes at 4°C). Supernatant was incubated with glutathione Sepharose 4B (GE Healthcare) in a gravity-flow column and incubated for two hours at 4˚C. The column was washed 3x in triton lysis buffer supplemented with 0.5 mM TCEP and 1x in triton lysis buffer supplemented to 330 mM NaCl and 0.5 mM TCEP. The complex was eluted from the column via incubation with Tobacco Etch Virus (TEV) Protease overnight at 4˚C, which cleaved between GST and DEPDC5. Eluted complexes were concentrated and purified to homogeneity by injection onto a Superose 6 (GE Healthcare) column equilibrated in Wash Buffer (25 mM HEPES, 130 mM NaCl, 2.5 mM $MgCl_2$, 2 mM EGTA, pH 7.4) supplemented with 0.5 mM TCEP (Figure 3.9).

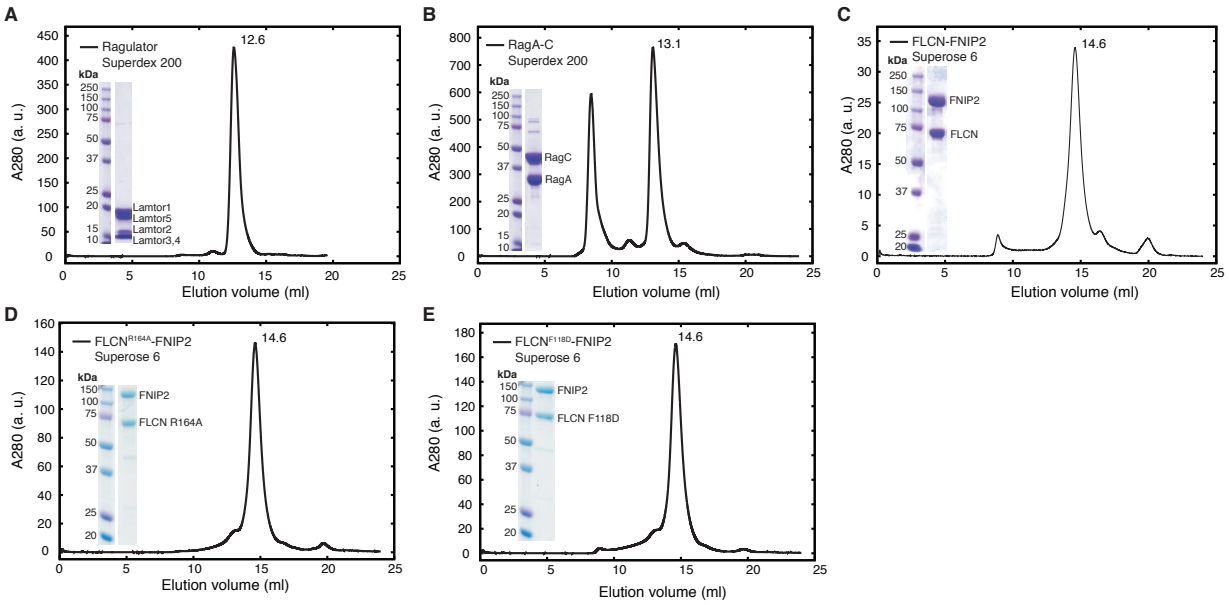

Figure 3.9 Purification of individual LFC components. *(**a**) S200 SEC elution profile for Ragulator and coomassie blue stained SDS-PAGE analysis of protein collected from the peak labeled with elution volume (12.6 ml). (**b**) S200 SEC elution profile for Rag GTPases and coomassie blue stained SDS-PAGE analysis of protein collected from the peak labeled with elution volume (13.1 ml). (**c**) Superose 6 SEC elution profile for FLCN:FNIP2 and coomassie blue stained SDS-PAGE analysis of protein collected from the peak labeled with elution volume (14.6 ml). (**d**) Superose 6 SEC elution profile for FLCN:FNIP2 containing FLCN^{R164A} mutation and coomassie blue stained SDS-PAGE analysis of protein collected from the peak labeled with elution volume (14.6 ml). (**e**) Superose 6 SEC elution profile for FLCN:FNIP2 containing FLCN^{F118D} mutation and coomassie blue stained SDS-PAGE analysis of protein collected from the peak labeled with elution volume (14.6 ml).*

Nucleotide loading

RagA:RagC^{D181N} heterodimers purified from SF9 cells were incubated with 5 mM EDTA in Calcium- and Magnesium-Free DPBS (Gibco^{TM}) supplemented with 0.5 mM TCEP for 20 minutes at 25°C. Then, the desired nucleotides were added at a 10-fold molar excess to the Rags and incubated for 20 minutes at 25°C. $MgCl_2$ was added to a final concentration of 20 mM and incubated for 10 minutes at 25°C. The Rags were then buffer-exchanged at 4°C to remove unbound nucleotide into Wash Buffer (25 mM HEPES, 130 mM NaCl, 2.5 mM $MgCl_2$, 2 mM EGTA, pH 7.4) supplemented with 0.5 mM TCEP via a PD-10 desalting column (GE Healthcare). When a diphosphate nucleotide-bound state was desired, triphosphate nucleotide-loaded Rag heterodimers were incubated with the corresponding GAP complex at a 1:100 GAP:Rag ratio at 37˚C for 30 minutes. Final nucleotide binding state of the Rags was verified via High Pressure Liquid Chromatography (HPLC) analysis (see below).

LFC Complex Assembly

To assemble the LFC complex, purified RagA^{GDP}:RagC$^{XTP\gamma S}$ and Ragulator were incubated for 30 minutes at 4°C at a 1:1.2 molar ratio. FLCN:FNIP2 was then added at a 1.2-fold excess relative to Rags and further incubated at 4°C for 30 minutes. This complex was hard spun to remove any precipitate at 17,000.0 *x g* for 10 minutes and then loaded onto a Superose 6 (GE Healthcare) column equilibrated in Wash Buffer supplemented with 0.5 mM TCEP. Fractions containing assembled LFC complex were verified by SDS PAGE and coomassie stain, after which identified fractions were collected, concentrated and kept at 4°C until use in experiments.

HPLC Analysis

Nucleotide binding state of Rag GTPases was assessed by boiling >30 μl of Rag complex (>1 mg/ml) for 5 minutes at 95°C followed by 10 min centrifugation at 17,000 *x g*. The supernatant, containing released nucleotides, was injected onto an HPLC column (ZORBAX Eclipse XDB-C18, Agilent Technologies). Nucleotides were eluted with HPLC buffer (10 mM tetra-n-butylammonium bromide, 100 mM potassium phosphate pH 6.5, 7.5% acetonitrile) and detected by absorbance at 260 nm.

HPLC GTPase or XTPase assay

HPLC-based GTPase or XTPase assays were performed by incubating >30 μl of substrate complex (>1 mg/mL Rags in the indicated nucleotide-binding state, with or without the addition of a 1.2-fold molar excess of Ragulator) with a GAP at a 1:100 GAP:Rag molar ratio for 30 minutes at 37˚C. Samples were immediately boiled for 5 minutes at 95°C followed by 10 min centrifugation at 17,000 *x g.* The supernatant was injected onto an HPLC column, as above. Relative amounts of unhydrolyzed nucleotide were reported by integrating the A260 peak intensity for the nucleotide of interest (i.e. XTP) for non-GAP and with GAP samples. Reported values are raw integrated intensities (a.u.).

HPLC Nucleotide Exchange Assay

HPLC-based RagA nucleotide exchange assays were performed by first preparing the indicated RagA^{GDP}:RagC$^{XTP\gamma S}$–containing complexes by incubating RagA^{GDP}:RagC$^{XTP\gamma S}$ Rags (that had been prepared by Gator1-treatment and subsequent SEC to remove Gator1) with a 1.2-fold molar excess of Ragulator and/or FLCN:FNIP2 (as indicated). Next, complexes containing 12.4 uM RagA^{GDP}:RagC$^{XTP\gamma S}$ or ^{XPPNHP} were incubated with 12.5 uM GTP for 30 minutes at 25˚C. The samples were buffer exchanged into GTP-free Wash Buffer + TCEP by dilution and concentration on a 30,000 MWCO concentrator column (Millipore). Samples were prepared for HPLC injection as described in HPLC Analysis (above). Relative levels of nucleotide exchange were reported by integrating the A280 peak intensity for GTP. Reported are experimental samples and control samples that lack GTP, as indicated in figures and figure legends. Mean and standard deviation of the mean of two replicates per condition are plotted.

Tryptophan Fluorescence RagC XTPase Assay

Fluorimetry experiments were performed on a Cary Eclipse Fluorescence Spectrophotometer (Agilent Technologies) using a quartz cuvette compatible with magnetic stirring, pathlength 10 mm (Starna Cells). Tryptophan fluorescence signal was collected using a 297 nm excitation (1.5 nm slit) and 340 nm emission (20 nm slit). Experiments were performed in HKM buffer (20 mM HEPES, 160 mM KoAc, 1 mM MgCl2, pH 7.2) supplemented with 0.5 mM TCEP at 37˚C with stirring. After addition of 525 μl HKM buffer to the cuvette, signal was zeroed. Kinetics data collection commenced with one second acquisition intervals, and 30 μg Rag GTPases or Rag GTPases-containing protein mixes composed of 30 μg Rag GTPases with a 1.2-fold molar excess of other proteins were pipetted into the cuvette. Once the signal equilibrated, GAP protein was pipetted into the cuvette at a 1:10 molar ratio of GAP: Rags. Data are displayed such that t=0 corresponds to GTP addition, and are normalized such that the fluorescent signal upon GAP addition is set to 1. Mean and standard error of the mean of three replicates per condition are plotted. It should be noted that control experiments indicate that intrinsic fluorescence of the Rag GTPases is dependent on RagC nucleotide binding state but not RagA nucleotide binding state.

mantGDP Nucleotide Exchange Assay

Experiments were performed with the same instrument and cuvette as described for tryptophan fluorescence assays (see above). Mant fluorescence signal was collected using a 360 nm excitation (10 nm slit) and 440 nm emission (10 nm slit). Experiments were performed in HKM buffer supplemented with 0.5 mM TCEP (see above) at 37˚C with stirring. After addition of 525 μl HKM buffer to the cuvette, signal was zeroed. Kinetics data collection commenced with one second acquisition intervals, and 15 μg $RagA^{mantGDP}$:$RagC^{XTP\gamma S \text{ or } XPPNHP}$ or pre-mixed $RagA^{mantGDP}$:$RagC^{XTP\gamma S \text{ or } XPPNHP}$ protein complexes composed of 15 μg Rags with a 1.2-fold molar excess of other proteins were pipetted into the cuvette. Once the signal equilibrated, GTP was pipetted into the cuvette at a final concentration of 500 nM. Data are displayed such that t=0 corresponds to GTP addition, and are normalized such that the fluorescent signal immediately following GTP addition is set to 1. Mant fluorescence signal decays by approximately half upon release from GTPase active site. Mean and standard error of the mean of two or three replicates per condition are plotted.

3.5 References

Ahmadian MR, Stege P, Scheffzek K, Wittinghofer A. 1997. Confirmation of the arginine-finger hypothesis for the GAP-stimulated GTP-hydrolysis reaction of Ras. *Nature structural biology* **4**: 686-689.

Ahmadian MR, Zor T, Vogt D, Kabsch W, Selinger Z, Wittinghofer A, Scheffzek K. 1999. Guanosine triphosphatase stimulation of oncogenic Ras mutants. *Proc Natl Acad Sci U S A* **96**: 7065-7070.

Baba M, Hong SB, Sharma N, Warren MB, Nickerson ML, Iwamatsu A, Esposito D, Gillette WK, Hopkins RF, 3rd, Hartley JL et al. 2006. Folliculin encoded by the BHD gene interacts with a binding protein, FNIP1, and AMPK, and is involved in AMPK and mTOR signaling. *Proc Natl Acad Sci U S A* **103**: 15552-15557.

Bar-Peled L, Chantranupong L, Cherniack AD, Chen WW, Ottina KA, Grabiner BC, Spear ED, Carter SL, Meyerson M, Sabatini DM. 2013. A Tumor suppressor complex with GAP activity for the Rag GTPases that signal amino acid sufficiency to mTORC1. *Science* **340**: 1100-1106.

Bar-Peled L, Schweitzer LD, Zoncu R, Sabatini DM. 2012. Ragulator is a GEF for the rag GTPases that signal amino acid levels to mTORC1. *Cell* **150**: 1196-1208.

Barlowe C, Schekman R. 1993. SEC12 encodes a guanine-nucleotide-exchange factor essential for transport vesicle budding from the ER. *Nature* **365**: 347-349.

de Araujo MEG, Naschberger A, Furnrohr BG, Stasyk T, Dunzendorfer-Matt T, Lechner S, Welti S, Kremser L, Shivalingaiah G, Offterdinger M et al. 2017. Crystal structure of the human lysosomal mTORC1 scaffold complex and its impact on signaling. *Science* **358**: 377-381.

Gong R, Li L, Liu Y, Wang P, Yang H, Wang L, Cheng J, Guan KL, Xu Y. 2011. Crystal structure of the Gtr1p-Gtr2p complex reveals new insights into the amino acid-induced TORC1 activation. *Genes Dev* **25**: 1668-1673.

Hasumi H, Baba M, Hong SB, Hasumi Y, Huang Y, Yao M, Valera VA, Linehan WM, Schmidt LS. 2008. Identification and characterization of a novel folliculin-interacting protein FNIP2. *Gene* **415**: 60-67.

Hasumi Y, Baba M, Ajima R, Hasumi H, Valera VA, Klein ME, Haines DC, Merino MJ, Hong SB, Yamaguchi TP et al. 2009. Homozygous loss of BHD causes early embryonic lethality and kidney tumor development with activation of mTORC1 and mTORC2. *Proc Natl Acad Sci U S A* **106**: 18722-18727.

Hong SB, Oh H, Valera VA, Stull J, Ngo DT, Baba M, Merino MJ, Linehan WM, Schmidt LS. 2010. Tumor suppressor FLCN inhibits tumorigenesis of a FLCN-null renal cancer cell line and regulates expression of key molecules in TGF-beta signaling. *Mol Cancer* **9**: 160.

Jeong JH, Lee KH, Kim YM, Kim DH, Oh BH, Kim YG. 2012. Crystal Structure of the Gtr1p(GTP)-Gtr2p(GDP) Protein Complex Reveals Large Structural Rearrangements Triggered by GTP-to-GDP Conversion. *Journal of Biological Chemistry* **287**: 29648-29653.

Kim E, Goraksha-Hicks P, Li L, Neufeld TP, Guan KL. 2008. Regulation of TORC1 by Rag GTPases in nutrient response. *Nature cell biology* **10**: 935-945.

Lawrence RE, Cho KF, Rappold R, Thrun A, Tofaute M, Kim DJ, Moldavski O, Hurley JH, Zoncu R. 2018. A nutrient-induced affinity switch controls mTORC1 activation by its Rag GTPase–Ragulator lysosomal scaffold. *Nature Cell Biology* **epub ahead of print**.

Levine TP, Daniels RD, Wong LH, Gatta AT, Gerondopoulos A, Barr FA. 2013. Discovery of new Longin and Roadblock domains that form platforms for small GTPases in Ragulator and TRAPP-II. *Small GTPases* **4**: 62-69.

Meng J, Ferguson SM. 2018. GATOR1-dependent recruitment of FLCN-FNIP to lysosomes coordinates Rag GTPase heterodimer nucleotide status in response to amino acids. *J Cell Biol*.

Nickerson ML, Warren MB, Toro JR, Matrosova V, Glenn G, Turner ML, Duray P, Merino M, Choyke P, Pavlovich CP et al. 2002. Mutations in a novel gene lead to kidney tumors, lung wall defects, and benign tumors of the hair follicle in patients with the Birt-Hogg-Dube syndrome. *Cancer cell* **2**: 157-164.

Nookala RK, Langemeyer L, Pacitto A, Ochoa-Montano B, Donaldson JC, Blaszczyk BK, Chirgadze DY, Barr FA, Bazan JF, Blundell TL. 2012. Crystal structure of folliculin reveals a hidDENN function in genetically inherited renal cancer. *Open Biol* **2**: 120071.

Pacitto A, Ascher DB, Wong LH, Blaszczyk BK, Nookala RK, Zhang N, Dokudovskaya S, Levine TP, Blundell TL. 2015. Lst4, the yeast Fnip1/2 orthologue, is a DENN-family protein. *Open Biol* **5**: 150174.

Panchaud N, Peli-Gulli MP, De Virgilio C. 2013. Amino acid deprivation inhibits TORC1 through a GTPase-activating protein complex for the Rag family GTPase Gtr1. *Science signaling* **6**: ra42.

Peli-Gulli MP, Sardu A, Panchaud N, Raucci S, De Virgilio C. 2015. Amino Acids Stimulate TORC1 through Lst4-Lst7, a GTPase-Activating Protein Complex for the Rag Family GTPase Gtr2. *Cell Rep* **13**: 1-7.

Petit CS, Roczniak-Ferguson A, Ferguson SM. 2013. Recruitment of folliculin to lysosomes supports the amino acid-dependent activation of Rag GTPases. *J Cell Biol* **202**: 1107-1122.

Rebsamen M, Pochini L, Stasyk T, de Araujo ME, Galluccio M, Kandasamy RK, Snijder B, Fauster A, Rudashevskaya EL, Bruckner M et al. 2015. SLC38A9 is a component of the lysosomal amino acid sensing machinery that controls mTORC1. *Nature* **519**: 477-481.

Sancak Y, Bar-Peled L, Zoncu R, Markhard AL, Nada S, Sabatini DM. 2010. Ragulator-Rag complex targets mTORC1 to the lysosomal surface and is necessary for its activation by amino acids. *Cell* **141**: 290-303.

Sancak Y, Peterson TR, Shaul YD, Lindquist RA, Thoreen CC, Bar-Peled L, Sabatini DM. 2008. The Rag GTPases bind raptor and mediate amino acid signaling to mTORC1. *Science* **320**: 1496-1501.

Saxton RA, Sabatini DM. 2017. mTOR Signaling in Growth, Metabolism, and Disease. *Cell* **169**: 361-371.

Schmidt LS, Linehan WM. 2018. FLCN: The causative gene for Birt-Hogg-Dube syndrome. *Gene* **640**: 28-42.

Shen K, Huang RK, Brignole EJ, Condon KJ, Valenstein ML, Chantranupong L, Bomaliyamu A, Choe A, Hong C, Yu Z et al. 2018. Architecture of the human GATOR1 and GATOR1-Rag GTPases complexes. *Nature* **556**: 64-69.

Shen K, Sabatini DM. 2018. Ragulator and SLC38A9 activate the Rag GTPases through noncanonical GEF mechanisms. *Proc Natl Acad Sci U S A* **115**: 9545-9550.

Shen K, Valenstein ML, Gu X, Sabatini DM. 2019. Arg78 of Nprl2 catalyzes GATOR1-stimulated GTP hydrolysis by the Rag GTPases. *J Biol Chem*.

Su MY, Morris KL, Kim DJ, Fu Y, Lawrence R, Stjepanovic G, Zoncu R, Hurley JH. 2017. Hybrid Structure of the RagA/C-Ragulator mTORC1 Activation Complex. *Molecular cell* **68**: 835-846 e833.

Tsun ZY, Bar-Peled L, Chantranupong L, Zoncu R, Wang T, Kim C, Spooner E, Sabatini DM. 2013. The Folliculin Tumor Suppressor Is a GAP for the RagC/D GTPases That Signal Amino Acid Levels to mTORC1. *Molecular cell*.

Wang S, Tsun ZY, Wolfson RL, Shen K, Wyant GA, Plovanich ME, Yuan ED, Jones TD, Chantranupong L, Comb W et al. 2015. Metabolism. Lysosomal amino acid transporter SLC38A9 signals arginine sufficiency to mTORC1. *Science* **347**: 188-194.

Wu X, Bradley MJ, Cai Y, Kummel D, De La Cruz EM, Barr FA, Reinisch KM. 2011. Insights regarding guanine nucleotide exchange from the structure of a DENN-domain protein complexed with its Rab GTPase substrate. *Proc Natl Acad Sci U S A* **108**: 18672-18677.

Zhang D, Iyer LM, He F, Aravind L. 2012. Discovery of Novel DENN Proteins: Implications for the Evolution of Eukaryotic Intracellular Membrane Structures and Human Disease. *Frontiers in genetics* **3**: 283.

Zoncu R, Bar-Peled L, Efeyan A, Wang S, Sancak Y, Sabatini DM. 2011. mTORC1 senses lysosomal amino acids through an inside-out mechanism that requires the vacuolar H(+)-ATPase. *Science* **334**: 678-683.

Chapter 4

Structural and functional insights toward an integrated model of the Rag GTPase nucleotide cycle

Chapter Summary

Functional experiments have characterized features of distinct Rag nucleotide binding states, but a mechanistic understanding of how these states carry out distinct roles in regulating mTORC1 activity in the cell is hindered by a lack of structural information. An understanding of the conformational changes that the Rags undergo as well as of the binding interfaces engaged in interactions with effectors is needed to assemble a comprehensive model of the complete Rag nucleotide cycle. Here, I present the first structural comparison of Rags in the active and inactive nucleotide binding states, achieved in collaboration with members of the James Hurley lab. Next, a comprehensive model of the Rag nucleotide cycle is proposed. Finally, preliminary experiments are presented that address open questions that arise from the model. The chapter concludes with a discussion of promising areas of future research.

Portions of this chapter have been previously published in Su et al., or will be published Lawrence, Fromm et al. The structure of the active Rags was solved by Adam Yokom with assistance from Ashley Thelen, and the structure of the inactive Rags was solved by Simon Fromm with assistance from Rosalie Lawrence and Lindsey Young.

4.1 Background

Work from many laboratories over the past decade has enabled several groups to propose models for the complete nucleotide cycle of the heterodimeric Rag GTPases and how particular Rag nucleotide binding states shape mTORC1 activity (Lawrence et al. 2018; Shen and Sabatini 2018; Valvezan and Manning 2019). A key limitation toward building an integrative model has been a lack of information about the structural rearrangements that the Rags undergo upon transition between activating (mTORC1-binding) and inactivating (non-mTORC1 binding) nucleotide states. This chapter will review previously published work and present new structural data to inform a comprehensive model for Rag nucleotide cycling and subsequent activation and inactivation of mTORC1. I will conclude by highlighting key remaining questions and presenting some preliminary data toward addressing these questions.

While it was clear that the activating (RagA/B^{GTP}-RagC/D^{GDP}) and inactivating (RagA/B^{GDP}-RagC/D^{GTP}) Rag complexes had strikingly opposing effects on mTORC1 localization and activity, it was not clear what structural rearrangements occurred in the Rag heterodimer to achieve these functional outcomes. Elucidating the structural changes that occur upon nucleotide transition is necessary to understand mechanisms of effector engagement and regulation.

Furthermore, how Ragulator binding to the Rags affected Rag nucleotide state was elusive. It has been consistently observed that Ragulator binds more stably to the inactivating RagA/B^{GDP}:RagC/D^{GTP} complex than to the activating RagA/B^{GTP}:RagC/D^{GDP} complex, but the interaction interfaces between Rags and Ragulator were unknown (Sancak et al. 2010; Zoncu et al. 2011; Bar-Peled et al. 2012). Furthermore, reports that the Ragulator complex acted as a Guanine Nucleotide Exchange Factor were followed by contradictory reports (Shen and Sabatini 2018), and whether and how Ragulator controls Rag nucleotide binding states was unclear (Bar-Peled et al. 2012; Fu 2018).

Four papers published in late 2017 included structures of the *H. sapiens* Ragulator complex bound to Rag GTPase truncations or complete complexes (de Araujo et al. 2017; Su et al. 2017; Yonehara et al. 2017; Zhang et al. 2017). These reports were the first to establish the overall architecture of the Ragulator complex, which is composed of two Longin/Roadblock domain dimers (Lamtor2/Lamtor3 and Lamtor4/Lamtor5) enclosed within an elongated Lamtor1 peptide (**Figure 4.1a**). While none of these reports included high-resolution models of the Rag G domains, they did report atomic maps of the Rag C Terminal Domains (CTDs) (de Araujo et al. 2017; Yonehara et al. 2017). The Rag CTDs were shown to also form a Longin/Roadblock dimer and to make direct contact with the Lamtor2/ Lamtor3 roadblock dimer (**Figure 4.1a-c**). The Rag G domains project outward in the opposite direction from Ragulator (Su et al. 2017; Yonehara et al. 2017); this was surprising in light of the observation that Ragulator binding affinity was dependent upon G domain orientation, as no direct interactions between Rag G domains and Ragulator were shown (**Figure 4.1c**).

However, significant portions of Lamtor1 and Lamtor5 remained unstructured in all published reports, leaving open the possibility that the Lamtor1 or Lamtor5 N-terminal

residues directly contact Rag G domains. Rag-Ragulator reconstructions based on homology to yeast Gtr1/2 structures predict that the Lamtor1 NTD is projected to reach up toward the RagC/D G domain, whereas the Lamtor5 NTD is projected to extend toward the RagA/B G domain (**Figure 4.1b**). Whether and how the structurally invisible 96 residues at the Lamtor1 NTD or the 82 residues at the Lamtor5 contact and regulate the Rag G domains remains an important open question (Fu 2018).

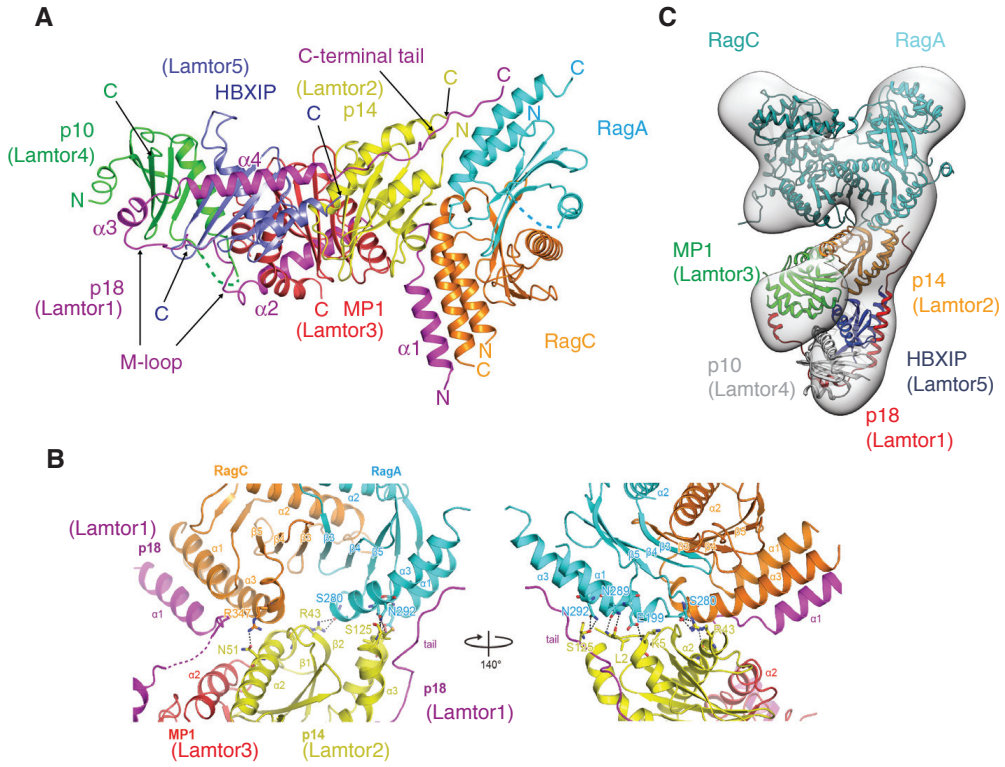

Figure 4.1 Architecture of the Rag-Ragulator complex. *(**a**) Ragulator is composed of two roadblock dimers (C7orf59/Lamtor4 with HBXIP/Lamtor5, and P14/Lamtor2 with Mp1/Lamtor3) clamped within an elongated p18/Lamtor1. The RagA and RagC C terminal domains form a roadblock dimer that sit atop the roadblock dimer composed of P14/Lamtor2 and Mp1/Lamtor3 roadblock dimer. (**b**) Zoom-in on the interface between the Ragulator and Rags complex. P18/Lamtor1 N terminus extends up toward RagC, while the p18/Lamtor1 C terminus extends toward RagA. Lamtor2 makes extensive contacts with both RagA and RagC C terminal domains. (**c**) Crystal structures of Ragulator and Active Gtr1/2 complex were modeled into a 3-D Cryo-EM reconstruction of a Ragulator-Active Rags (RagA$^{Q66L\text{-}GTP}$:RagC$^{D181N\text{-}XDP}$) complex. **a,b** adopted from Yonehara et al.(Yonehara et al. 2017) **c** adopted from Su et al.(Su et al. 2017)*

Notably, none of the four studies from 2017 reported an atomic model of the Rag G domains. Structures of the Rag homologs in yeast (Gtr1/2) were published in 2011 and 2012, including atomic resolution models of their G domains. The difficulty in resolving Rag G domains, along with the observation that Rags bind nucleotides with low affinity (discussed in Chapter 3 and Appendix I) suggest that in the absence of

stabilizing binding partners, they may sample multiple conformations, and be less ordered than small GTPase homologs.

One of the 2017 studies (Su et al. 2017) investigated RagA conformations using Hydrogen Deuterium eXchange (HDX). Su *et al.* found that when either Rag was loaded with a diphosphate nucleotide, the P loop showed 2-peak HDX signatures indicative of sampling two distinct conformations, while a single HDX peak was detected for triphosphate nucleotide-loaded Rags (Su et al. 2017). Notably, the addition of Ragulator to a $RagA^{GDP}$-containing complex collapsed away one peak and stabilized the other. These data suggest that Ragulator is able to influence the nucleotide binding properties of RagA, a finding that is consistent with the mant fluorimetry and HPLC results presented in Chapter 3. Notably, while RagC also showed two HDX peaks when bound to diphosphate nucleotdie, Ragulator binding did not collapse these peaks.

The first atomic model of the Rag GTPase G domains was reported as part of a Cryo-EM structure containing the Rags bound to the Gator1 GAP complex (Shen et al. 2018). The structure contained RagA loaded with the non-hydrolyzable nucleotide analog GPPNHP and RagC bearing an S75N mutation. The S75N mutation has been characterized both as stabilizing the GDP-bound state, and as being nucleotide empty (see Appendix I). In this structure, no nucleotide was visualized in the RagC nucleotide binding pocket.

A direct comparison of the full Rag structure and structures of the Gtr1/2 yeast homologs suggested structural divergence (Gong et al. 2011; Jeong et al. 2012a). While it had been shown that the Gtr1/2 G domains rotate away from one another upon conversion in the active GTP/GDP state relative to the GTP/GTP nucleotide bound state, the $RagA^{GPPNHP}$:$RagC^{empty}$ G domains were rotated away from each other to a more extensive degree than the $Gtr1^{GTP}$:$Gtr2^{GDP}$ G domains (Gong et al. 2011; Jeong et al. 2012a; Shen et al. 2018). However, prior to the work discussed in Chapter 3, no structure of Rags in the inactive GDP/GTP state had been reported.

This chapter will discuss our current understanding of the transition between inactive and active Rag nucleotide binding conformations. The mechanism of conversion from an inhibitory LFC to the active Rag complex remains unclear, and I will discuss hypotheses and preliminary evidence for the existence of an external factor that promotes Rag escape from the LFC and conversion to the fully activated conformation. To complete the discussion of the Rag nucleotide binding cycle, I will also present preliminary data suggesting that mTORC1 binding to the Rags regulates RagC nucleotide binding state.

Results

4.2.1 Elucidation of dynamic rearrangement between active and inactive Rags

In order to assess conformational transitions between active ($RagA^{GTP}$:$RagC^{GDP}$) and inactive ($RagA^{GDP}$:$RagC^{GTP}$) Rags, I contributed to a collaborative team that determined an ~8-9 Å structure of the 150 kDa Ragulator- $RagA^{GTP}$:$RagC^{XDP}$ complex (**Figure 4.2a**). No difference could be detected between the RagA and RagC G domain orientations between our active Rag-Ragulator structure and the previously reported GATOR1-RagA:RagC structure in a pseudo-active loading state ($RagA^{GTP}$:$RagC^{empty}$) (Shen et al. 2018) (**Figure 4.2a**). By aligning RagA:RagC in the inactive nucleotide state (from the LFC structure described in Chapter 3) with RagA:RagC in the active state, we found that both G domains reorient relative to the roadblock domains (**Figure 4.2b**). Similar behavior has been observed for Rag homologs Gtr1 and Gtr2 from *S. cerevisiae* (Gong et al. 2011; Jeong et al. 2012b). As a consequence, the cleft between the RagA and RagC G domains is nearly twice as wide in the inactive ($RagA^{GDP}$:$RagC^{GTP}$) as the active ($RagA^{GTP}$:$RagC^{GDP}$) state (**Figure 4.2c**).

This modification of the intra-G domain cleft restricts GTPase client engagements. For example, without this cleft opening, the FLCN:FNIP2 longin heterodimer would be sterically unable to bind RagA:RagC as observed in the LFC. Docking of active $RagA^{GTP}$:$RagC^{GDP}$ onto the FLCN:FNIP2 longin heterodimer to generate a hypothetical binding model leads to steric clashes. This explains structurally why the LFC does not form in nutrient replete conditions (**Figure 4.2d**). It remains to be seen how the Rag G domain rearrangement upon activation impacts interactions with other Rag effectors, such as Raptor or Gator1. Besides the LFC, the only other Rag structure containing a G-domain interactor is that of $RagA^{GppNHp}$:$RagC^{empty}$ with Gator1 (Shen et al. 2018). In this structure, the Depdc5 subunit of Gator1 interacts directly with the RagA nucleotide binding pocket, likely stabilizing the basally loosely-bound Rag A nucleotide. The binding orientation captured in this structure is likely inhibitory toward Gator1 GAP activity, as the Nprl2 domain containing the catalytic arginine residue required for GAP activity is positioned distally from the RagA G domain (Shen et al. 2018; Shen et al. 2019).

Fascinatingly, the Nprl2 and Nprl3 subunits of Gator1 assume longin domain folds. This raises the possibility that Gator1 could interact with the Rag GTPases in a conformation in which there is a similar longin dimer-roadblock dimer interface as reported for FLCN:FNIP2 and the Rag G domains in Chapter 3. At this time, it is unclear whether such a complex could possibly exist between a longin dimer-containing complex and the Rag GTPases when they are in their $RagA^{GTP}$:$RagC^{GTP}$ orientation, which I believe to be the predominant GAP substrate for both Gator1 and FLCN:FNIP2 in cells (although this is not proven). For such a complex to exist, the longin dimer would have to rearrange significantly to fit into the Rag G domains in their $RagA^{GTP}$:$RagC^{GTP}$ orientation. A key landmark in the field will be the determination of a structure of Rag GTPases with a GAP protein in its catalytically active conformation.

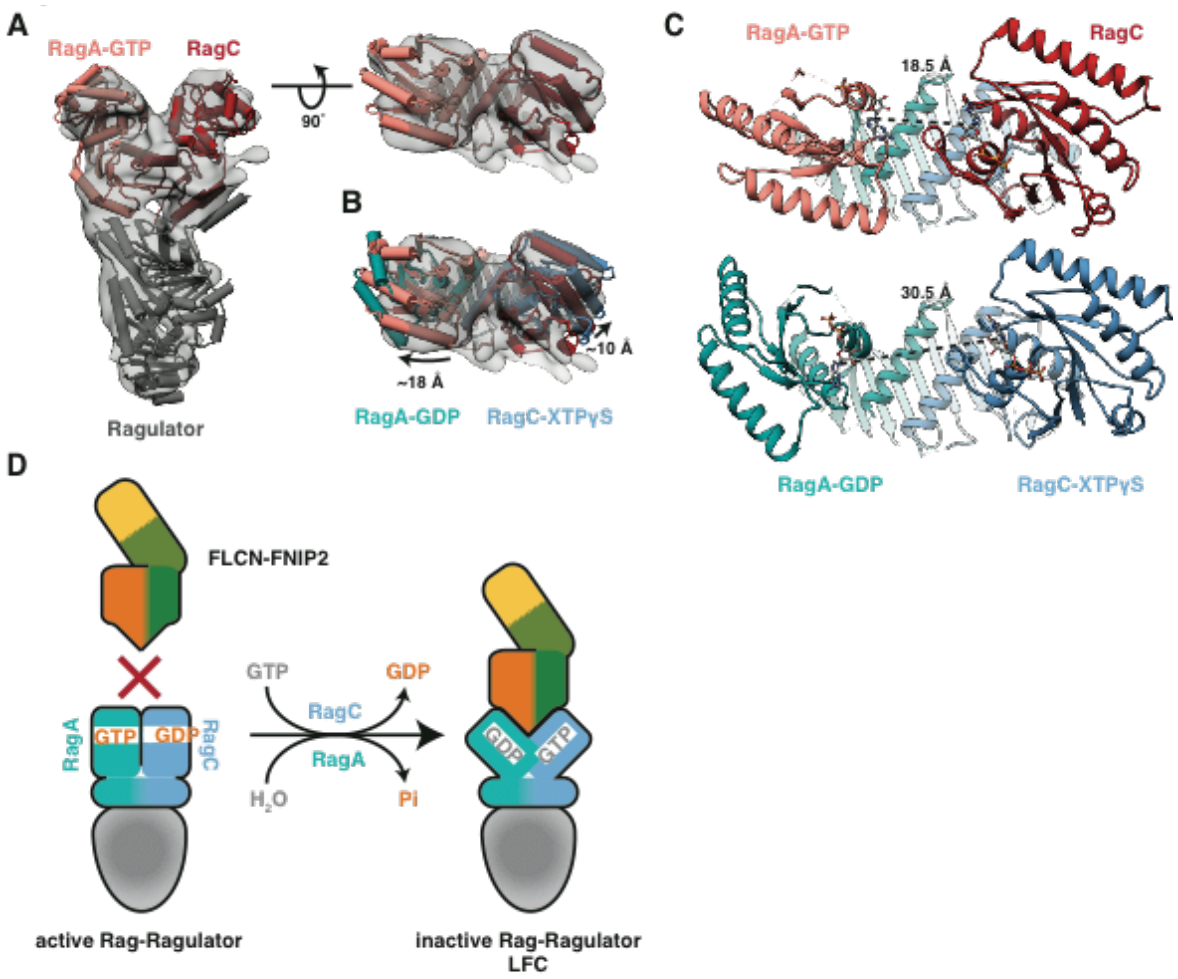

Figure 4.2 Rag conformational change upon conversion between active and inactive states. ***(a)*** Side (left) and top (right) view of the cryo-EM structure of Ragulator-RagA^{GTP}:RagC^{XDP} (gray, transparent). Rigid-body fitted atomic models for Ragulator (dark gray) and RagA^{GTP}:RagC (light red, red) are displayed. (**b**) Top view of the active Rag-Ragulator structure as in (a) with the atomic model of RagA^{GDP}:RagC^{XTPγS} from the LFC overlaid (cyan, blue). Model alignment was based on the constant roadblock domains of RagA:RagC. Extend of the G domain rotations are indicated. (**c**) Nucleotide-nucleotide distance in active (top) and inactive (bottom) RagA:RagC. The nucleotide distance for active RagA:RagC is based on a hypothetical model build by aligning the RagA and RagC G domains of the inactive LFC structure to the G domains of the pseudo-active RagA^{GTP}:RagC model. (**d**) Structure-based model for the nucleotide dependent formation of the LFC.

4.2.2 Comprehensive model of the Rag nucleotide cycle

Emerging data that provides both dynamic and structural details of Rag interactions with nucleotides, regulators, and effectors informed the complete model of the Rag nucleotide binding cycle that I present below.

In low nutrient conditions, the Rags are predominantly found in a stable lysosomal complex, and are in the RagA/B^{GDP}:RagC/D^{GTP} nucleotide binding conformation. The Rags are most stably maintained in the RagA/B^{GDP}:RagC/D^{GTP} nucleotide conformation when they are a member of the Lysosomal Folliculin Complex (LFC) composed of Ragulator, RagA/B^{GDP}:RagC/D^{GTP}, and FLCN:FNIP2. However, RagA/B^{GDP}:RagC/D^{GTP} also binds stably to Ragulator without FLCN:FNIP2, and preliminary evidence suggests that other proteins may also bind and maintain an inactive RagA/B^{GDP}:RagC/D^{GTP}-Ragulator complex (see sections 4.2.1 and 4.2.3) (Shen et al. 2018). One hypothesis is that the roadblock-longin interaction interface visualized for the inactive Rags and FLCN:FNIP2 in the LFC structure may be assumed between the Rags and other binding partners, such that FLCN:FNIP2 is not the only factor that may act to maintain the inactivating state.

In step '**1**' of the nucleotide cycle, the stable LFC (or alternative) complex is disrupted, by an as-yet-unknown process (see section 4.2.3 for more discussion on this topic). Once the LFC is disrupted, RagA/B undergoes spontaneous nucleotide exchange, which results in a RagA/B^{GTP}:RagC/D^{GTP} loaded state (step '**2**'). In this state, Rag affinity for Ragulator is decreased, and the Rags begin to spatially cycle between a lysosomal and a cytoplasmic state (as discussed in Chapter 2 and (Lawrence et al. 2018). Loading of RagA/B with GTP also enables step '**3**': FLCN:FNIP2 RagC GAP activity (as discussed in Chapter 3).

The resulting RagA/B^{GTP}:RagC/D^{GDP} complex is competent to recruit mTORC1 to the lysosome (step '**4'**). The Ragulator-active Rag-mTORC1 complex assembles transiently; mTORC1 cycles between a lysosomal and a cytoplasmic state in a Rag-dependent manner (step '**5**'; see Chapter 2 and (Lawrence et al. 2018). Unpublished data suggests that RagC has a low affinity for GDP nucleotide, and mTORC1 binding to RagA/B^{GTP}:RagC/D^{GDP} stabilizes RagC GDP binding (see section 4.2.4). Thus, mTORC1 release that occurs during spatial cycling may also prompt RagC nucleotide exchange (step '**6**'), which likely reloads RagC with GTP due to the 10:1 GTP:GDP cytoplasmic nucleotide ratio (Bos et al. 2007).

I posit that after each cycle of mTORC1 recruitment to the lysosome, the Rags are returned to the intermediate RagA/B^{GTP}:RagC/D^{GTP} state. Then, depending on the current cellular conditions, they may be re-converted to the activating RagA/B^{GTP}:RagC/D^{GDP} state by FLCN:FNIP2 GAP activity (returning to step '**3**' of the cycle) if nutrient levels remain high, or they may be converted to the inactivating RagA/B^{GDP}:RagC/D^{GTP} state by Gator1 GAP activity if nutrient levels fall (step '**7**'). Gator1 GAP activity hence activates a series of events that results in the formation of a stable LFC in which FLCN:FNIP2 GAP activity is inhibited (consistent with observations reported in (Meng and Ferguson 2018). FLCN:FNIP2 GAP activity is inhibited upon its assembly into the LFC, which strengthens the cellular commitment to converting the Rag pool to the inactivating conformation in response to decreased nutrient levels.

This model highlights the transient nature of each of the Rag heterodimer's nucleotide binding states, and emphasizes the requirement for Rag binding partners to maintain particular states. The GAP complexes Gator1 and FLCN:FNIP2 are critical in orchestrating Rag nucleotide binding conformation, and play additional regulatory roles

to their canonical GAP functions—Gator1 activity prompts the formation of a FLCN:FNIP2 interaction interface that ultimately acts to control the GDP-bound state of RagA. This feature sets the Rags apart from other small GTPases, which utilize both GEFs and GAPs to manage their nucleotide binding cycle. Instead, I posit that the Rags' low affinity for diphosphate nucleotide is a defining feature, and results in a distinct nucleotide binding cycle relative to canonical small GTPases.

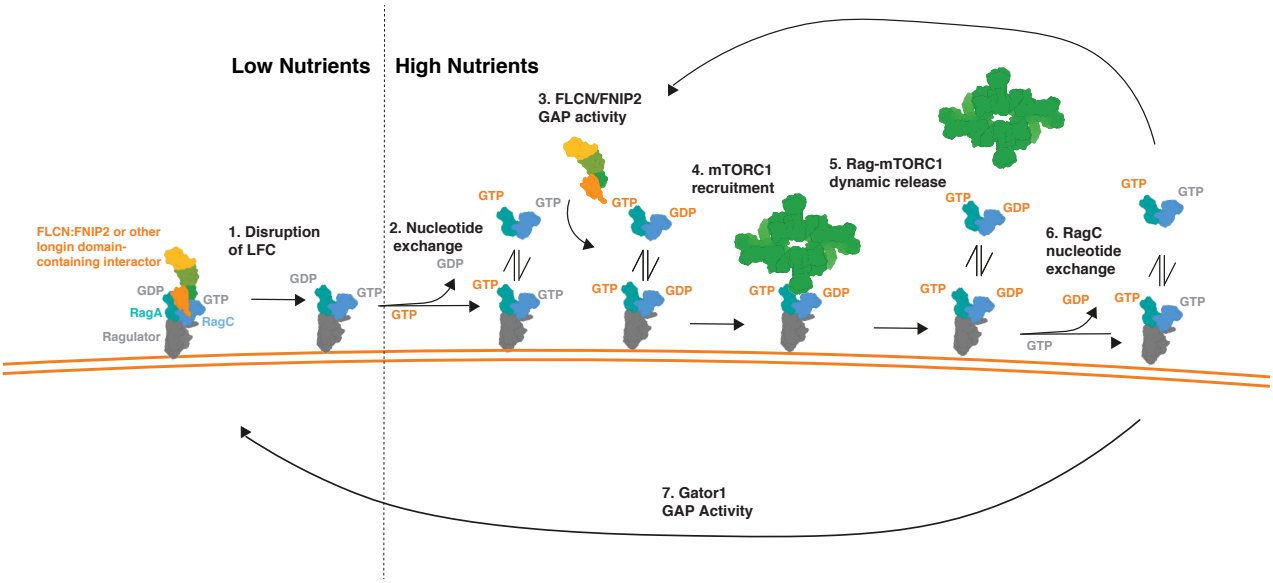

Figure 4.3 Model of the complete Rag GTPase nucleotide cycle. *Description of steps in the Rag nucleotide cycle can be found in the text for section 4.2.2. In this figure, the "activating" nucleotide conformations are indicated in orange, and the inactivating nucleotide conformations are indicated in grey.*

4.2.3 How do Rags escape inhibition by the LFC?

A key open question is how the Rags are released from their inhibited state in the LFC and ultimately converted to their fully active state. Experiments presented in Chapter 3 suggest a pathway to Rag activation can be achieved by disrupting the LFC, which would promote auto-loading of RagA with GTP and convert FLCN:FNIP2 to a GAP-competent state, ultimately resulting in RagC nucleotide hydrolysis to the GDP-bound active form.

An intriguing candidate for a factor that could mediate Rag nucleotide binding transition is the SLC38A9 amino acid permease. SLC38A9 has been reported to act as both an amino acid and a cholesterol sensor (Jung et al. 2015; Rebsamen et al. 2015; Wang et al. 2015; Castellano et al. 2017), and to mediate amino acid efflux from the lysosome (Wyant et al. 2017). SLC38A9 is composed of a transmembrane region (that mediates the permease function), as well an N-terminal cytosolic domain (Jung et al. 2015; Rebsamen et al. 2015). Furthermore, a recent paper reported that a purified SLC38A9 cytosolic domain bound directly to the Rags and both inhibited nucleotide loading onto RagA and promoted GDP release from RagA (Shen and Sabatini 2018).

The authors of this paper concluded that SLC38A9 acts as a noncanonical GEF toward RagA.

Based on these data, I tested the hypothesis that the purified SLC38A9 cytosolic domain (**Figure 4.3a**) promotes Rag nucleotide exchange in the context of the LFC. Contrary to expectation, the mant fluorimetry assays showed that the SLC38A9 cytosolic domain had the effect of stabilizing mant nucleotide onto Rags, both for a $RagA^{mantGDP}$:$RagC^{XTP\gamma S}$ + Ragulator substrate and for a $RagA^{mantGDP}$:$RagC^{XTP\gamma S}$ + Ragulator + FLCN:FNIP2 (full LFC) substrate (**Figure 4.3b**). In fact, complexes containing the SLC38A9 cytosolic domain showed an even lower rate of nucleotide exchange than the LFC on its own, which does show a gradual mant signal decay. The fact that the mant fluorimetry traces were identical for the sample containing SLC38A9 cytosolic domain + $RagA^{mantGDP}$:$RagC^{XTP\gamma S}$ + Ragulator, and SLC38A9 cytosolic domain + $RagA^{mantGDP}$:$RagC^{XTP\gamma S}$ + Ragulator + FLCN:FNIP2 suggest that SLC38A9 has the dominant effect on the RagA nucleotide binding pocket orientation, perhaps by competing FLCN:FNIP2 off and stably binding the Rag G domain.

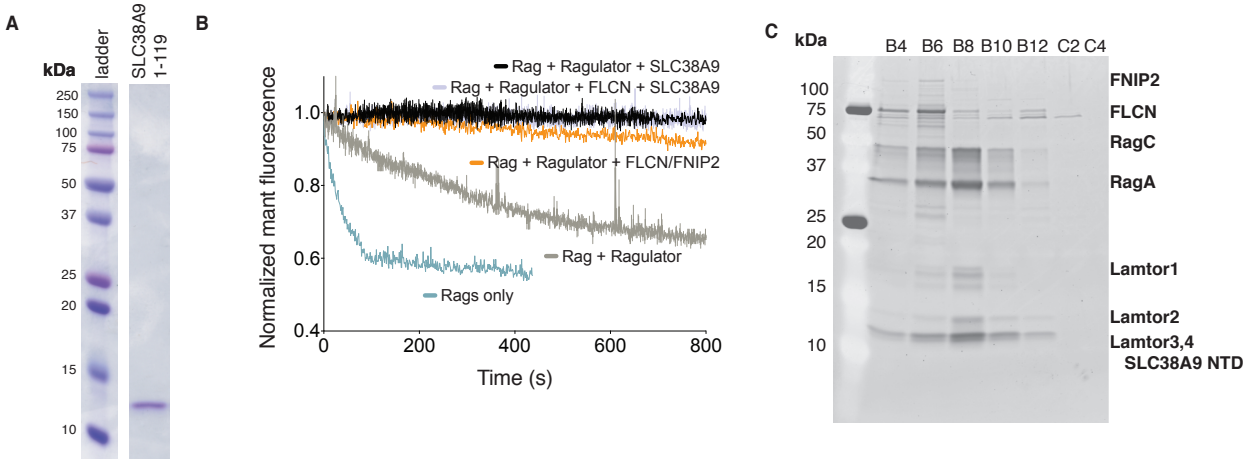

Figure 4.4 SLC38A9 Cytosolic Domain stabilizes RagA GDP-binding. *(**a**) Coomassie gel showing purified SLC38A9 cytosolic domain. (**b**) RagA nucleotide exchange visualized by mant fluorescence. GTP replacement of mantGDP was monitored for $RagA^{mantGDP}$:$RagC^{XTP\gamma S}$ alone (blue), in complex with Ragulator only (grey), with Ragulator and SLC38A9 NTD (black), with Ragulator and FLCN:FNIP2 (orange), or with Ragulator, SLC38A9 NTD, and FLCN:FNIP2 (purple). Mean and Standard Error of the Mean (SEM) are plotted. (**c**) SYPRO-stained gel electrophoresis analysis of SEC experiment analyzing elution of complexes formed upon after co-incubation of $RagA^{mantGDP}$:$RagC^{XTP\gamma S}$, Ragulator, FLCN:FNIP2, and SLC38A9 NTD. Elution fractions are indicated above the gel.*

To test whether SLC38A9 displaces FLCN:FNIP2 from the LFC, I combined $RagA^{mantGDP}$:$RagC^{XTP\gamma S}$ with a 1.2-fold molar excess of Ragulator, FLCN:FNIP2, and the SLC38A9 CTD and analyzed complex formation via SEC. Because the SLC38A9 NTD (13.4 kDa) is a very similar size to Mp1/Lamtor3 (13.6 kDa), the results are difficult to

interpret. However, there is an intermediate fraction that appears to be enriched for Rags, Ragulator, and SLC38A9 NTD, whereas the first eluted fraction clearly contains FLCN:FNIP2 and may contain relatively less SLC38A9 (**Figure 4.3c**). More work will be required to rule out the possilbity that SLC38A9 binding is not mutually exclusive with LFC complex formation, but preliminary results suggests that SLC38A9 forms a stable complex with $RagA^{mantGDP}$:$RagC^{XTP\gamma S}$ and Ragulator.

4.2.4 Characterization of RagC nucleotide affinity

To elucidate the full Rag nucleotide cycle, I performed preliminary experiments to assess RagC nucleotide affinity. Using a mant fluorescence assay to assess release of mant-labeled xanthine nucleotide from the $RagC^{D181N}$ xanthine-specific mutant nucleotide binding pocket, I found that RagC spontaneously exchanges mantXDP but not mantXTP for unlabeled XTP (**Figure 4.5a**). Unlike what was observed for RagA (**Figure 3.5c**), binding to Ragulator neither stabilized nor destabilized RagC mantXDP nucleotide, which does not support the previously proposed model that Ragulator acts as a 'biased RagC GEF' (Shen and Sabatini 2018). This suggests that the GDP-bound state of RagC is short-lived, as the plentiful GTP:GDP ratio in the cytoplasm would result in rapid nucleotide exchange back to the GTP-bound state, unless some other factor acts to stabilize RagC nucleotide binding.

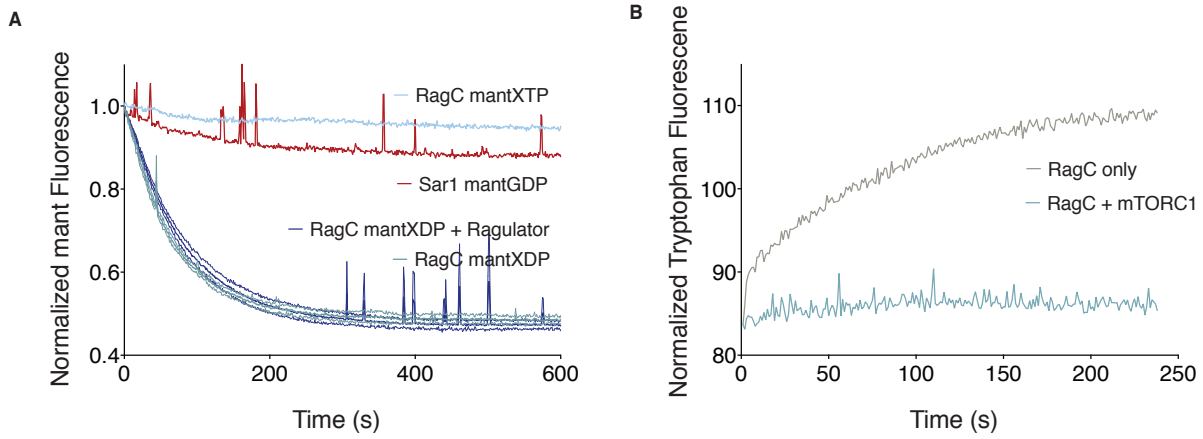

Figure 4.5 RagC has a low affinity for GDP; mTORC1 stabilizes RagC GDP interaction. (a) *mant GEF assay, in which normalized mant fluorescence intensity is plotted, representing release of indicated mant-labeled nucleotide upon the addition of unlabeled triphosphate nucleotide. One representative trace (RagC mantXTP and Sar1 mantGDP) or the mean and SEM of two traces (RagC mantXDP and RagC mantXDP + Ragulator) are plotted. (**b**) Tryptophan fluorescence nucleotide exchange assay in which GDP-loaded RagC nucleotide exchange is visualized in the absence and presence of superstoichiometric amounts of mTORC1. Following GTP addition to the cuvette at t=0, increased signal corresponds to GTP reloading (and displacement of GDP) in the RagC nucleotide binding pocket. One representative trace is plotted.*

One candidate for a RagC binding partner that could influence nucleotide affinity is mTORC1 itself. mTORC1 binds preferentially to GDP-bound RagC according to studies using both the $RagC^{S75N}$ mutant that preferentially binds GDP, and *in vitro* studies of XDP-loaded RagC (Tsun et al. 2013; Lawrence et al. 2018). I monitored RagC nucleotide exchange via a tryptophan fluorescence nucleotide exchange assay in the absence and presence of superstoichiometric amounts of mTORC1. I found that while $RagC^{WT}$ spontaneously exchanged GDP for GTP, when superstoichiometric amounts of mTOR1 were added, GTP exchange was no longer observed (**Figure 4.5b**).

These data suggest that mTORC1 is not only a client of the active ($RagA/B^{GTP}$:$RagC/D^{GDP}$) Rags, but also that mTORC1 and the Rags co-regulate one another. The 'affinity switch' property of the Rags detailed in Chapter 2 builds in a mechanism for the dissolution of the lysosomal Rag-mTORC1 complex, as the active-state GTP-bound RagA/B partner has a high off-rate from Ragulator, and dynamic release of the Rags from Ragulator is thought to also promote mTORC1 unbinding (see Chapter 2 and (Lawrence et al. 2018). Further work to dissect the co-regulatory relationship between RagC nucleotide binding state and mTORC1 recruitment may be a fruitful future direction.

4.2.5 Open questions

Ultimately, the goal of studying mechanisms of Rag GTPase conversion between states is to understand the physical process of mTORC1 recruitment to the lysosome. Many open questions in this area remain: what is the interaction interface between the Rags and mTORC1, itself an 800 kDa heterohexamer? Are multiple copies of the Rag-Ragulator scaffold required for mTORC1 docking at the lysosome? If so, does mTORC1 recruitment require or template the assembly of a lysosomal supercomplex containing multiple copies of Rags and Ragulator?

Another area of intrigue is the observation that many of the components of the Rag regulatory pathway contain roadblock/longin domains, and that these structural building blocks can be assembled into both activating and inactivating supercomplexes. I hypothesize that there may be additional as-yet-unidentified Rag interaction partners that contain Roadblock domains, and that these interactors may be involved in the assembly of functional mTORC1 signaling complexes on the lysosome. For example, how is Rheb oriented such that it is aligned to allosterically activate mTORC1? Are there factors that coordinate the relative orientations of Rag and Rheb relative to mTORC1 to ensure effective allosteric interactions? Rag-Rheb relative orientations?

The extent to which the Rag GAP complexes, FLCN:FNIP2 and Gator1, rearrange in order to assume their active conformation is also unclear. Evidence suggests that FLCN:FNIP2 dynamically relocalizes within the cell in response to nutrients, in a manner that controls its enzymatic activity (Petit et al. 2013; Tsun et al. 2013; Wolfson et al. 2017). The cellular location of Gator1 in varying nutrient states is less clear; a key open question is whether Gator1 activity is also controlled by or correlated with subcellular localization.

The field of nutrient sensing by mTORC1 at the lysosome has advanced by leaps and bounds during the past five years that I have spent in the Zoncu lab, and I look forward to watching more future discoveries.

4.3 References

Bar-Peled L, Schweitzer LD, Zoncu R, Sabatini DM. 2012. Ragulator is a GEF for the rag GTPases that signal amino acid levels to mTORC1. *Cell* **150**: 1196-1208.

Bos JL, Rehmann H, Wittinghofer A. 2007. GEFs and GAPs: critical elements in the control of small G proteins. *Cell* **129**: 865-877.

Castellano BM, Thelen AM, Moldavski O, Feltes M, van der Welle RE, Mydock-McGrane L, Jiang X, van Eijkeren RJ, Davis OB, Louie SM et al. 2017. Lysosomal cholesterol activates mTORC1 via an SLC38A9-Niemann-Pick C1 signaling complex. *Science* **355**: 1306-1311.

de Araujo MEG, Naschberger A, Furnrohr BG, Stasyk T, Dunzendorfer-Matt T, Lechner S, Welti S, Kremser L, Shivalingaiah G, Offterdinger M et al. 2017. Crystal structure of the human lysosomal mTORC1 scaffold complex and its impact on signaling. *Science* **358**: 377-381.

Fu Y. 2018. Molecular mechanisms for mTORC1 activation via coordinated nucleotide loading of the Rag GTPases. *Master Thesis*.

Gong R, Li L, Liu Y, Wang P, Yang H, Wang L, Cheng J, Guan KL, Xu Y. 2011. Crystal structure of the Gtr1p-Gtr2p complex reveals new insights into the amino acid-induced TORC1 activation. *Genes Dev* **25**: 1668-1673.

Jeong JH, Lee KH, Kim YM, Kim DH, Oh BH, Kim YG. 2012a. Crystal structure of the Gtr1p(GTP)-Gtr2p(GDP) protein complex reveals large structural rearrangements triggered by GTP-to-GDP conversion. *J Biol Chem* **287**: 29648-29653.

-. 2012b. Crystal Structure of the Gtr1p(GTP)-Gtr2p(GDP) Protein Complex Reveals Large Structural Rearrangements Triggered by GTP-to-GDP Conversion. *Journal of Biological Chemistry* **287**: 29648-29653.

Jung J, Genau HM, Behrends C. 2015. Amino Acid-Dependent mTORC1 Regulation by the Lysosomal Membrane Protein SLC38A9. *Mol Cell Biol* **35**: 2479-2494.

Lawrence RE, Cho KF, Rappold R, Thrun A, Tofaute M, Kim DJ, Moldavski O, Hurley JH, Zoncu R. 2018. A nutrient-induced affinity switch controls mTORC1 activation by its Rag GTPase-Ragulator lysosomal scaffold. *Nature cell biology*.

Meng J, Ferguson SM. 2018. GATOR1-dependent recruitment of FLCN-FNIP to lysosomes coordinates Rag GTPase heterodimer nucleotide status in response to amino acids. *J Cell Biol*.

Petit CS, Roczniak-Ferguson A, Ferguson SM. 2013. Recruitment of folliculin to lysosomes supports the amino acid-dependent activation of Rag GTPases. *J Cell Biol* **202**: 1107-1122.

Rebsamen M, Pochini L, Stasyk T, de Araujo ME, Galluccio M, Kandasamy RK, Snijder B, Fauster A, Rudashevskaya EL, Bruckner M et al. 2015. SLC38A9 is a component of the lysosomal amino acid sensing machinery that controls mTORC1. *Nature* **519**: 477-481.

Sancak Y, Bar-Peled L, Zoncu R, Markhard AL, Nada S, Sabatini DM. 2010. Ragulator-Rag complex targets mTORC1 to the lysosomal surface and is necessary for its activation by amino acids. *Cell* **141**: 290-303.

Shen K, Huang RK, Brignole EJ, Condon KJ, Valenstein ML, Chantranupong L, Bomaliyamu A, Choe A, Hong C, Yu Z et al. 2018. Architecture of the human GATOR1 and GATOR1-Rag GTPases complexes. *Nature* **556**: 64-69.

Shen K, Sabatini DM. 2018. Ragulator and SLC38A9 activate the Rag GTPases through noncanonical GEF mechanisms. *Proc Natl Acad Sci U S A* **115**: 9545-9550.

Shen K, Valenstein ML, Gu X, Sabatini DM. 2019. Arg-78 of Nprl2 catalyzes GATOR1-stimulated GTP hydrolysis by the Rag GTPases. *J Biol Chem* **294**: 2970-2975.

Su MY, Morris KL, Kim DJ, Fu Y, Lawrence R, Stjepanovic G, Zoncu R, Hurley JH. 2017. Hybrid Structure of the RagA/C-Ragulator mTORC1 Activation Complex. *Molecular cell* **68**: 835-846 e833.

Tsun ZY, Bar-Peled L, Chantranupong L, Zoncu R, Wang T, Kim C, Spooner E, Sabatini DM. 2013. The Folliculin Tumor Suppressor Is a GAP for the RagC/D GTPases That Signal Amino Acid Levels to mTORC1. *Molecular cell*.

Valvezan AJ, Manning BD. 2019. Molecular logic of mTORC1 signalling as a metabolic rheostat. *Nature Metabolism* **1**.

Wang S, Tsun ZY, Wolfson RL, Shen K, Wyant GA, Plovanich ME, Yuan ED, Jones TD, Chantranupong L, Comb W et al. 2015. Metabolism. Lysosomal amino acid transporter SLC38A9 signals arginine sufficiency to mTORC1. *Science* **347**: 188-194.

Wolfson RL, Chantranupong L, Wyant GA, Gu X, Orozco JM, Shen K, Condon KJ, Petri S, Kedir J, Scaria SM et al. 2017. KICSTOR recruits GATOR1 to the lysosome and is necessary for nutrients to regulate mTORC1. *Nature* **543**: 438-442.

Wyant GA, Abu-Remaileh M, Wolfson RL, Chen WW, Freinkman E, Danai LV, Vander Heiden MG, Sabatini DM. 2017. mTORC1 Activator SLC38A9 Is Required to Efflux Essential Amino Acids from Lysosomes and Use Protein as a Nutrient. *Cell* **171**: 642-654 e612.

Yonehara R, Nada S, Nakai T, Nakai M, Kitamura A, Ogawa A, Nakatsumi H, Nakayama KI, Li S, Standley DM et al. 2017. Structural basis for the assembly of the Ragulator-Rag GTPase complex. *Nat Commun* **8**: 1625.

Zhang T, Wang R, Wang Z, Wang X, Wang F, Ding J. 2017. Structural basis for Ragulator functioning as a scaffold in membrane-anchoring of Rag GTPases and mTORC1. *Nat Commun* **8**: 1394.

Zoncu R, Bar-Peled L, Efeyan A, Wang S, Sancak Y, Sabatini DM. 2011. mTORC1 senses lysosomal amino acids through an inside-out mechanism that requires the vacuolar H(+)-ATPase. *Science* **334**: 678-683.

Appendix 1

Nucleotide binding properties of the Rag GTPases

A1.1 The Rag GTPases cannot be *de novo* loaded with diphosphate nucleotides

The Rag GTPases appear to be distinct from most small GTPases in their nucleotide binding properties. This section is a summary of experiments characterizing Rag nucleotide binding that allowed for effective protocols to generate reliably- and uniformly-labeled Rag GTPases over the course of my thesis research. The realization that the Rag GTPases have unique nucleotide binding properties was a critical insight that enabled many of the experiments reported in Chapters 3 and 4, and was achieved via work by Do Jin Kim, Ming Yuan Su, Simon Fromm, and myself.

Standard GTPase nucleotide loading protocols utilize a chelating agent, here Ethylenediaminetetraacetic acid (EDTA), to strip bound nucleotide via chelation of magnesium (Mg^{2+}) ion that coordinates nucleotide binding in the GTPase active site. EDTA incubation is followed by introduction of the desired nucleotide(s), and finally reintroduction of Mg^{2} (see Chapter 3 methods). In all *in vitro* experiments reported in this thesis, we utilized Rag heterodimers harboring the RagC D181N mutation, which engenders a preference for binding to Xanthosine over Guanosine nucleotides. It should be noted that the preference for Xanthosine is not absolute; it is estimated that the D181N mutant bestows a 10-fold bias of Xanthosine over Guanosine nucleotide binding (Bar-Peled et al. 2012), and it is expected that some of the RagC protein successfully binds GTP when no competing XTP is present (for example, in cells).

When we performed EDTA reloading reactions with varying nucleotide combinations, HPLC analysis indicated that Rags were effectively reloaded with triphosphate nucleotides, but that diphosphate nucleotides did not effectively load (**Figure A1.1a**). However, we were able to generate uniformly-loaded Rag combinations including diphoshpate nucleotides by incubating $RagA^{GTP}$:$RagC^{XTP}$ with catalytic amounts of either the Gator1 RagA GAP complex or the FLCN:FNIP2 RagC GAP complex (**Figure A1.1b**). These Rag products remained stably bound to diphosphate nucleotides even after a Size Exclusion Chromatography (SEC) run to remove the GAP (data not shown). This result suggests that stable diphosphate-loaded Rag GTPases can be generated, but perhaps that the diphosphate-bound conformation can be accessed upon nucleotide hydrolysis but is not readily sampled in EDTA-chelation conditions.

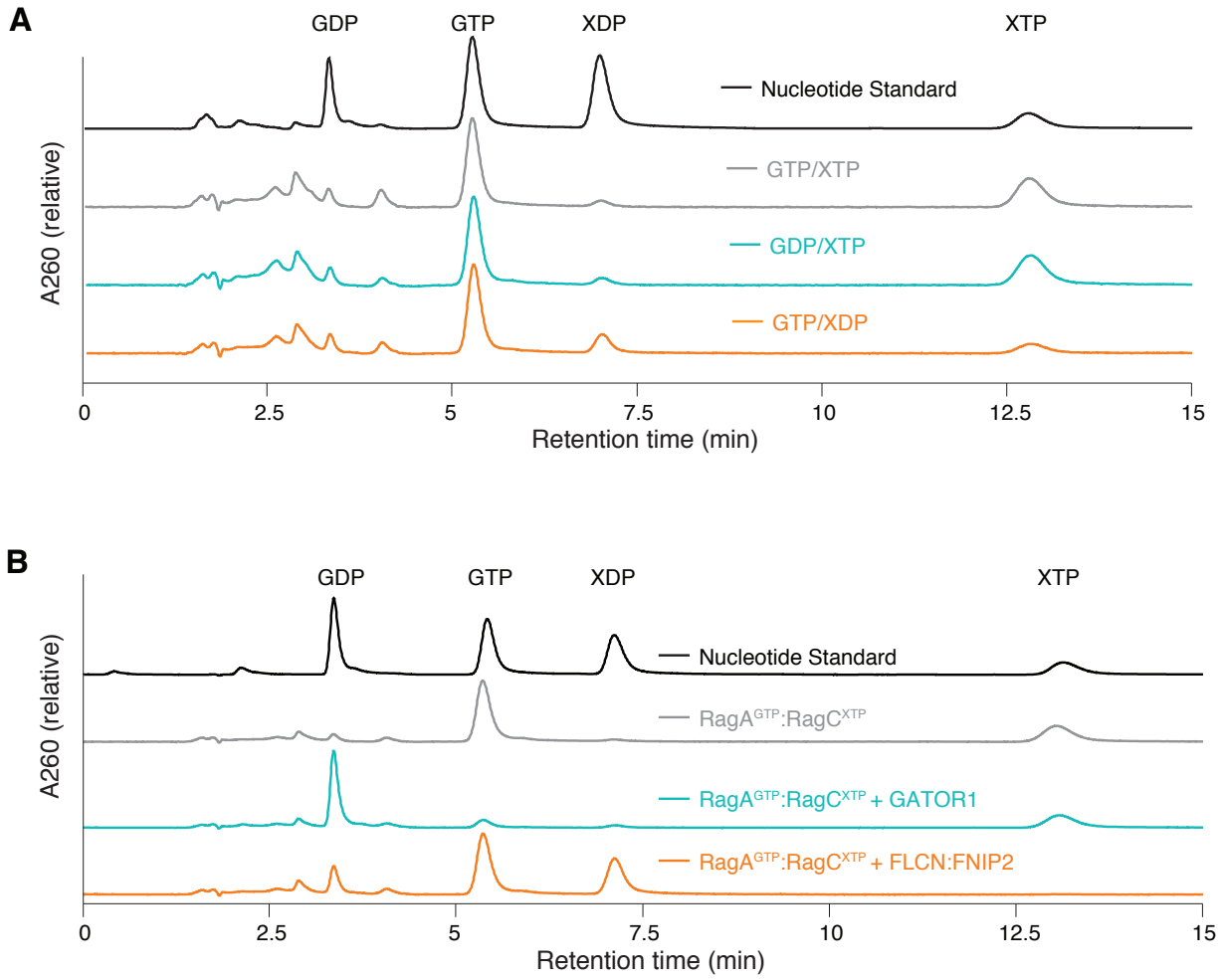

Figure A1.1 Diphosphate nucleotide-loaded Rags can be generated via GAP treatment, but not via de novo loading. *(**a**) Nucleotide elution profiles from High Performance Liquid Chromatography (HPLC) analysis of Rag nucleotide binding states. Rag heterodimers containing a the RagC Xanthine-binding D181N mutant were loaded with the indicated nucleotides (grey: GTP, XTP; teal: GDP, XTP; orange: GTP,XDP), boiled to release bound nucleotide, and analyzed via HPLC. A nucleotide standard consisting of 50 uM GDP, GTP, XDP, and XTP is shown in black. (**b**) Nucleotide elution profiles from High Performance Liquid Chromatography (HPLC) analysis of Rag nucleotide binding states. Rags heterodimers were loaded with GTP and XTP to generate $RagA^{GTP}$:$RagC^{XTP}$, boiled to release bound nucleotide, and HPLC elution profile is shown (grey). $RagA^{GTP}$:$RagC^{XTP}$ were incubated with FLCN:FNIP2 (orange) or Gator1 (teal) then analyzed by HPLC. A nucleotide standard consisting of 50 uM GDP, GTP, XDP, and XTP is shown in black.*

A1.2 EDTA stripping is only partially effective at unloading Rags purified from cells

We wondered whether the Rags were not being effectively loaded with diphosphate nucleotides because of an unusually high affinity for triphosphate nucleotides. One explanation for the results presented in A1.2 is that upon purification from SF9 cells, most of both of the RagA and RagC nucleotide pockets are occupied with GTP, and reloading is limited by the lack of release of triphosphate nucleotide from the nucleotide binding pocket. We assessed the nucleotide binding state of Rags upon purification from SF9 cells, prior to any nucleotide reloading, and observed one GTP peak (**Figure A1.2a**). We asked whether GTP could be dislodged from the Rags upon EDTA chelation, and incubated the Rags with EDTA for one hour followed by buffer exchange to remove unbound nucleotide. We observed a reduction in the GTP peak of roughly 50% (by integrating the peak area).

We next asked whether this "unloaded" Rag substrate might be more effectively loaded with diphosphate nucleotides. We observed a small, substoichiometric XDP peak (**Figure A1.2b**), and no discernible GDP peak. These results suggest that the Rags do have some capacity for diphosphate nucleotide loading when they begin in an empty rather than a triphosphate nucleotide-loaded state at the start of the EDTA reloading protocol. This interpretation is supported by the observation that RagC is more easily reloaded with XDP than RagA is with GDP, assuming that RagC is more thoroughly stripped of nucleotide by the unloading step than is RagC. However, even when ~50% of the nucleotide was lost upon unloading (**Fig A1.2a**), only a small fraction of the Rags were effectively reloaded with diphosphate nucleotide (**Figure A1.2b**).

These data support utilizing GAPs to generate diphosphate nucleotide-loaded Rags in a uniform and reliable manner, and cast doubt on results reported in studies that utilize *de novo* EDTA loading to generate diphosphate nucleotide-loaded Rags (Bar-Peled et al. 2012; Shen et al. 2017; Shen et al. 2018). My concerns about the reported results from these studies are compounded by the fact that they do not report HPLC or other analyses that can comprehensively indicate the nucleotide binding status of their Rag GTPase preparation. In the future, I hope reporting an analysis of the nucleotide binding status of the GTPase starting material will become standard practice in the Rag field, as it will help to avoid confusion when comparing results between studies.

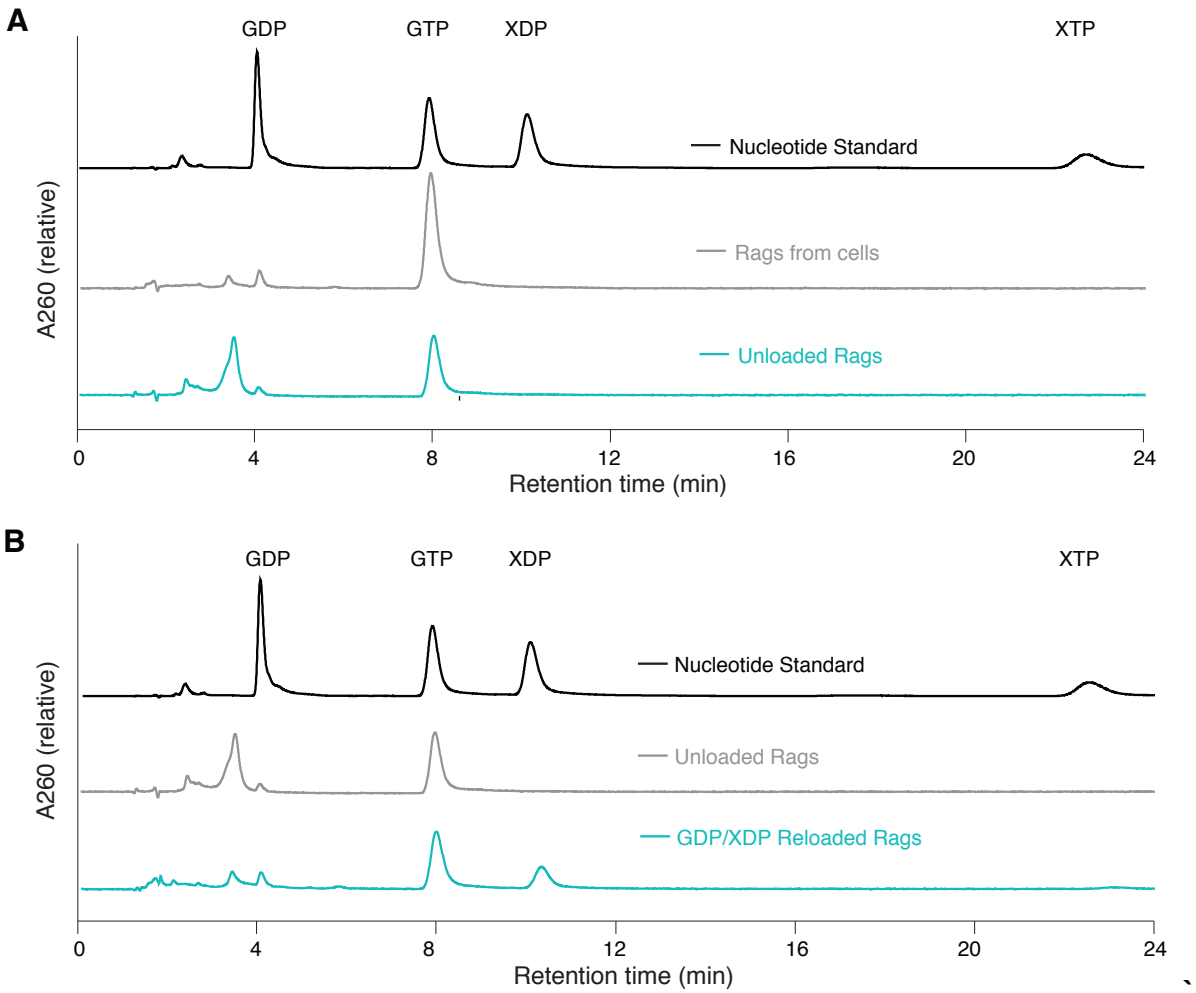

Figure A1.2 EDTA stripping is only partially effective at unloading Rags purified from cells, and only marginally improves diphosphate-nucleotide loading. (**a**) Nucleotide elution profiles from High Performance Liquid Chromatography (HPLC) analysis of Rag nucleotide binding states. Rag heterodimers containing a the RagC Xanthine-binding D181N mutant purified from SF9 cells before nucleotide reloading were boiled to release bound nucleotide and analyzed via HPLC. (grey). The same Rags were EDTA-treated to attempt to strip bound nucleotide as described in (Shen and Sabatini 2018), boiled to release bound nucleotide, and analyzed via HPLC (blue). A nucleotide standard consisting of 50 uM GDP, GTP, XDP, and XTP is shown in black. (**b**) Nucleotide elution profiles from High Performance Liquid Chromatography (HPLC) analysis of Rag nucleotide binding states. Rag heterodimers containing a the RagC Xanthine-binding D181N mutant purified from SF9 cells before nucleotide reloading were boiled to release bound nucleotide and analyzed via HPLC. (grey). The same Rags reloaded with GDP and XDP were boiled to release bound nucleotide, and analyzed via HPLC (blue). A nucleotide standard consisting of 50 uM GDP, GTP, XDP, and XTP is shown in black.

A1.3 References

Bar-Peled L, Schweitzer LD, Zoncu R, Sabatini DM. 2012. Ragulator is a GEF for the rag GTPases that signal amino acid levels to mTORC1. *Cell* **150**: 1196-1208.

Shen K, Choe A, Sabatini DM. 2017. Intersubunit Crosstalk in the Rag GTPase Heterodimer Enables mTORC1 to Respond Rapidly to Amino Acid Availability. *Mol Cell* **68**: 821.

Shen K, Huang RK, Brignole EJ, Condon KJ, Valenstein ML, Chantranupong L, Bomaliyamu A, Choe A, Hong C, Yu Z et al. 2018. Architecture of the human GATOR1 and GATOR1-Rag GTPases complexes. *Nature* **556**: 64-69.

Shen K, Sabatini DM. 2018. Ragulator and SLC38A9 activate the Rag GTPases through noncanonical GEF mechanisms. *Proc Natl Acad Sci U S A* **115**: 9545-9550.